Pulsed Ultrasonic Fields

Numeric Methods and Measurements

Nils Sponheim

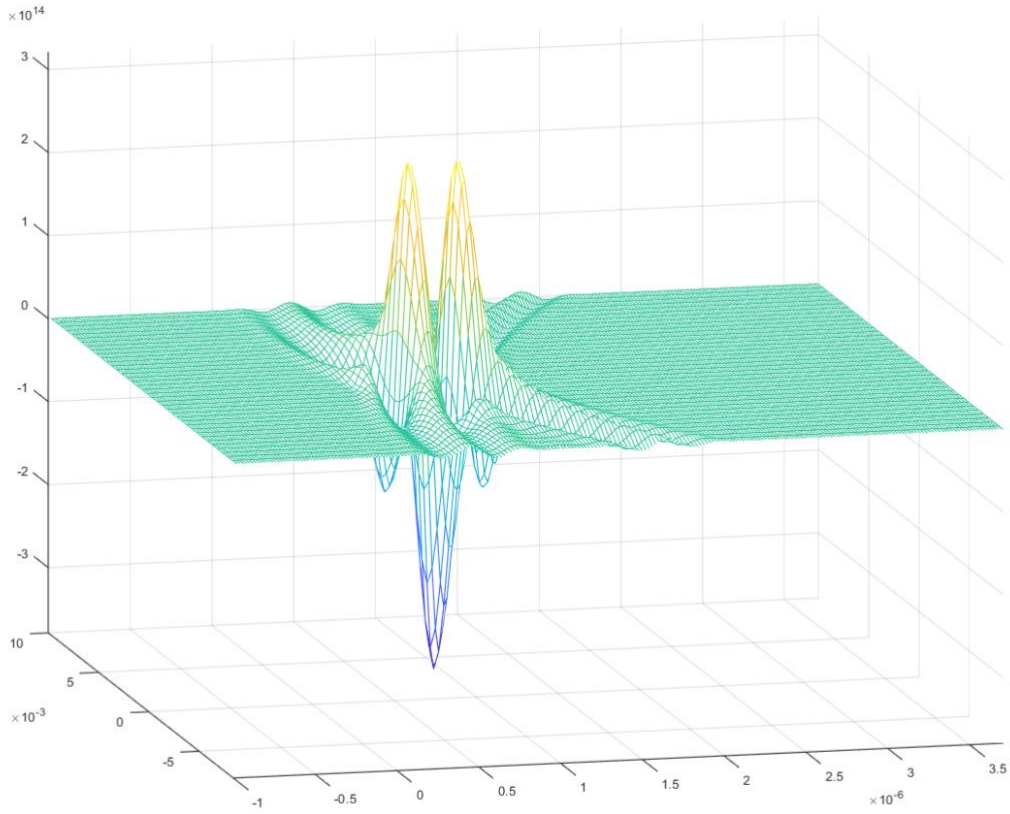

University Library
OsloMet – Oslo Metropolitan University
Spring 2025

OsloMet Skriftserien 2025 nr. 5

ISSN 2535-6992 (online)

ISBN 978-82-8364-673-3 (online)

OsloMet – storbyuniversitetet

Universitetsbiblioteket

Skriftserien

St. Olavs plass 4,

0130 Oslo,

Telefon (47) 64 84 90 00

Postadresse:

Postboks 4, St. Olavs plass

0130 Oslo

Godkjent og kvalitetssikret av instituttleder Astrid Oust Janbu, Institutt for maskin, elektronikk og kjemi, Fakultet for teknologi, kunst og design.

Abstract

This report is a summary of the medical ultrasound activity at Oslomet over several years. The modelling of pulsed field propagation and generation is based on the method of the spatial impulse response method. A novel numeric algorithm for calculating the spatial impulse response has been developed and tested. The novel algorithm uses weighted binning to reduce the numeric noise in the calculation and the computation time can therefore be reduced. The method can be used for any source function. The method has been tested by comparison to piecewise analytic solutions and measurements. The measurements have been done in a water tank with several transducers as sources. Some of the transducer's impulse responses were modified by digital inverse filtering. Measurements of pulse responses and beam profiles have verified the calculation method. Measurements of harmonic generation and propagation has been demonstrated, showing a narrower beam profile. Depth resolution was measured by applying deconvolution and the theoretical minimum of one-half period was achieved.

Sammendrag

Denne rapporten er en oppsummering av den medisinske ultralydaktiviteten ved Oslomet gjennom flere år. Modelleringen av pulset bølgeutbredelse og generering er basert på metoden med den romlige impulsrespons (SIR). En ny numerisk algoritme for beregning av den romlige impulsresponsen er utviklet og testet. Den nye algoritmen bruker vektet diskretisering for å redusere den numeriske støyen i beregningen, og beregningstiden kan derfor reduseres. Metoden kan brukes for alle kildefunksjoner. Metoden er testet ved sammenligning med stykkevise analytiske løsninger og målinger. Målingene er gjort i en vanntank med flere transdusere som kilder. Noen av transduserens impulsresponser ble modifisert med digital invers filtrering. Målinger av pulsrespons og stråleprofiler har verifisert beregningsmetoden. Målinger av harmonisk generering og utbredelse er demonstrert, og viser en smalere stråleprofil. Dybdeoppløsning ble målt ved å bruke dekonvolusjon og det teoretiske minimum på en halv periode ble oppnåd

Contents

List of Tables

List of Figures

Definitions/abbreviations

SIR Spatial Impulse Response

IMT Intima Media Thickness

PZT **Lead zirconate titanate**, also called **lead zirconium titanate** and commonly abbreviated as **PZT**, is an inorganic compound with the chemical formula $Pb[Zr_xTi_{1-x}]O_3$ ($0 \leq x \leq 1$).. It is a ceramic perovskite material that shows a marked piezoelectric effect,

KLM a transmission line model after Krimholtz, Leedom and Matthaei[16].

PMMA Polymethyl methacrylate(PMMA), is a transparent and versatile synthetic resin widely known as acrylic or plexiglass.

PVDF Polyvenylidene Fluoride, a plastic film used in hydrophones due to its piezo-electric properties.

PA75 A transducer manufactured by Precision Acoustics with focus at 75mm.

PAplan An unfocused transducer manufactured by Precision Acoustics with a quaterwave matchinglayer

PATR A transducer for transmit and receipt manufactured by Precision Acoustics.

PS Polystyrene

.

1 Introduction

Medical ultrasound imaging utilizes piezo-electric transducers driven in pulsed mode. The quality of the image depends on the pulses shaped by the transducer. Simulations of the pulsed ultrasonic fields is therefore a tool to understand the physical limitations of the ultrasonic imaging technique. Calculations of pulsed wave fields require temporal information. The method of choice is the Spatial Impulse Response method (SIR). The method was first published by Tupholm [1] in 1969. The method was brought to the attention of the ultrasound community by Stephanishen [2,3] in 1981.

The method reduces the calculation of pulsed fields to a calculation of the Spatial Impulse Response (SIR). The SIR is the velocity potential of the source when the source excites the medium with an impulse function. Several methods of calculation have been published. They can be categorized as analytic methods and purely numeric methods. The analytic methods assume that a spherical impulse is propagating with the speed of sound from an observation point. The intersection between the wave front and the source function is found and yields the analytic solution. The result is a set of piecewise analytic functions, valid over a given time range. The observation space must also be divided into several regions where different solutions are valid. The piecewise analytic functions and the different regions of validity result in complex calculation schemes. In addition, different source functions have different solutions. The first analytic solutions for a planar circular disc and for a planar rectangular disc, was published in the first papers by Stephanishen [[2],[3]] in 1971. Arditi et al [5] published an analytic solution for a focused circular disc in 1981. Dietz et al [6] published a solution for annular arrays in 1978, using a subtraction technique. Due to circular symmetry, circular sources have simpler solutions than rectangular sources. The first to find an analytic solution for a focused rectangular source were Penttinen and Luukkala [7] in 1976. Apodization was added to the solution for a rectangular source by Harris [8] in 1981 and by Tjøtta [9] in 1982. These solutions are complicated to program and is followed by a lot of logical programming and testing for validation. Several papers have been published on the attempt to simplify the algorithms. A bandlimited approach was published by D'hooge et al [10] in 1997 and a faster algorithm was published by Ortega et al [11] in 2014. A simpler solution for the planar rectangular source including phased arrays was published by Cheng at al [12] in 2011.

A major disadvantage of the analytic solutions is that a separate algorithm is needed for each source function. Numeric algorithms on the other hand, can be designed to

support any source function. We start by dividing the source into elements, at least smaller then half the wavelength. Each element is given an amplitude and a time delay, so that an amplitude matrix and a time delay matrix define the source function. The amplitude matrix is used to define the shape of the source and any apodization. The time delay matrix is used to define focusing and beam steering. For the numeric method, in general we assume that each source element radiates an impulse with the specified amplitude and time delay. At the observation point, we can sum up the contribution from all source elements. In 1990, Jensen [13] published a numeric method that assumes that the observation point is in the far field of each source element and that the SIR is a trapezoid. At the observation point, the contribution of each source element is summed up to yield the total SIR of the source.

In this report, we will use a numeric method to calculate the pulsed pressure fields. The shape of the source function and apodization will be defined by an amplitude matrix, A, and the focusing and beam steering will be defined by a time delay matrix τ. We assume that each source element radiates a Dirac's delta function. At the observation point, we can sum up the contributions from each source element as a sum of delta pulses in a time array. The novelty of the method is that each contribution is entered into the time array with weighted binning. With this method, each contribution is shared between the two closest time elements so that the time average of the two equals the exact arrival time of this contribution. The weighted binning algorithm has previously been validated in Sponheim [[14]] for circular sources and in Sponheim [15] for rectangular sources.

In chapter 2 the theory of the SIR-method is summarized, and the novel numeric method is presented. A one-dimensional transducer model is also presented. The use of inverse filtering to improve the performance of the transducer and lens design for focusing of the beam is introduced.

In chapter 3 calculations based on the theory in chapter 2 are performed. First the numeric method is validated. Second, calculations based on the transducer model are shown. Finally, various ways of calculating and presenting pulsed fields are presented. The MATLAB codes used in this chapter are listed in the appendix.

Chapter 4 is devoted to the measurements. The water tank and all the instruments used are presented. The rest of the chapter is divided into sections for each transducer. The transducers have been designed for different purposes.

2 Theory

Relevant theoretical aspects are presented in this section.

2.1 Spatial Impulse response Method

Figure 2.1
Geometry for calculation of the spatial impulse response.

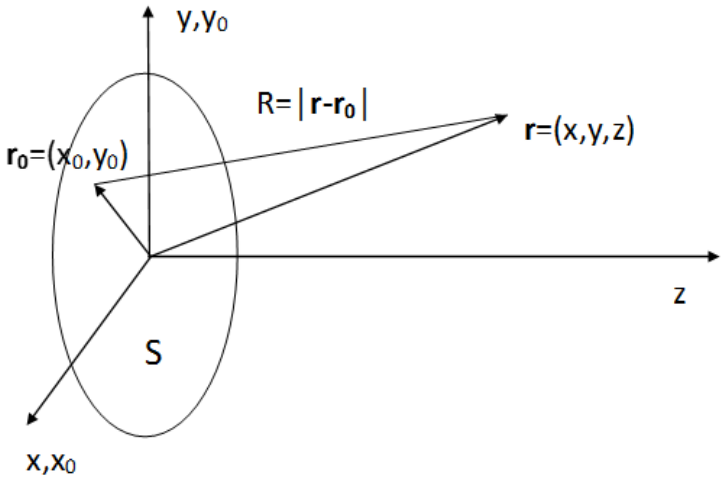

The Rayleigh integral for a piston source in an infinite baffle radiating into infinite half-space (z>0) is:

$$\varphi(\vec{r},t) = \int_S \frac{v_n(\vec{r}_0, t - R/c)}{2\pi R} dS \tag{2.1}$$

Where ϕ is the velocity potential at point $\vec{r}$ at time t, v_n is the normal velocity at the source surface S in position $\vec{r}_0$, R is the distance between $\vec{r}$ and $\vec{r}_0$, and c is the speed of sound, see Figure 2.1. We assume that the normal velocity at the source have the same time dependence v(t) for all S, but that the amplitude A($\vec{r}_0$) and the time delay τ($\vec{r}_0$) can be a function of $\vec{r}_0$ at the source in order to achieve apodization and focusing. Thus, we have:

$$v_n(\vec{r}_0, t) = A(\vec{r}_0) v\big(t - \tau(\vec{r}_0)\big) \tag{2.2}$$

And

$$\varphi(\vec{r},t)=\int_S \frac{A(\vec{r}_0)v(t-\frac{R}{c}-\tau(\vec{r}_0))}{2\pi R}dS \tag{2.3}$$

By applying the convolution theorem for the Dirac δ-function, we get:

$$\varphi(\vec{r},t)=\int_{-\infty}^{\infty} v(\sigma)\int_S \frac{A(\vec{r}_0)\delta\left(t-\frac{R}{c}-\tau(\vec{r}_0)-\sigma\right)}{2\pi R}dS\,d\sigma$$
$$=v(t)*h(\vec{r},t) \tag{2.4}$$

where * denotes convolution and

$$h(\vec{r},t)=\int_S \frac{A(\vec{r}_0)\delta(t-{}^{R}/_{c}-\tau(\vec{r}_0))}{2\pi R}dS \tag{2.5}$$

is the spatial impulse response (SIR) of the source. The SIR is the resulting velocity potential when the source S excites the infinite half-space with a Dirac's δ-function, $v(t)=\delta(t)$. The pressure field is found from the velocity potential as:

$$p(\vec{r},t)=\rho\frac{d}{dt}\varphi(\vec{r},t)=\rho\frac{d}{dt}v(t)*h(\vec{r},t) \tag{2.6}$$

where ρ is the mass density of the medium.

The calculation of pulsed pressure fields has been reduced to the calculation of the SIR for a given source function, defined by A and τ.

2.2 Numeric calculation of SIR

Figure 2.2
Geometry for numeric calculation of the spatial impulse response.

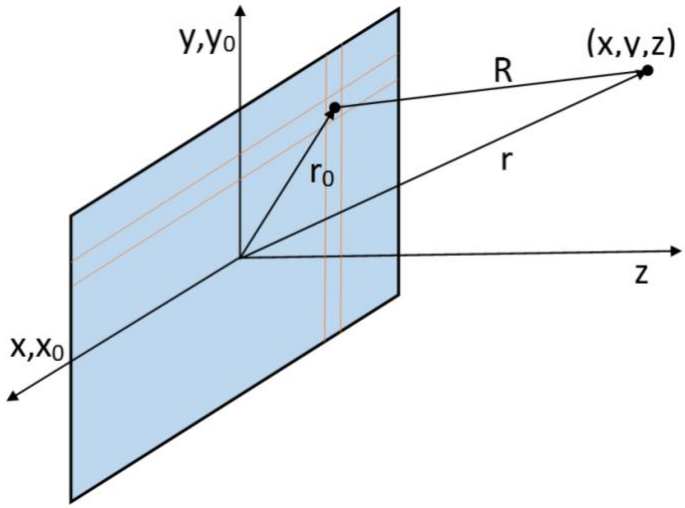

Numeric calculations of the spatial impulse response are done by dividing the source into N by M source elements that are Δx_0 by Δy_0 in size, so that the width of the source is $L_X=N\Delta x_0$ and the height of the source is $L_Y=M\Delta y_0$. The coordinates of the source are (x_0, y_0) with origo at the center of the source, that coincides with the origo of the spatial coordinates (x, y, z). The z-axis is also the acoustic axis of the source. Figure 2.2 shows the geometry of an arbitrary source element in position $\mathbf{r_0}$ = (x_0, y_0). The indices n and m are positive integers that runs from 1 to N and M, respectively. The position of each element should be at the center of the respective element. The length of $\mathbf{r_0}$ for element (n, m) is therefore given by:

$$|r_0| = \sqrt{{x_0}^2 + {y_0}^2} = \sqrt{((\left(n - \frac{(N+1)}{2}\right)\Delta x_0)^2 + ((\left(m - \frac{(M+1)}{2}\right)\Delta y_0)^2}$$

The observation point is at $\mathbf{r}$ = (x, y, z). The distance between source element (n, m) and the observation point is given by:

$$R_{nm} = \sqrt{(x - x_0)^2 + (y - y_0)^2 + z^2}$$
$$= \sqrt{(x - \left(n - \frac{(N+1)}{2}\right)\Delta x_0)^2 + (y - \left(m - \frac{(M+1)}{2}\right)\Delta y_0))^2 + z^2}$$

The spatial impulse response becomes a sum over all source elements where the source is defined by the amplitude matrix A_{nm} and the time delay matrix τ_{nm}. i_{nm} is the time index in the time array for element (n, m):

$$h(\vec{r},i) = \sum_{m=1}^{M}\sum_{n=1}^{N} \Delta_{nm}\, h(i_{nm}) = \sum_{m=1}^{M}\sum_{n=1}^{N} \frac{A_{nm}}{2\pi R_{nm}} \Delta x_0 \Delta y_0 / \Delta t \quad with \;\; i_{nm} = \left[\frac{R_{nm}-z}{c\Delta t} + \frac{\tau_{nm}}{\Delta t}\right]$$

The spatial impulse response at the observation point is calculated as a time discrete function with time resolution Δt. The contribution to the SIR from element (n, m) arrives at $t = R_{nm}/c+\tau_{nm}$. We shall use retarded time defined as T=t-z/c, to shorten the time discrete array for the SIR. The time index for element (n, m) will be $i_{nm} = T_{nm}/\Delta t$, but $T_{nm}/\Delta t$ is a real number, and an index must be an integer. A simple conversion of a real number to an integer will add numeric noise to the SIR. We shall therefore apply the method of weighted binning [14][15]. The method of weighted binning shares the contribution of a source element between the two closer time elements of the SIR. The weighted time average of the two equals the exact arrival time, see Figure 2.3[15]. We separate the real time index, i_{nm}, into an integer time index, i, and a rest value, Δi, given by:

$$\Delta i = i_{nm} - i = {}^{T_{nm}}/_{\Delta t} - i$$

Δi is a real number between zero and one and can be used to share the contribution of source element (n, m) between time element i and i+1. If the contribution from source element (n,m) to the SIR is Δh_{nm} , we can add $(1-\Delta i)\Delta h_{nm}$ to time element i and $\Delta i \Delta h_{nm}$ to time element i+1.

$$\Delta_{nm}h(i) = (1-\Delta i)\frac{A_{nm}}{2\pi R_{nm}}\Delta x_0 \Delta y_0/\Delta t \qquad and \qquad \Delta_{nm}h(i+1)$$
$$= \Delta i \frac{A_{nm}}{2\pi R_{nm}}\Delta x_0 \Delta y_0/\Delta t$$

The weighted time average of these to contributions will be the exact arrival time, T_{nm}, from source element (n, m). The time weighted contribution is:

$$i\Delta t \cdot (1-\Delta i)\Delta h_{nm} + (i+1)\Delta t \cdot \Delta i \Delta h_{nm} = \Delta t(i+\Delta i)\Delta h_{nm} = T_{nm}\Delta h_{nm}$$

which equals the exact time weighted contribution from element (n, m).

Figure 2.3
Two time-elements of the SIR time array, i and i+1.

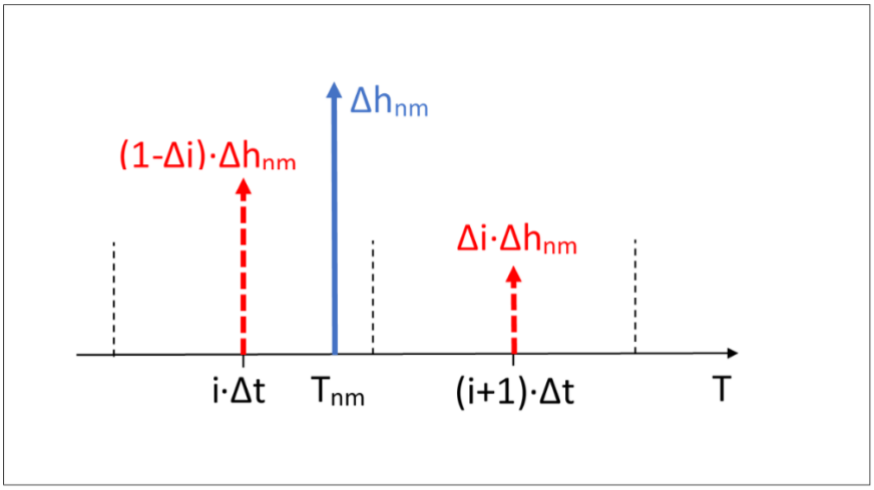

The blue solid arrow represents the contribution from source element (n, m) arriving at retarded time T_{nm}. The two red dashed arrows represent the weighted binning contribution from the same source element.

2.3 Transducer model

All transducers in this project are circular disc transducer with a diameter of several wavelengths across and half a wavelength thick. These transducers can with good approximation be modelled as simple one-dimensional thin disc piezo-electric transducer. The model used, is referred to as the KLM-transmission line model after Krimholtz, Leedom and Matthaei [16]. The transducer is modelled as a transmission line with a half period thickness at the design frequency. The electro-acoustic coupling is modelled at the center of the disc, see Figure 2.4.

Figure 2.4
The KLM-transmission line model of a thin disc piezoelectric transducer.

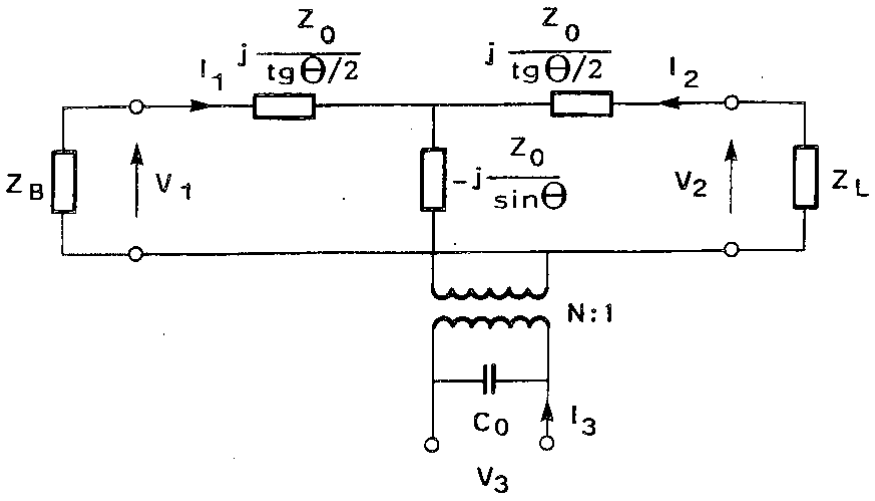

Here the following definitions are used:

Wavenumber: $k_0 = \omega\sqrt{\rho/\kappa}$

Angular thickness: $\theta = k_0 t$

Acoustic Impedance: $Z_0 = k_0 \kappa A/\omega$

Capacitance: $C_0 = \varepsilon_0 \varepsilon A/t$

Coupling factor: $N = hC_0 = C_0/d_{33}$

The notations are:

Angular frequency: ω

Mass density: ρ

Compressibility: κ

Dielectric constant: $\varepsilon_0 \varepsilon^S$ (constant strain)

Piezoelectric constant: $h = 1/d_{33}$

Thickness of disc: t

Area of disc: A

Backing impedance: Z_B

Load impedance: Z_L

Front port force: V_1

Velocity into front port: I_1

Back port force: V_2

Velocity into back port: I_2

Voltage at electric port: V_3

Current into electric port: I_3

The equivalent circuit in Figure 2.4 can be used to calculate the electric input impedance of the transducer as: $Z_{in}(\omega) = V_3(\omega)/I_3(\omega)$.

The transfer function from voltage at the electric port to the acoustic velocity at the front port can be found as: $H(\omega) = I_2(\omega)/V_3(\omega)$.

Finally, the impulse response of the transducer can be found as the inverse Fourier transform of H(ω): $h(t) = \mathcal{F}^{-1}\{H(\omega)\}$.

To increase the bandwidth of the transducer, we can add a quarter wave matching layer at the front. The matching layer can be modelled as its cascade matrix:

$$\begin{pmatrix} V_2 \\ I_2 \end{pmatrix} = \begin{pmatrix} cos\theta & -jZ_0 sin\theta \\ j\dfrac{sin\theta}{Z_0} & -cos\theta \end{pmatrix} \begin{pmatrix} V_1 \\ I_1 \end{pmatrix}$$

Here θ is the angular thickness of the matching layer and Z_0 is its acoustic impedance. Index 1 is towards the active element and index 2 is towards the acoustic front. This model can be used for several matching layers in cascade if required. We can also increase the bandwidth by using a heavy backing.

2.3 Inverse filtering and pulse forming

Spatial resolution is one of the critical parameters in imaging together with signal to noise ratio. In medical ultrasound imaging, the pulse form influence both the axial resolution and the signal to noise ratio of the image. The transmitted pulse is formed by a piezoelectric transducer and by the excitation of the transducer. The pulse length influences the axial resolution, and the pulse length is inversely proportional with the bandwidth of the transducer. The signal to noise ratio depends on the energy of the transmitted pulse, but the amplitude of the transmitted acoustic pressure is limited by the allowed mechanical index in medical imaging. The only way to increase the pulse energy is to increase the length of the pulse. This trade-off between resolution and SNR does not have an optimal solution and will depend on the imaging application. It is usual to consider a two-period pulse of the center frequency, f0, to be optimal for general purpose imaging. This pulse will give an acceptable axial resolution, $\Delta z=2c/f0$, where c is the speed of sound. The transducer must therefore have a bandwidth of at least 50%. If the transducer has a wider bandwidth, the pulse can be formed by the excitation of the transducer. Another important aspect of the pulse form is what is normally referred to as the tail of the pulse. This is caused by the after ringing of the resonant transducer and should be made as short and small as possible, since it has a negative influence on both resolution and signal to noise ratio.

The transmitted pulse, y(t), of a transducer can be found as the convolution of the transducers impulse response, h(t), and the excitation signal, x(t):

$$y(t) = h(t) * x(t)$$

where * denotes convolution. Applying the Fourier transform on this equation, we get:

$$Y(f) = H(f) \bullet X(f)$$

where Y(f) is the frequency spectrum of the transmitted pulse, X(f) is the frequency spectrum of the excitation pulse and H(f) is the frequency response of the transducer. The impulse response of a transducer can be found from a mathematical model of the transducer or from a measurement of the transmitted pulse, ym(t), with a Dirac's delta function, δ(t), as excitation.

$$y_m(t) = h(t) * \delta(t) = h(t) \leftrightarrow Y_m(f) = H(f)$$

Let us then assume that we have a description of the ideal imaging pulse, p0(t), and want to find the excitation pulse, x0(t), that will produce the ideal imaging pulse.

$$p_0(t) = h(t) * x_0(t) = y_m(t) * x_0(t) \leftrightarrow P_0(f) = H(f)X_0(f) = Y_m(f)X_0(f)$$

Thus, we get:

$$X_0(f) = \frac{P_0(f)}{H(f)} = \frac{P_0(f)}{Y_m(f)} \leftrightarrow x_0(t) = \mathcal{F}^{-1}\left\{\frac{P_0(f)}{Y_m(f)}\right\}$$

The ideal excitation pulse is found as the inverse Fourier transform of the frequency spectrum of the ideal imaging pulse divided by the measured frequency response of the transducer. This technique is referred to as invers filtering or deconvolution. The frequency spectrum of the ideal excitation pulse becomes singular if the frequency response of the transducer has zeroes. The transducers are mostly constructed as a damped half wavelength resonator. These transducers will have a zero in the frequency response at twice the resonance frequency. Mathematically, we can say that the inverse Fourier transform does not exist. The measured frequency response of the transducer will have low values compared to added noise in the measurement for large frequency bands. Applying the inverse formula in these frequency bands will only amplify the noise in the experiment. It is therefore necessary to select the frequency band for which we can apply the technique and to have a realistic suggestion for the ideal imaging pulse.

2.4 Acoustic lens design

Planar disc-transducers are easier to make if matching layers are to be added. To focus the acoustic beam of the transducer we will need lenses. In this project a silicon rubber with speed of sound equal to approximately 1000 m/s has been used. This gives a refractive index of n = 1.5 and a planar/concave lens can be made to focus the beam. This is a practical shape of a lens as the planar side can be attach to the transducer and the concave side toward the window in a measurement tank. Using simple geometric ray theory for the lens design, we find in the literature [ref.] that the focal length can be calculated as:

$$F = \frac{R}{n-1}$$

Where F is the focal length, n is the refractive index and R is the radius of the concave surface. With a refractive index of 1.5 and a desired focal length F we get:

$$R = \frac{F}{2}$$

A molding form with the required radius can be made and the lens molded in it with the other surface planar.

3 Calculations

3.1 Varification of the novel numeric method

Verification of the novel numeric method can be done by comparison with an analytic method. The simplest analytic solution is that of a circular planar disc. Figure 3.1 shows the geometry.

Figure 3.1
Geometry for calculation of the SIR of a planar circular disc in Tabel 3.1.

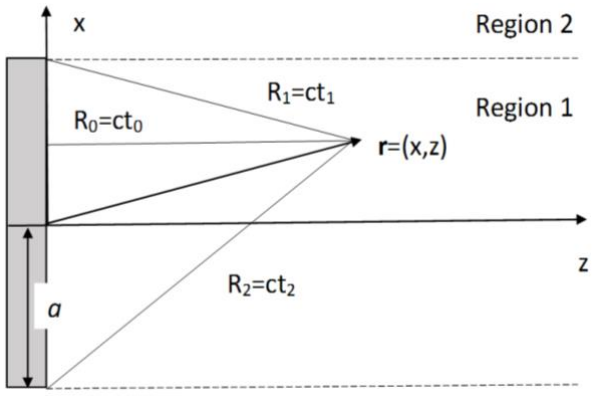

An analytic solution for a planar circular disc with radius *a* can be found in Stephanishen [2]. The infinite half space (z > 0) is divided into two regions. Region 1 is the geometric shadow of the disc defined as the cylinder with radius a, and axis along the acoustic axis defined equal to the z-axis. Region 2 is the rest of the infinite half space. Figure 3.1 shows the geometry as a two-dimensional problem due to circular symmetry. The critical time points for this geometry are the first arrival time t_0 corresponding to the normal distance between the source and the observation point (x, y, z), t_1, the propagation time between the closer edge of the disc and the observation point and t_2, the propagation time between the further edge and the observation point. Table 3.1 presents the results.

Table 3.1
The Spatial Impulse Response. The piecewise analytic solution of the SIR for a planar circular disc of radius $\boldsymbol{a}$.

$h(\boldsymbol{r},t)=$	Region 1	Region 2
0	$t<t_0$	$t<t_1$
c	$t_0<t<t_1$	Not appl.
$\frac{c}{\pi}\arccos\left(\frac{c^2t^2-z^2+x^2-a^2}{2x\sqrt{c^2t^2-z^2}}\right)$	$t_1<t<t_2$	$t_1<t<t_2$

On the acoustic axis (x=0) the SIR will be a rectangular function equal to c between the critical time points t_0 and $t_1=t_2$. We need to sample SIR and calculate for discrete time points. To reduce the length of the time array, we introduce the retarded time $T=t-t_0$ so that $T_0=0$ and $T_1=t_1-t_0$. The time length of the SIR on-axis is:

$$\Delta T = t_1 - t_0 = \left(\sqrt{a^2+z^2}-z\right)/c \qquad (3.1)$$

ΔT will decrease with z and the SIR will approach a δ-function as z increases. We observe from (2.6) that SIR shall be convolved with v(t) to find the pressure. The front velocity of the transducer v(t) is a band limited signal and therefore also the pressure pulse. The sampling frequency of the SIR must therefore be greater than twice the transducer bandwidth. However, the area under the curve of the SIR must be correct, to correctly calculate the pressure field. This requires an accurate calculation of the SIR around the critical time points t_0, t_1 and t_2 to make sure that the area under the curve is correct.

To compare the purely numeric calculation and the piecewise analytic calculation of the SIR, we chose the source function to be a planar circular disc with radius a=6.35mm. We also chose to divide the source into elements that are Δx=0.1mm by Δy=0.1mm for the numeric calculation so that A_{nm} is a 127 by 127 matrix. The circular source is modelled by assigning a value of 1 to all elements with center

inside the circle of radius *a,* and 0 to all elements with center outside the circle. The source can easily be apodised by changing the values of A_{nm} accordingly. All elements in τ_{nm} are set to zero to model a non-focused source. Focusing can be included by calculating the time delay of the elements of τ_{nm} to form a spherical wave front.

Most medical imaging transducers use frequencies well below 25 MHz so the required sampling frequency will be 50 MHz; the required time resolution is Δt=20ns. Figure 3.2 shows the on-axis SIR at a distance z=20mm for the analytic calculation (solid green line) and the numeric calculation (dashed blue line). At t_0 (T=0) the analytic SIR has been given the value c/2=750m/s to give SIR the correct area under the curve. In the other end of the rectangular function, at the time element located at 660ns that includes T_1 = 655.91ns, the analytic SIR has been given the value c((660-655.91)ns/20ns)=443m/s in order to give SIR the correct area under the curve at the end of the rectangular function. Between the critical time points T_0=0 and T_1 the SIR is given the value of c=1500m/s.

To compare the two results, we define a root mean square error function:

$$E = \sqrt{\frac{1}{I}\sum_{i}^{I}(H_{num}(i) - H_{ana}(i))^2} \qquad (3.2)$$

$H_{num}(i)$ is the numerically calculated SIR and $H_{ana}(i)$ is the analytically calculated SIR. Applying this formula to the results shown in Figure 3.2, we get E=14m/s which is 0.9% of the average value of c=1500m/s.

The above calculations of the SIR are for an on-axis observation point where the SIR is a rectangular function. In order to test the algorithm further, we chose an observation point in region 2 where the analytic solution is an analytic function between the time points t_1 and t_2. The analytic function goes to zero at both t_1 and t_2 and adjustments around these time points is not required. shows the SIR for an observation point at distance 40mm and 10mm off-axis, (z, x) = (40mm, 10mm), calculated with the analytic solution in Table 3.1 (solid green line) and the numeric algorithm (dashed blue line). The rms-error calculated with (10) gives E = 2.0m/s which is 0.6 % of the maximum value of 330m/s.

Figure 3.2
The on-axis SIR at distance 20mm. The solid line is the analytic result, and the dashed line is the result from the novel numeric algorithm.

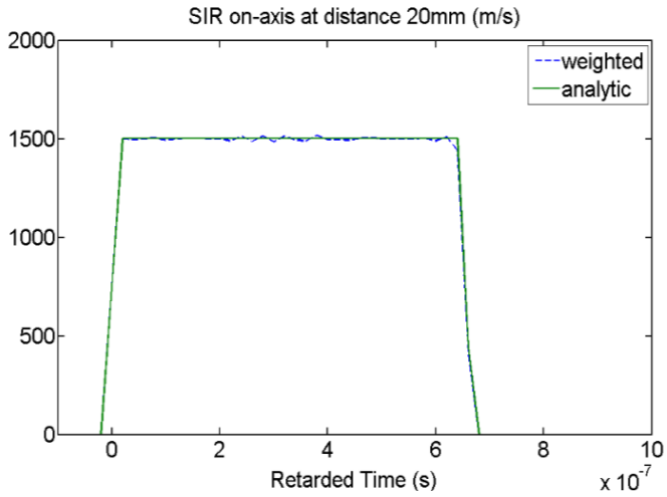

Figure 3.3
The off-axis SIR at observation point (z, x) = (40, 10) mm. The solid line is the analytic result, and the dashed line is the result from the novel numeric algorithm.

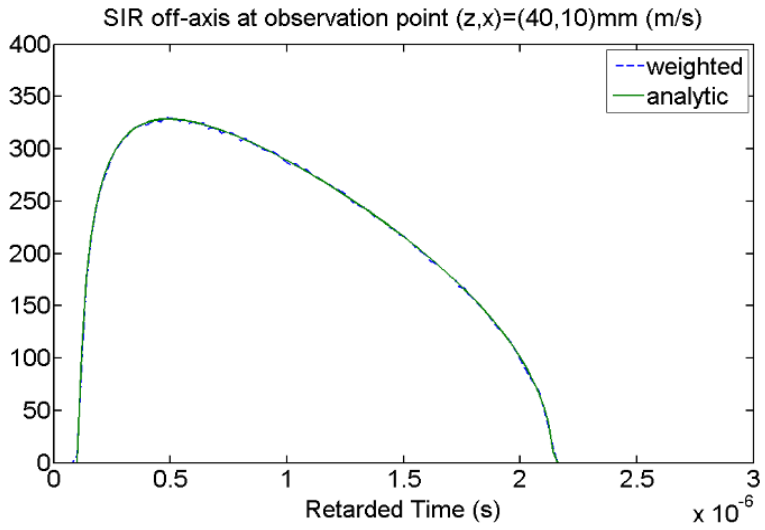

A critical area for analytic calculation of the SIR is at and around the focal point. At the focal point the SIR becomes a Dirac delta function, δ(t). Figure 3.4 shows the SIR of a focused disc of diameter 15mm and a focal length of 75mm at the focal point.

Figure 3.4
Numeric calculation of the SIR at the focal point.

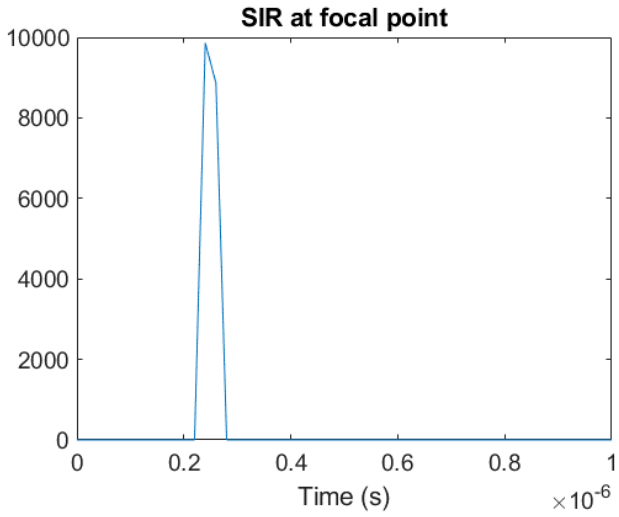

The SIR in Figure 5 is centered at 0.25μs equal to the time delay at the center of the source and the contribution from the source elements are distributed in the two closest bins of each 20ns. The half value length of the SIR is therefore 40ns.

3.2 Transducer calculations

A test transducer was designed during my PhD-work [17] at The Electronics Laboratory at NTH (today SINTEF/NTNU). It was made of a circular disc of PZ27 (Ferroperm, Denmark) with diameter 12.7mm and thickness tuned to 3MHz. The disc was equipped with a quarter-wave matching layer at the front with an acoustic impedance of 4.25 Mrayl and speed of sound equal to 2800m/s. The backing of the disk was made of Devenycell, a porous mechanically stiff material with estimated acoustic impedance of 0.4 Mrayl and high losses at 3MHz. This transducer is used as an example when doing the following calculations. The Matlab program transducer1.m can calculate the electrical input impedance, the frequency response from the electrical port to the acoustic front and the companion impulse response using the transmission line model described in Chapter 2.3.

Figure 3.5 shows the electric input impedance of the transducer. The transducer is capacitive, as expected, except around resonance at 3MHz. Between 2 and 4MHz the input impedance has a real component, and power is coupled to the acoustic front.

Figure 3.7 shows the amplitude of the frequency response from the electric port to the acoustic front and Figure 3.8 shows the impulse response of the transducer, found as the inverse Fourier transform of the frequency response. This impulse response is the normal front velocity of the transducer provided that the electric excitation is a Dirac delta function. The center frequency of the transducer is 3MHz and the FWHM-bandwidth is 1.5MHz or 50%. This is in good agreement with the fact that the main part of the pulse is approximately two periods long. The relatively short tail of the pulse is due to the bell-shape of the amplitude response. This pulse is well suited for imaging purposes as it will give a depth resolution of about 1mm, but also contain an adequate amount of energy.

Figure 3.5
Electric input impedance of transducer1

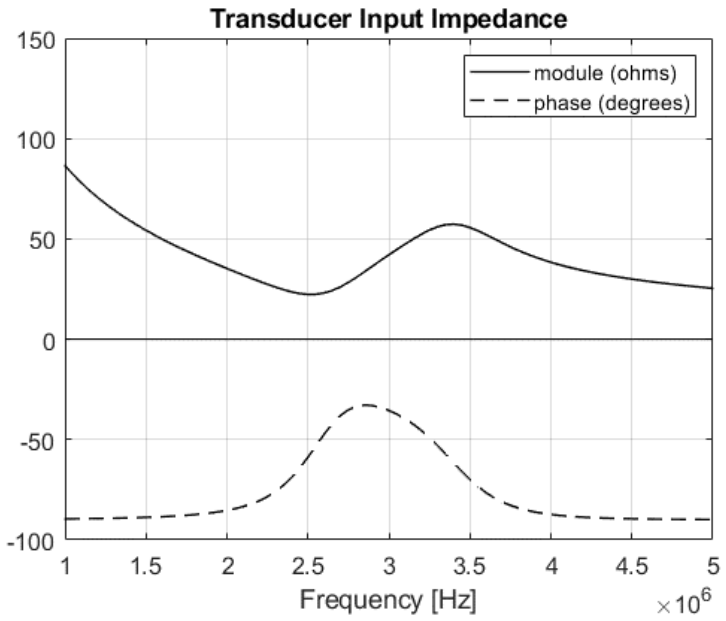

Figure 3.6
Impulse response of transducer 1

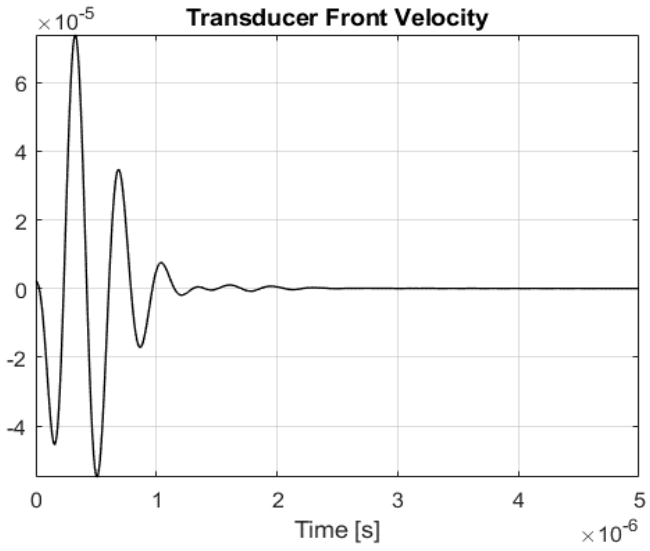

Figure 3.7
Frequency response of transducer 1.

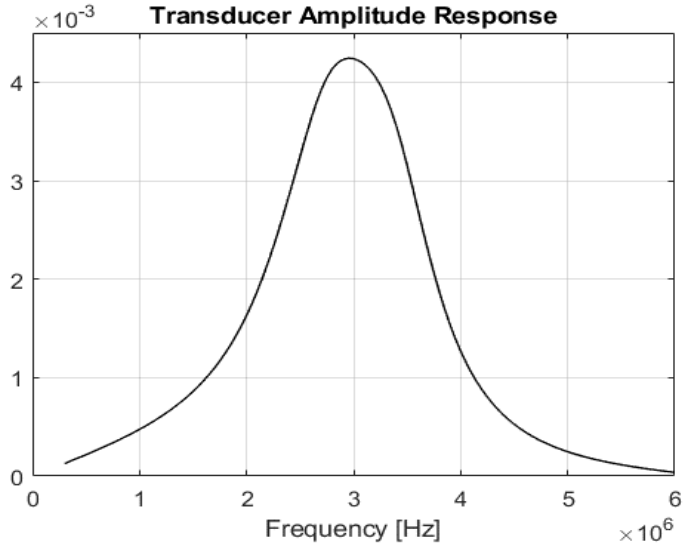

3.3 Calculation of pulsed fields

Figure 3.8
Overview of programs for calculation of pulsed ultrasonic fields.

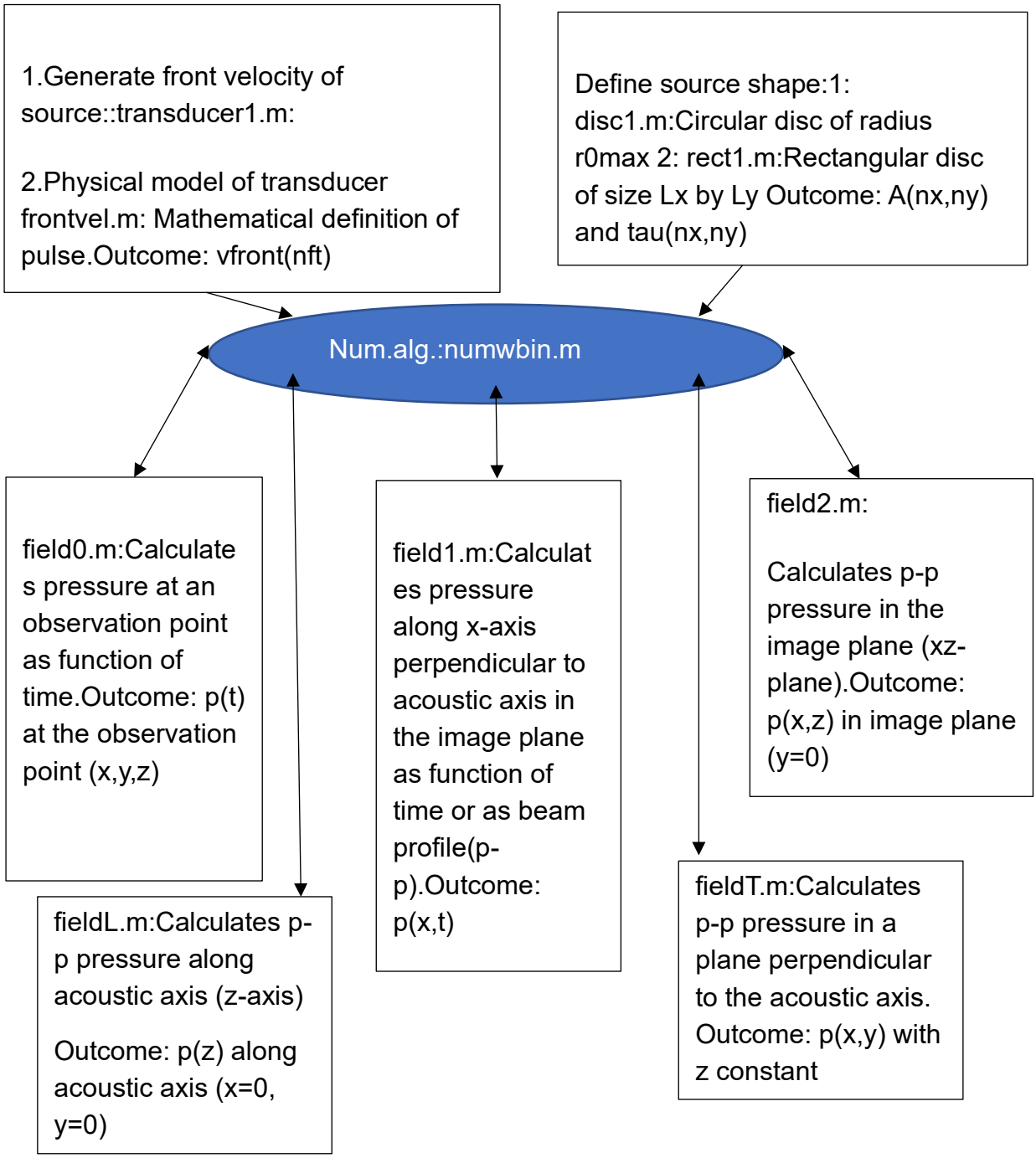

Figure 3.8 shows an overview of the programs used to calculate the pulsed ultrasonic fields. The pulsed fields are calculated for different observation geometries with the different field programs. They all use the same numeric algorithm that is based on weighted binning. But prior to embarking on the field calculation, the source must be defined. The source is defined by the normal velocity on the front of the source and by the shape of the source surface. The normal velocity of the source can be generated by two different programs. The simplest program is frontvel.m. This program is just a mathematical description of a pulse that can be used in the calculations of the fields. A more complex program is transducer1.m. This program is a mathematical model of a thin disc piezo-electric disc. The program calculates the electric input impedance of the transducer, the frequency response from the electric port to the front velocity of the transducer and the corresponding impulse response of the transducer. This impulse response is used as the front velocity in the calculations. This require that the transducer is excited with an impulse at the electric port. The pulse is shown in Figure 3.6.

The shape of the source front must also be defined before calculating the field. In medical ultrasound, two different shapes are in regular use. These are circular disc transducers and rectangular transducers as phased arrays or linear arrays. A circular disc transducer can be defined with the program disc1.m. The inputs to this program are the diameter of the disc and the focal length of the disc. Figure 3.10 shows the source function time-delay of a disc with diameter 12.7mm and focal length 75mm. The amplitude is planar, see Figure 3.9 because there is no apodization and the time delay is parabolic with focus in the focal point. The source elements are 0.1mm by 0.1mm. This size of the elements is considered small enough as the wavelength at 3MHz is 0.5mm.

A rectangular transducer can be defined with the program rect1.m. The inputs to this program are the length and the width of the transducer front as well as the focal length in azimuth, Fx, and elevation, Fy.

When the source is properly defined, the field calculations can start. The parameters and the results from the source definition programs must be stored in the working space of MATLAB. The pressure field is a function of the observation coordinates, (x, y, z), as well as time, p (x, y, z, t). To present the calculations, the 4-dimensional function is simplified by calculating the field along characteristic axis and planes. The time dimension is in most calculations reduced to a peak-peak value of the pressure. The spatial axes are standardized, so that the z-axis is the acoustic axis starting at

the center of the source and the x-axis is defining the image plane, so that the xz-plane is the assumed image plane of a 2D-ultrasound scanner.

The program field0.m calculates the pressure field in a single observation point as function of time, p(t). Figure 3.11 shows the pressure pulse at the focal point for a circular disc with diameter 12.7mm and focal length 75mm.

The program field1.m calculates the pressure field along the x-axis at a given z-position. The field is presented as a pulse in space as a function of time or as a beam profile. Figure 3.12 shows the pressure pulse as a function of time and distance from the acoustic axis. At the acoustic axis we can see the pulse shape as function of time like the plot in Figure 3.11. Distal from the axis we can see the characteristic center wave followed by the edge wave. Figure 3.13 shows the beam profile at depth 100mm as function of distance from the axis. The solid curve shows the peak-peak pressure where the time dimension is reduced to the difference between the maximum and the minimum pressure. The dashed curve represents the pulse energy integrated over time.

Figure 3.9
The source amplitude of a circular disc of diameter 12.7mm.

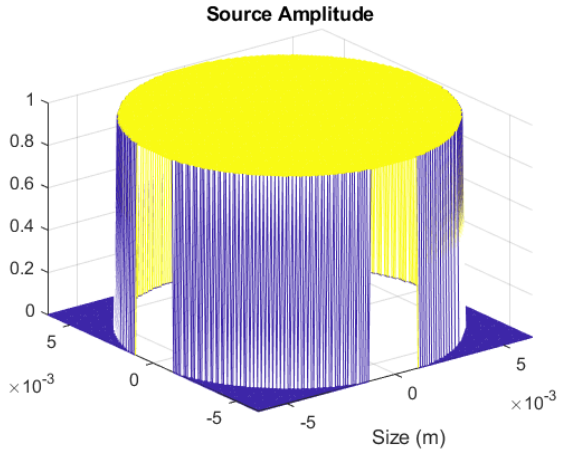

Figure 3.10
The source time delay of a circular disc of diameter 12.7mm and a focal length of 75mm.

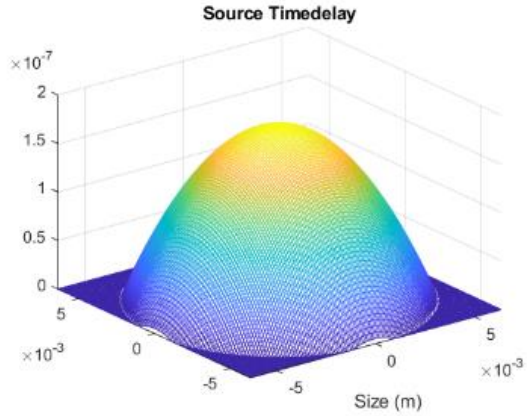

Figure 3.11
Pressure pulse at focus of the circular disc described above.

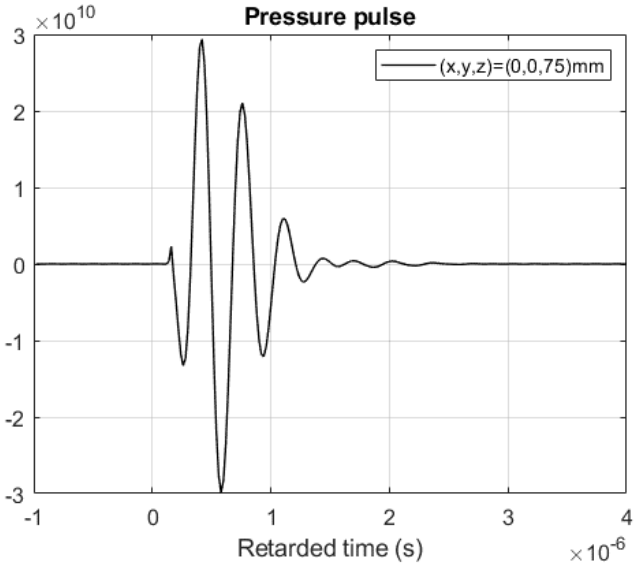

Figure 3.12
Pressure pulse at distance 100mm as a function of time and distance from the axis.

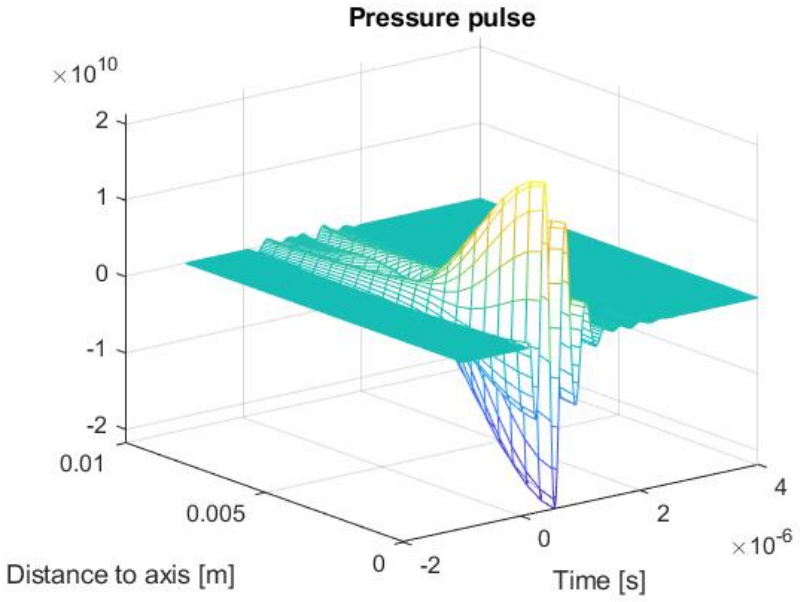

Figure 3.13
Beam profile at depth 100mm as function of distance from the axis.

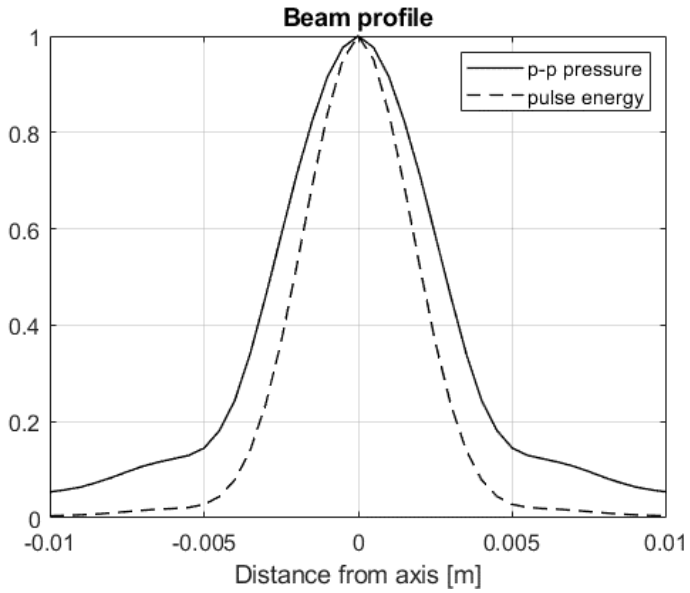

The program field2.m calculates the peak-peak pressure in the image plane, p (x, z). Figure 3.14 shows the peak pressure beam in the image plane, z is the image depth and x is the distance from acoustic axis. Figure 3.15 shows a contour plot of the same beam as in Figure 3.14. The distance between the contours are 3dB. The 0dB

point is at depth z = 50mm and x = 0. Figure 3.16 shows the contour plot when the beam profiles are normalized at each depth of the same beam as in both Figure 3.14 and Figure 3.15.

Figure 3.14
Peak pressure beam in the image plane (x, z).

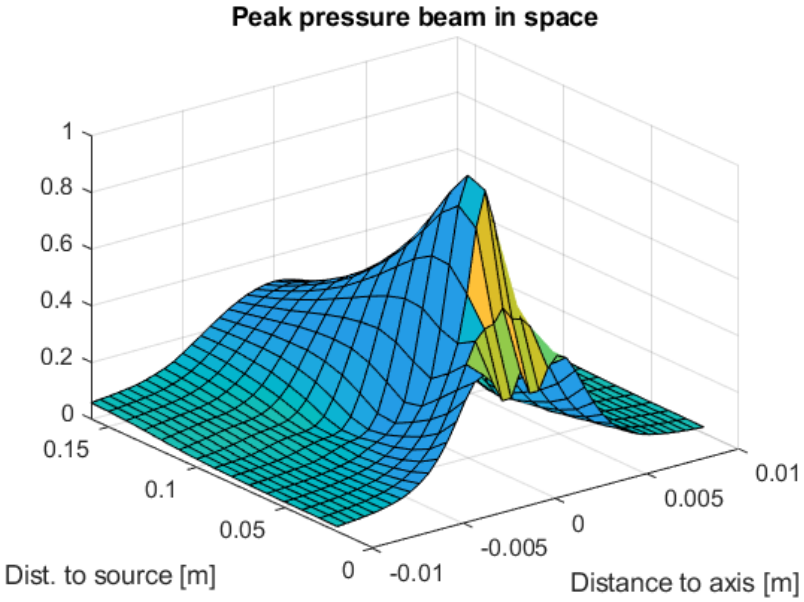

Figure 3.15
Contour plot of peak pressure beam in image plane. The contours are 3dB apart. Starting at 0dB at (x, z) = (0, 50mm) and ending at -30dB.

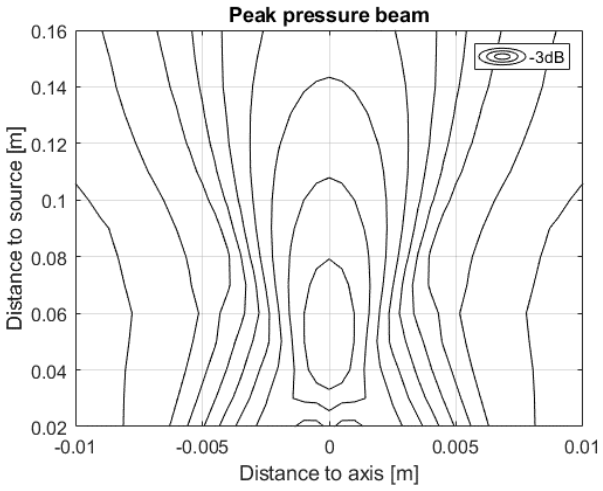

Figure 3.16
Contour plot of peak pressure beam in image plane. The beam profiles are normalized at each depth.

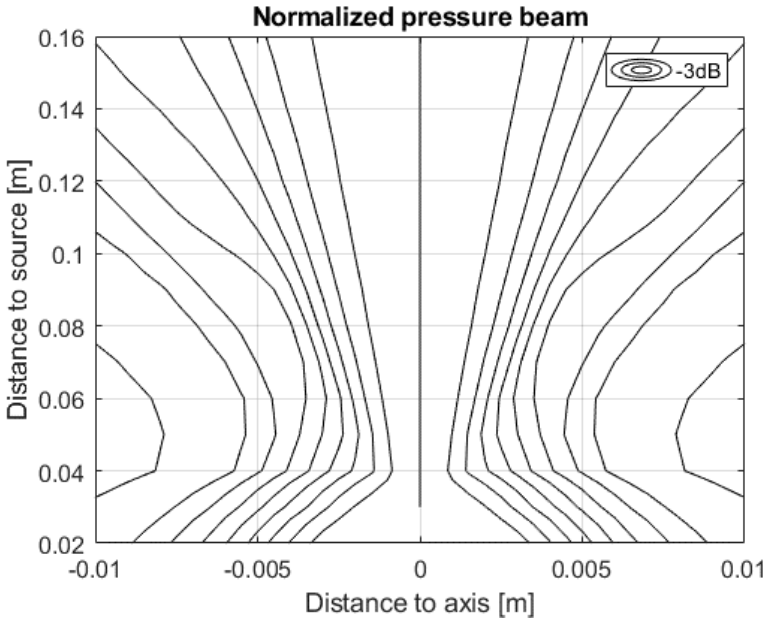

The program fieldL.m calculates the peak pressure field along the acoustic axis, p(z). Figure 3.17 shows the peak pressure along the acoustic axis also referred to as the z-axis. These calculations show us at what depth the highest pressure occurs. The transducer in these calculations is focused at 75mm. Diffraction causes the beam waist to be closer to the source. A planar source will have a beam waist at a distance a^2/λ, where λ is the wavelength and a is the radius of the source. In the calculations we have used a radius of 6.35mm and the wavelength of the center frequency is 0.5mm. The distance to the beam waist of the planar source is therefore 80mm. If we use inverse addition of 75mm and 80mm, we get 40mm, which is close to the maximum of the plot in Figure 3.17.

Finally, the program fieldT.m calculates the pressure field transversal to the acoustic axis at a given depth, p (x, y). This is to accommodate the rectangular shaped sources, for circular sources the transversal field will have circular symmetry. To demonstrate this program, we simulate a rectangular transducer with dimension 20mm in the x-direction by 10mm in the y-direction and give it a focus of 75mm in the image plan (x-direction) and no focus in the y-direction (elevation). We apply the

rect1.m program to generate the source function. For completeness we will also generate the front velocity function with the program frontvel.m. Figure 3.18 shows the front velocity and Figure 3.19 its spectrum. The simulated pulse is a tree-period Hanning weighted pulse with center frequency of 3MHz. The pulse is like the calculated pulse of the circular transducer shown in Figure 3.6. Figure 3.20 shows the amplitude and Figure 3.21 the time delay of the rectangular source with focal length 75mm in the image plan. Figure 3.22 shows the peak pressure transvers to the acoustic axis at depth 75mm which is at the same depth as the focus in the image plane. Figure 3.23 shows the contour plot of the peak pressure at depth 75mm.

Figure 3.17
Peak pressure along the acoustic axis (z – axis).

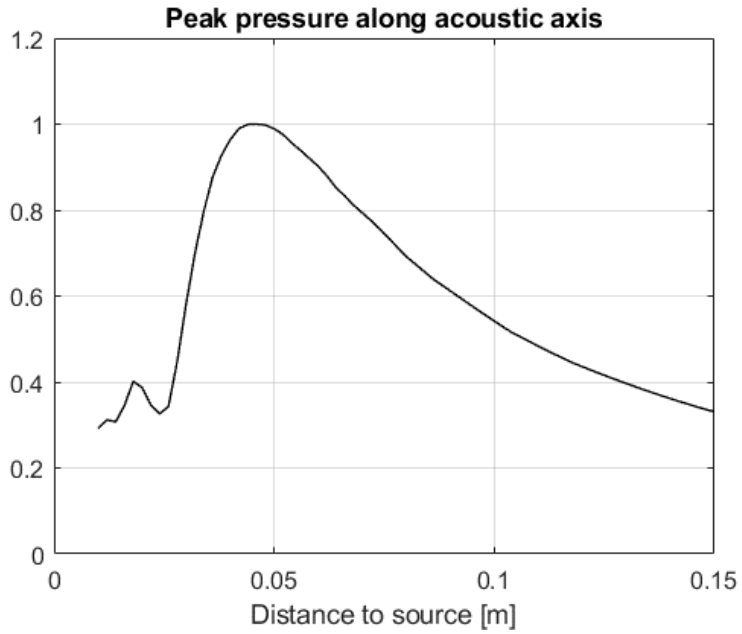

Figure 3.18
Front velocity pulse of the rectangular transducer.

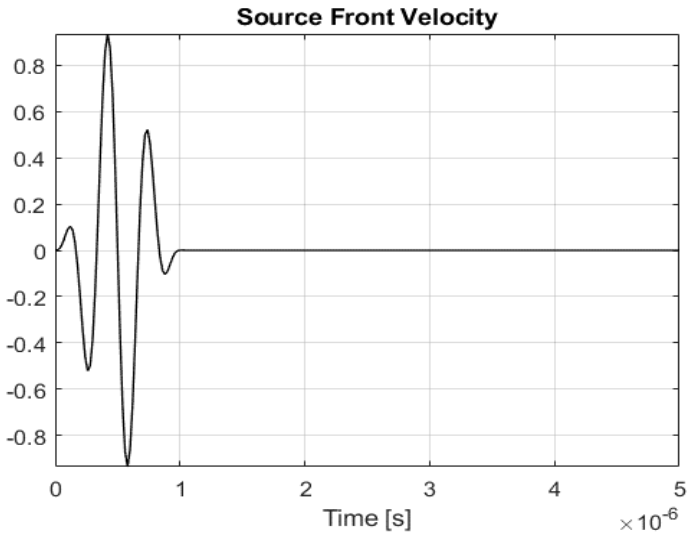

Figure 3.19
Front velocity spectrum of the rectangular transducer.

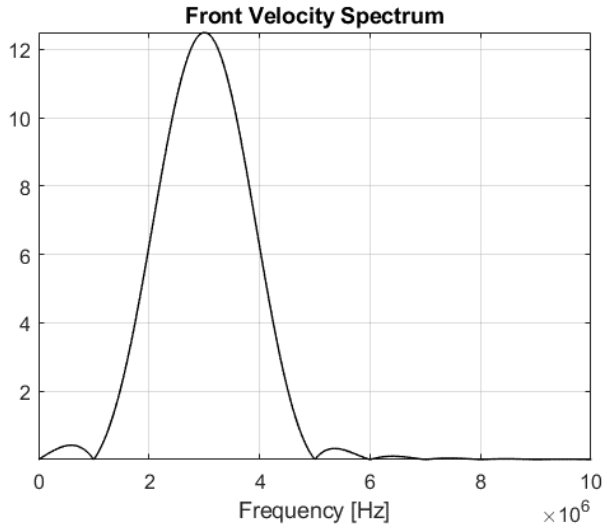

Figure 3.20
Source amplitude of the rectangular transducer.

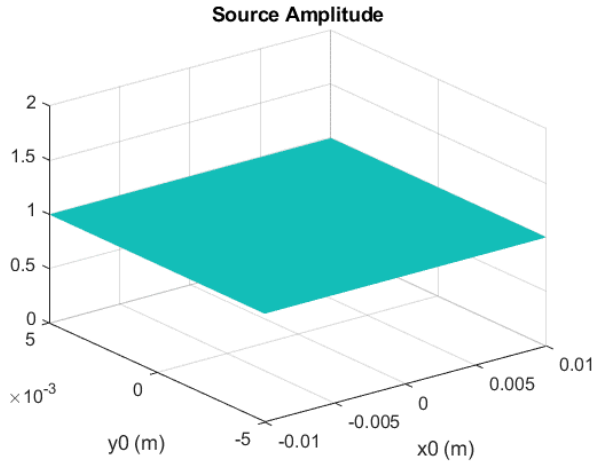

Figure 3.21
The source time delay of the rectangular transducer (20 x 10mm).

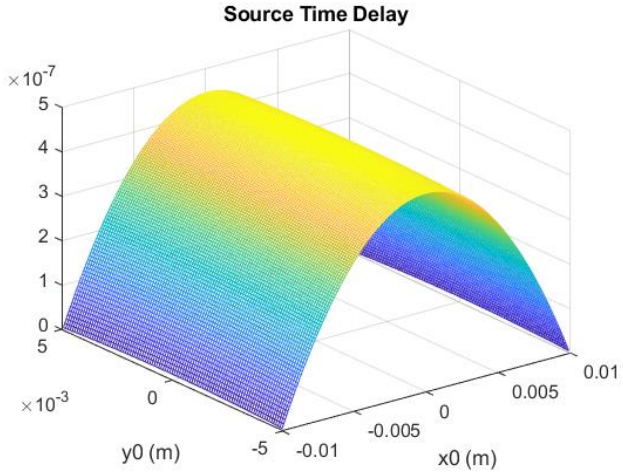

Figure 3.22
Transvers pressure beam orthogonal to the acoustic axis at depth 75mm.

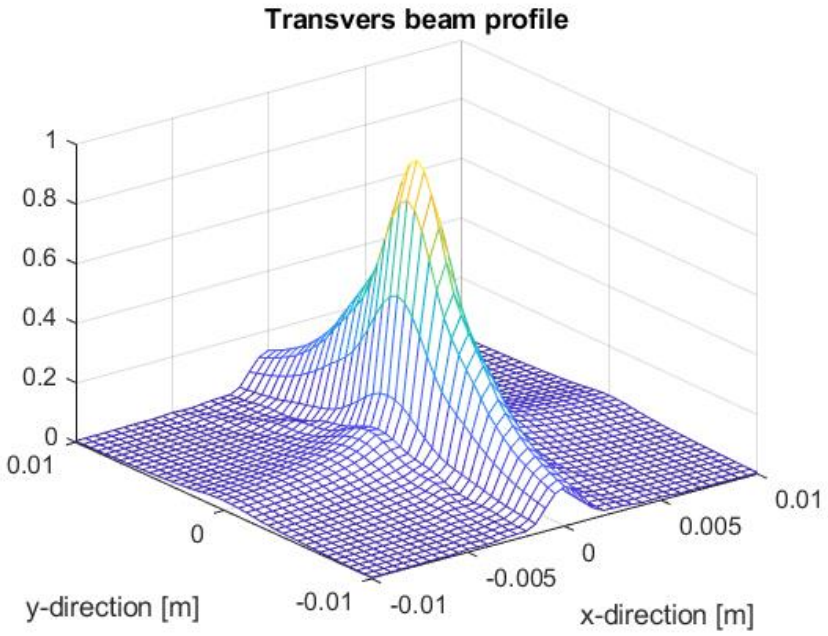

Figure 3.23
Contour plot of the transvers pressure of the rectangular transducer at depth 75mm.

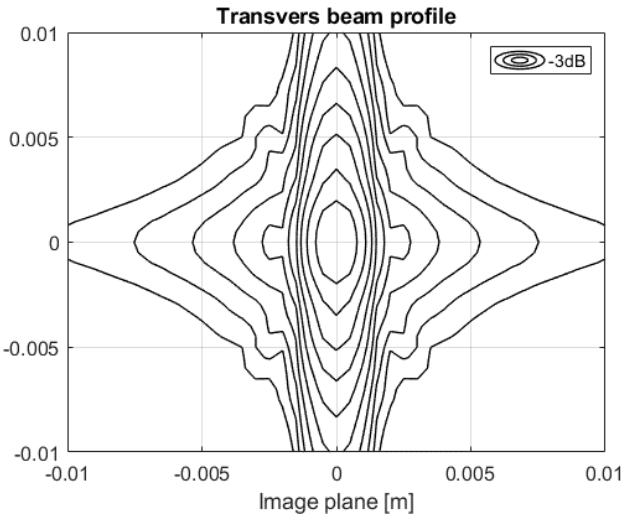

4 Measurements

4.1 The Experiment set-up

Figure 4.1
Measurement set-up

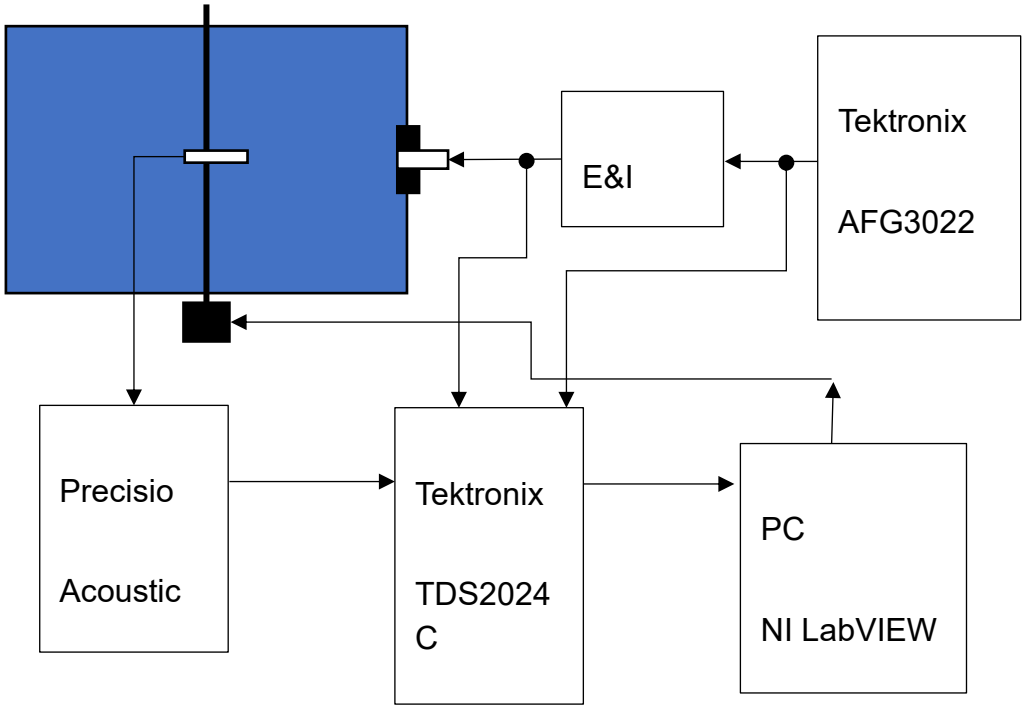

Figure 4.1 shows the experimental set-up. The water tank measures 30cm by 30cm by 55cm. The hydrophone is placed in the tank by a hydrophone holder that is attached to a manual three-dimensional positioning mechanism. This mechanism is attached to a sledge for automatic one-dimensional scanning, driven by a step motor. The hydrophone is a 0.5mm PVDF needle hydrophone from Precision Acoustics Ltd. (Dorchester, UK). It comes with a pre-amplifier and a power supply. The hydrophone including the pre-amplifier is calibrated over a bandwidth of 1-20MHz and the sensitivity is around 200mV/MPa. A Tektronix Digital Storage Oscilloscope, TDS2024C, captures the signal from the pre-amplifier. A PC with National Instrument LabVIEW software read the data from the oscilloscope and

present the waveform together with the frequency spectrum on the screen. The data can be exported from LabVIEW as an Excel-file or as a bitmap image.

The transducer is mechanically attached to an acoustic window in a short side of the tank. The excitation signal to the transducer is generated by an arbitrary function generator from Tektronix, AFG3022B. A power RF-amplifier from E&I (Electronics & Innovation Ltd., Rochester, NY, USA) Model A075 amplifies the signal. The PC controls the step motor through a National Instruments USB-6008. The tank system can also perform an automatic beam profile scan, driven by a LabView program.

4.2 Measurements of transducer1

Transducer1 is a transducer made of a planar circular disc of Pz27 (Ferroperm, Denmark) with a quarter wave matching and a light backing. The diameter of the disc is 12.7mm. The transducer was described in chapter 2.3, where also the impulse response and amplitude response were calculated. To measure the impulse response of a transducer, we will need an impulse as input signal. No signal generator can produce a pulse that is infinitely short and has infinite amplitude, but the signal generator can produce a pulse good enough for the purpose. Figure 4.2 shows a generator pulse with half maximum of 40ns and Figure 4.3 its frequency spectrum. The -3dB frequency of the spectrum is at 9MHz. The pressure pulse must be measured in the focal point where the SIR is a delta function. A lens with focal length of 75mm was attached to the transducer and the measurements ware done at distance 75mm on the acoustic axis. Figure 4.4 shows the impulse response and Figure 4.5 the frequency response of transducer1 when excited with the 40ns pulse. The amplitude spectrum shows that the transducer also has a resonance 10MHz. This is the resonance where the piezo-electric disc is one and a half wavelength thick. To avoid the excitation of this third harmonic mode of the transducer, we can excite the transducer with a rectangular pulse of length 100ns because a 100ns pulse will have a frequency spectrum with a zero at 10MHz. Figure 4.6 shows the pulse response and Figure 4.7 shows the amplitude response of the transducer when excited with the 100ns pulse. The resonance at 10MHz is gone while the resonance at 3MHz is preserved. The resulting pressure pulse is a good imaging pulse and in good agreement with the simulation of the impulse response in Figure 3.6. The impulse response calculated in Figure 3.6 is the normal front velocity of the transducer. We cannot measure this directly, but the pressure pulse in the focal point of the transducer is the time derivative of the velocity potential, which is the convolution of the spatial impulse response, the excitation pulse and the front velocity. If both the spatial impulse response and the excitation pulse are relatively

short compared to the front velocity, the pressure pulse will be the time derivative of the front velocity. The pressure pulse can under the above-mentioned conditions serve as a measure of the impulse response of the transducer except for a 90-degree phase shift.

Figure 4.2
The impulse used as input signal for measurement of the impulse response.

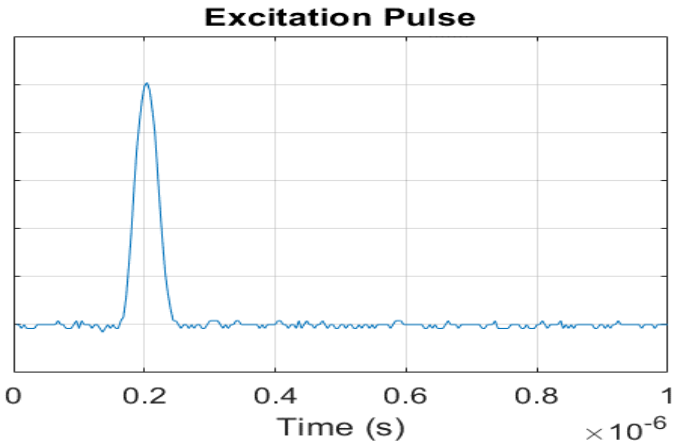

Figure 4.3
The frequency spectrum of the above impulse.

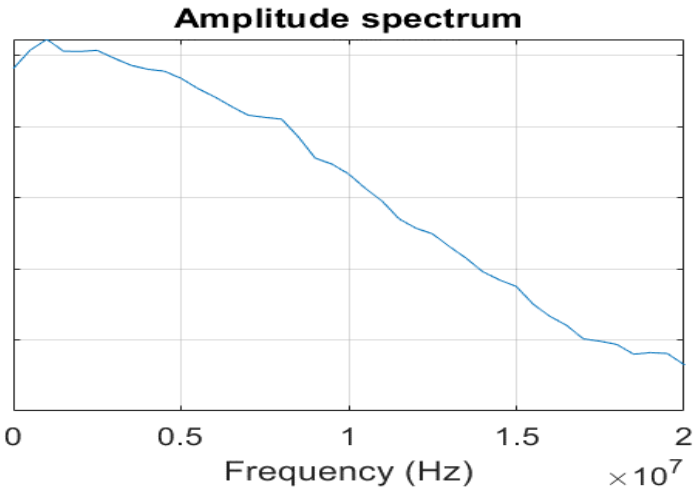

Figure 4.4
Impulse response of transducer 1.

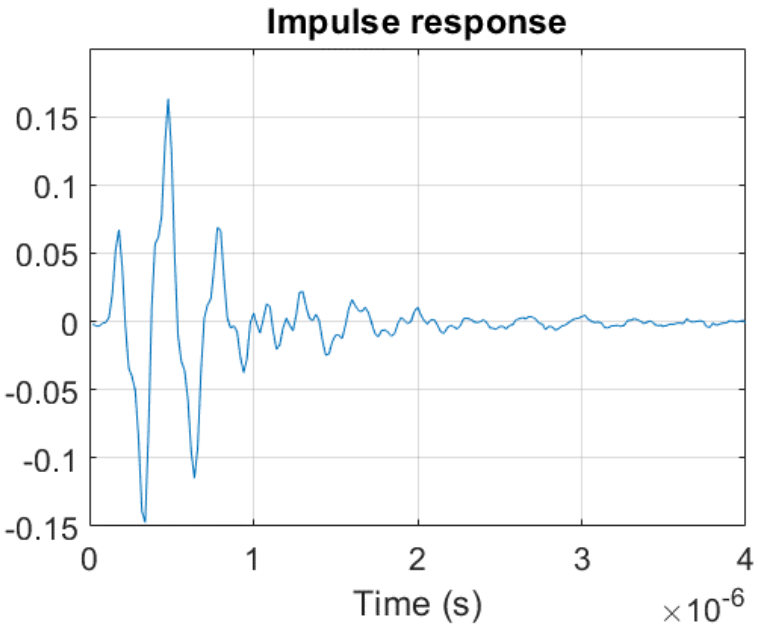

Figure 4.5
Frequency response of transducer 1 excited with the 40ns-pulse.

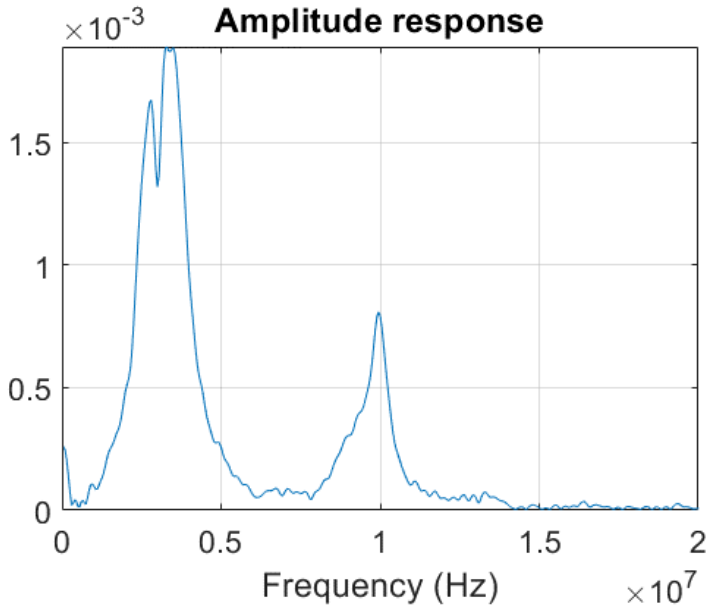

Figure 4.6
The on-axis pressure pulse of transducer1when excited with the 100ns-pulse

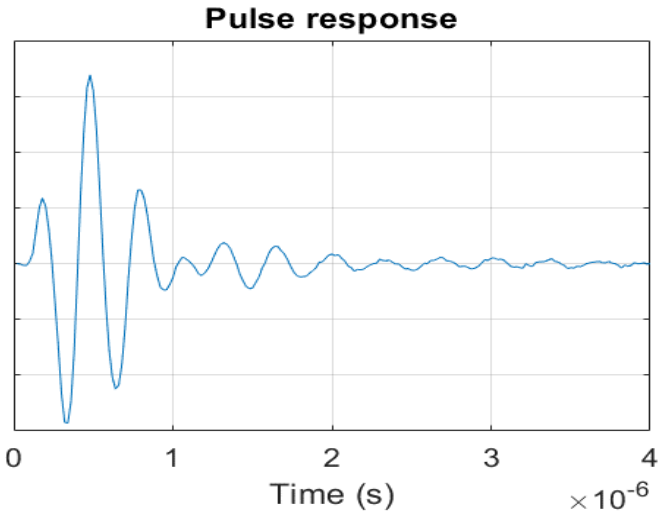

Figure 4.7
The frequency spectrum of the above pulse.

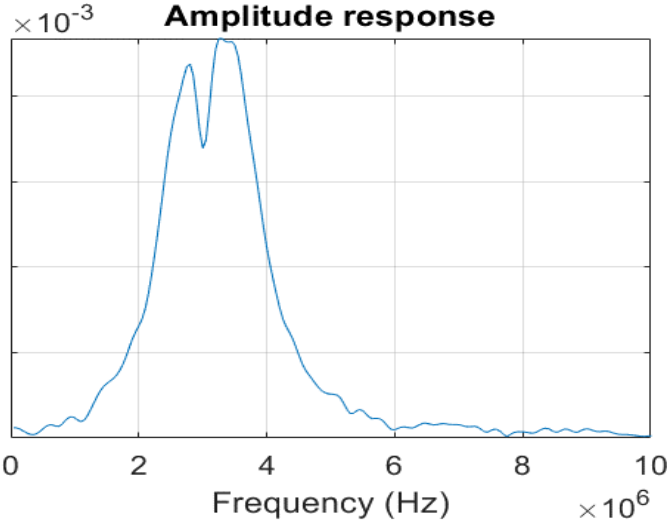

The pressure pulse length determines the depth resolution in ultrasound imaging. The beam width determines the transvers resolution. In the water tank we can measure the beam profile of the transducer and compare it with the calculated beam profile using field1.m.

Figure 4.9 through Figure 4.19 shows the calculated and measured beam profiles at z = 20, 30, 50, 70, 100, and 150mm of transducer1 with a planar front or infinite focal length. The solid curves are peak-peak pressure, and the dashed curves are pulse energy. The calculations shows that the beam is at its narrowest between 70 and

100mm. Also, the measurements show that the beam is at its narrowest between 70 and 100mm.The dashed curves representing the pulse energy calculation and measurements are somewhat narrower than the peak-peak beam profiles (solid lines). However, the peak-peak beam profiles are the most used way of calculating beam width and we will therefore use these values. The depth at which the beam is at its narrowest is called the beam waist. The beam waist is found at depth $z = a^2/\lambda$, where a is the radius of the transducer and λ is the wavelength. For transducer1 this gives z = 80mm. However, even at beam waist the half value diameter of the beam is about 7mm measured by the peak-peak value and about 4mm measured by the pulse energy. The agreement between the calculations and measurements are good in the far field, beyond beam waist. In the near field there are some differences probably caused by that the transducer doesn't vibrate entirely as a piston. A noticeable feature of the measured beam profiles is their lack of symmetry. This must be due to the production of the transducer. Firstly, leads must be soldered to the electrodes at some point and secondly, the disc is glued to a porous backing and the support may not be equal over the disc area. This leads to asymmetries in the measurements as can be seen in Figure 4.9 and Figure 4.11.

Figure 4.8
Non-focused calculated beam profiles at depth z=20mm

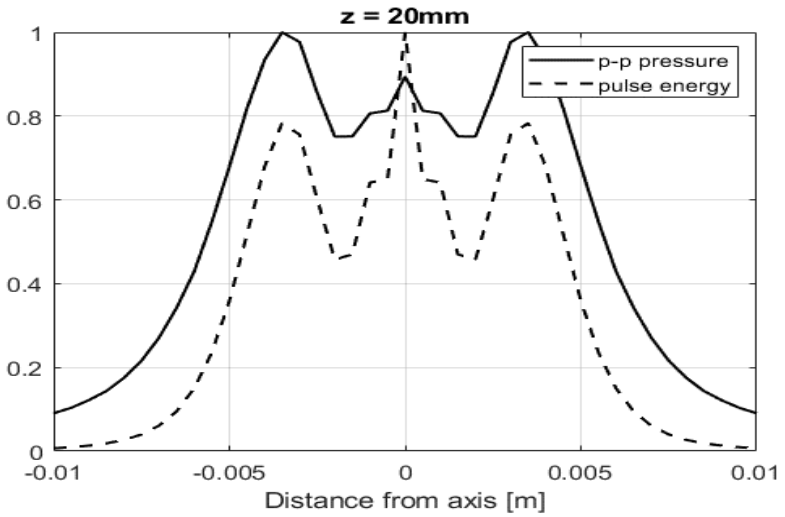

Figure 4.9
Measured beam profiles at depth z=20mm.

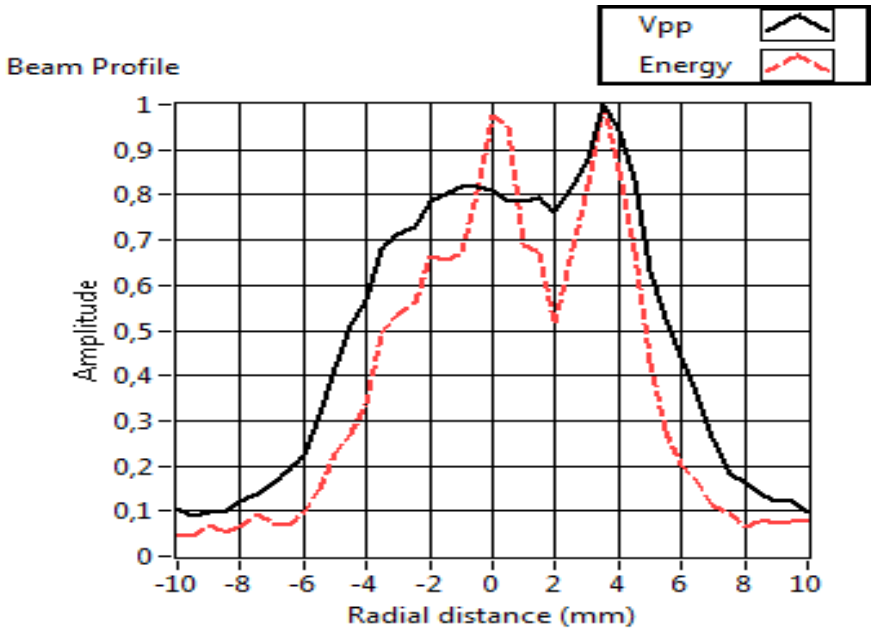

Figure 4.10
Calculated beam profile at depth z=30mm.

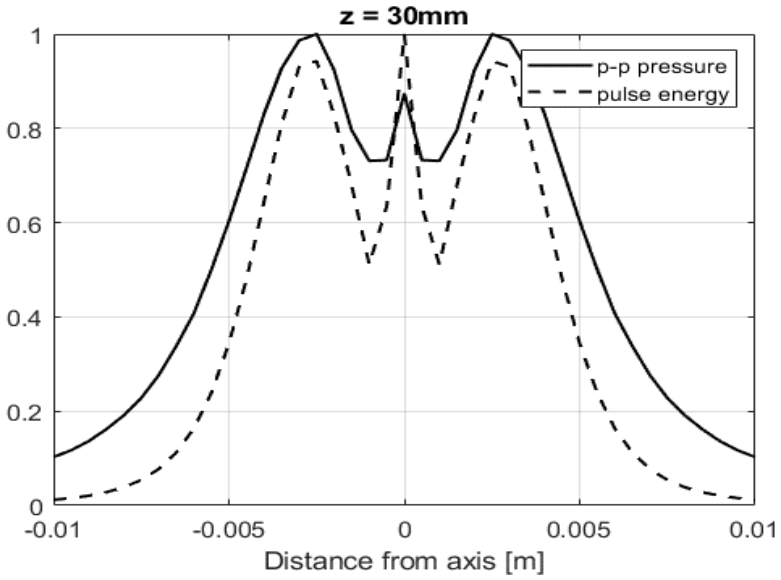

Figure 4.11
Measured beam profile at depth z=30mm

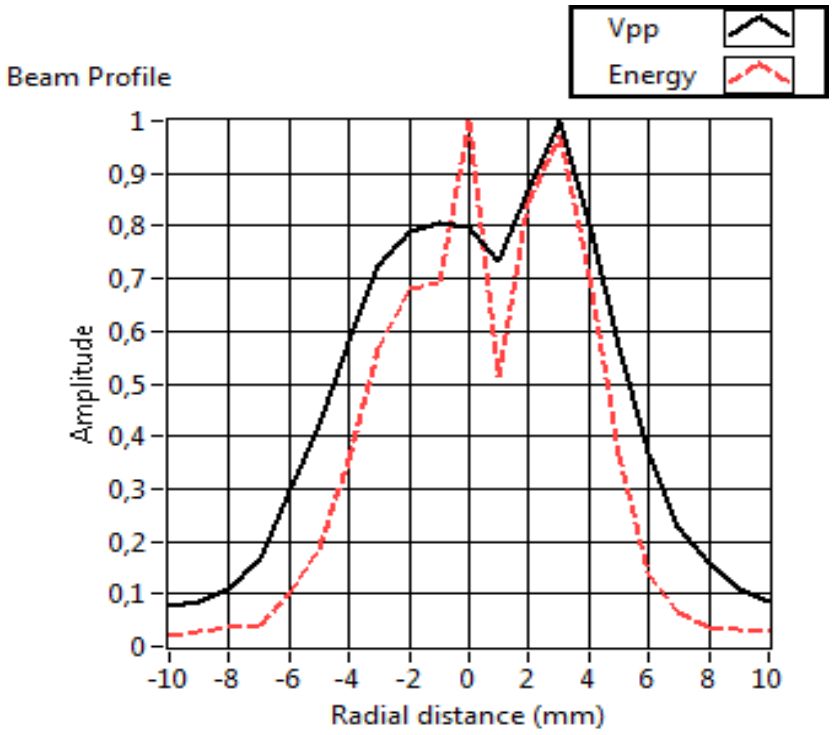

Figure 4.12
Calculated beam profile at z=50mm.

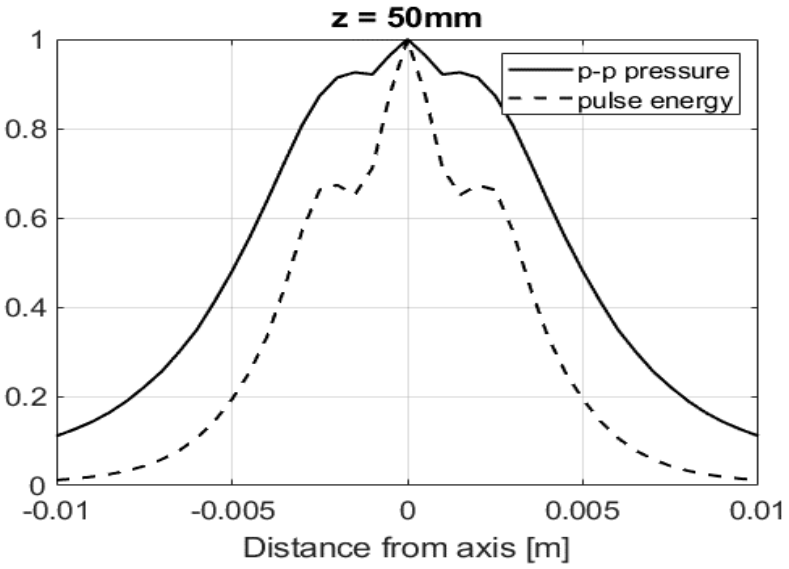

Figure 4.13
Measured beam profile at z=50mm.

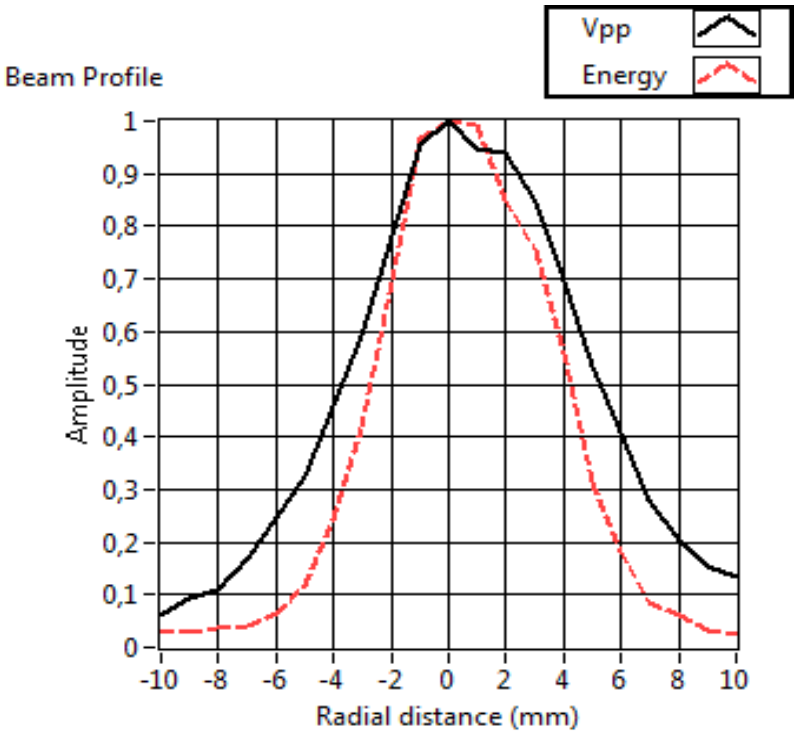

Figure 4.14
Calculated beamprofile at z=70mm.

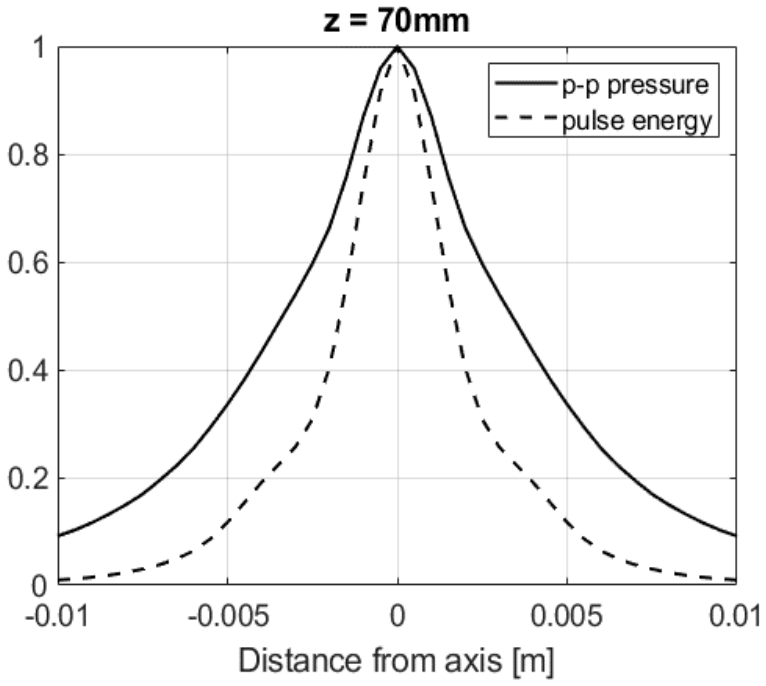

Figure 4.15
Measured beamprofile at 70mm.

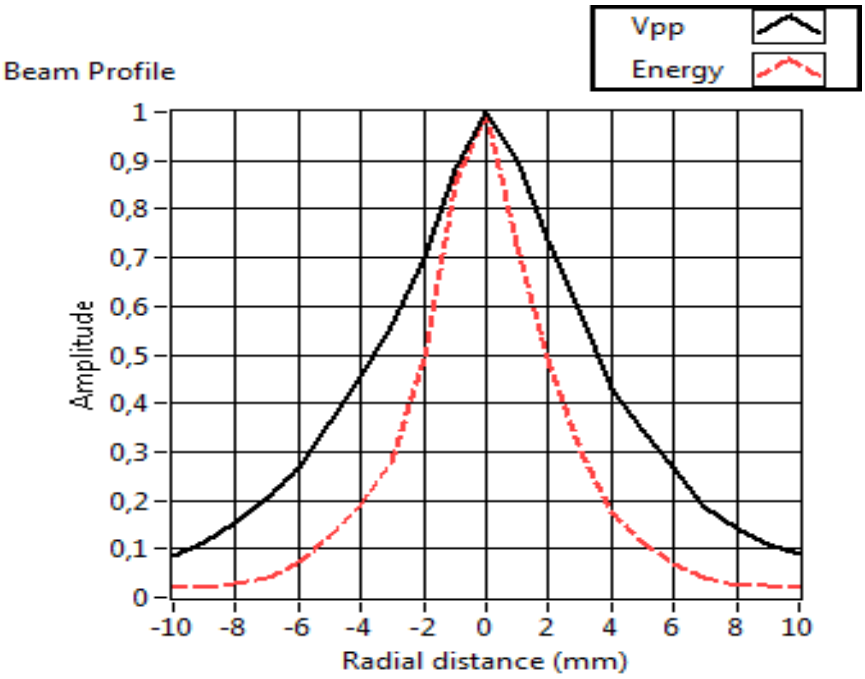

Figure 4.16
Calculated beamprofile at 100mm.

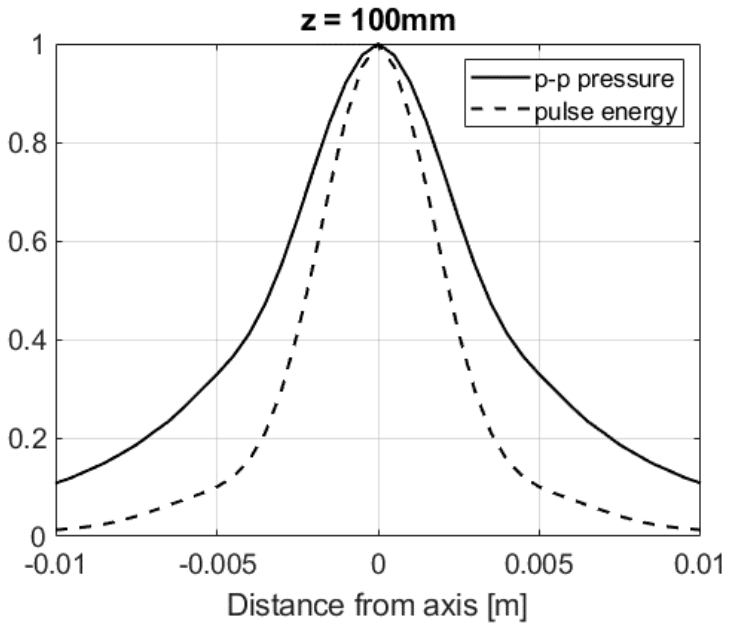

Figure 4.17
Measured beamprofile at 100mm.

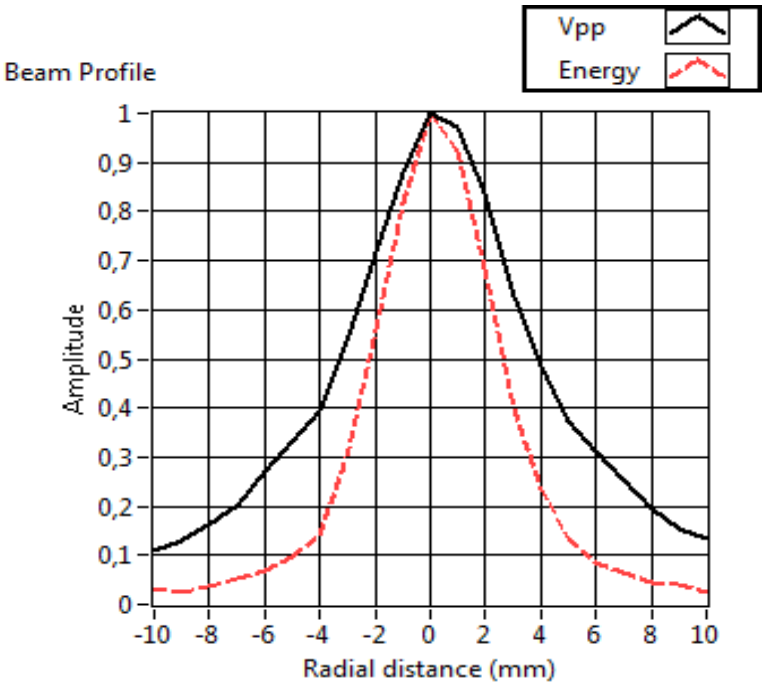

Figure 4.18
Calculated beam profile at 150mm.

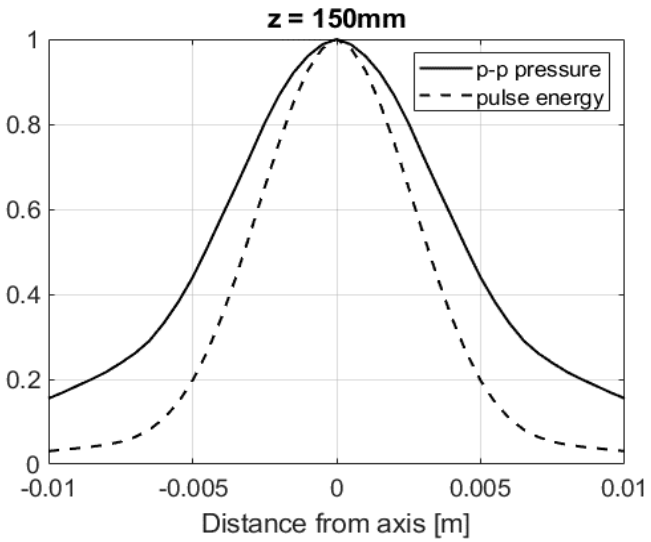

Figure 4.19
Measured beam profile at z=150mm.

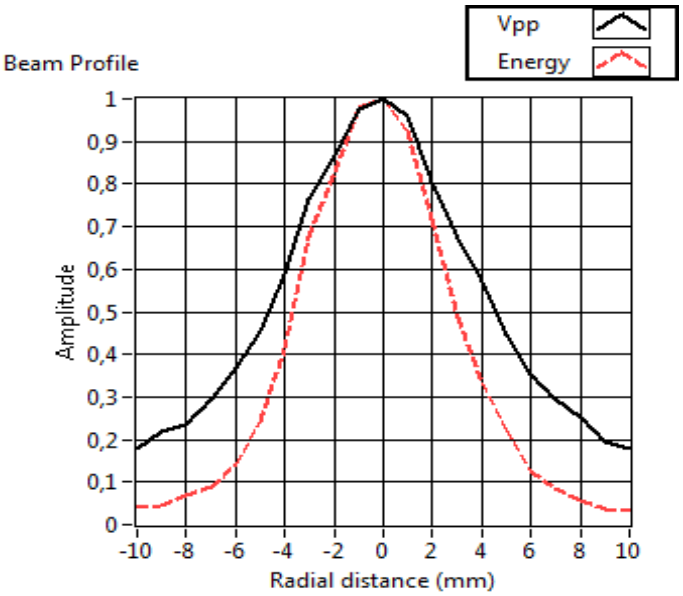

Figure 4.20
Beam profiles focused at 75mm at depth 20mm

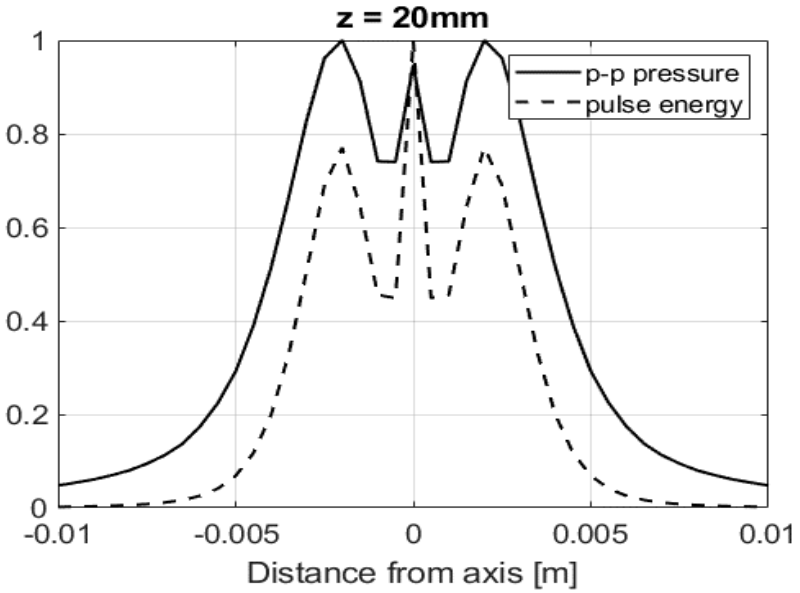

Figure 4.21
Measured beamprofile at z=20mm.

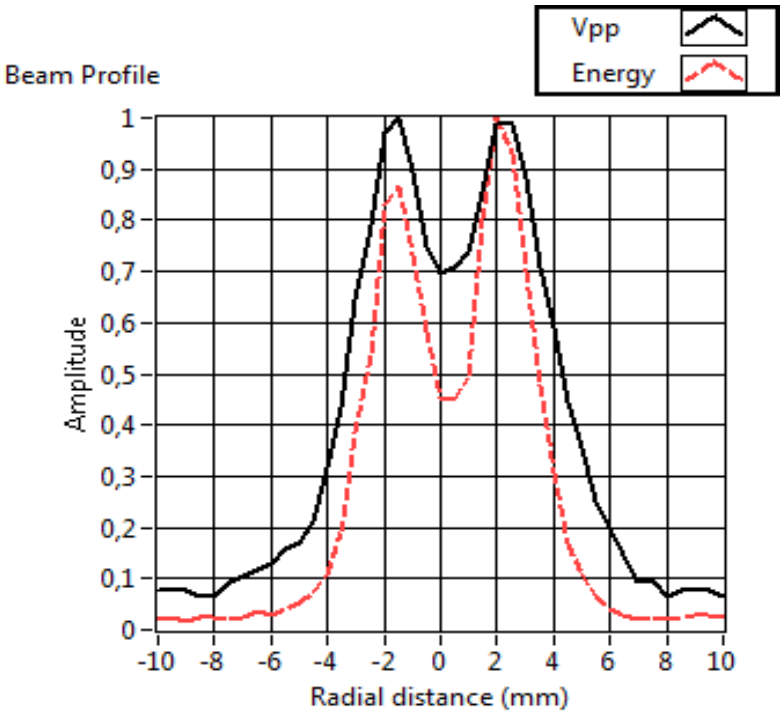

Figure 4.22
Calculated beam profile at z=30mm.

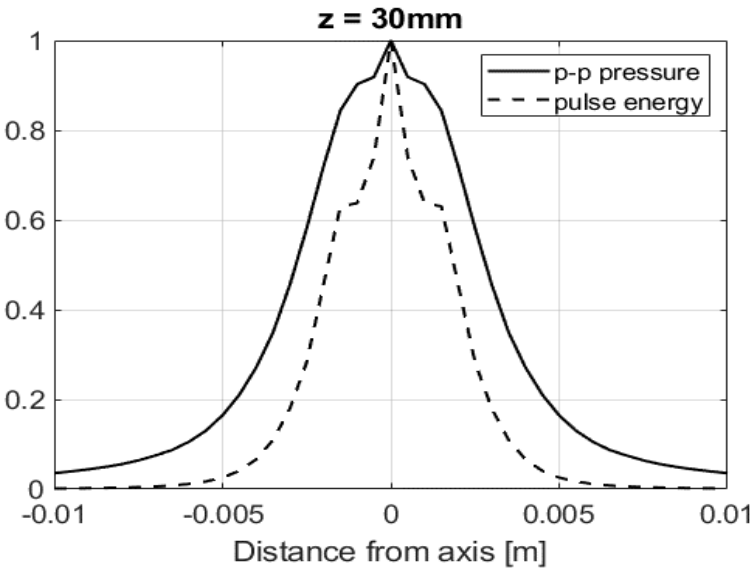

Figure 4.23
Measured beam profile at z=30mm.

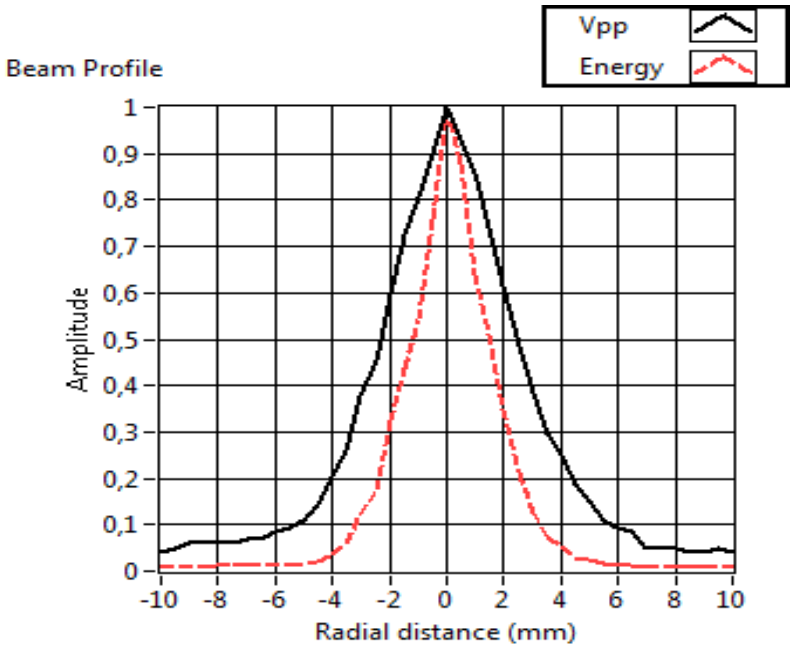

Figure 4.24
Calculated beam profile at z=50mm.

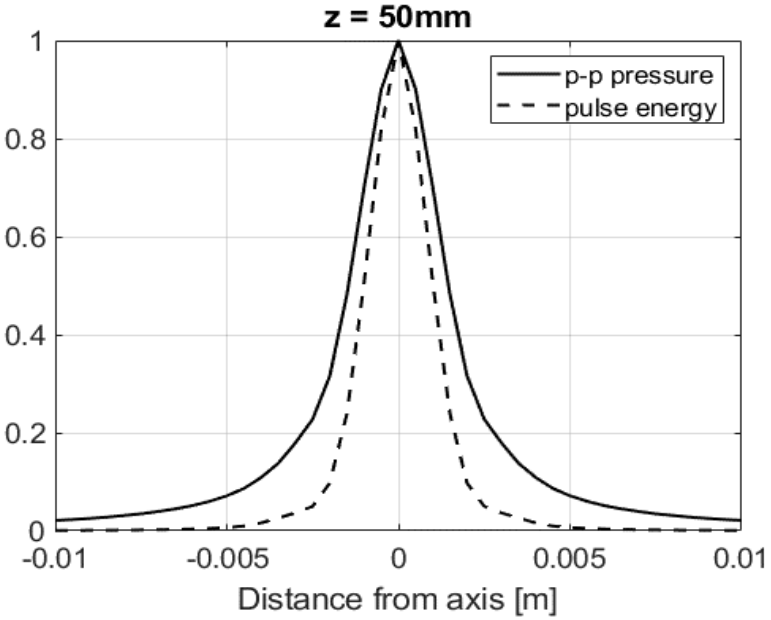

Figure 4.25
Measured beam profile at z=50mm.

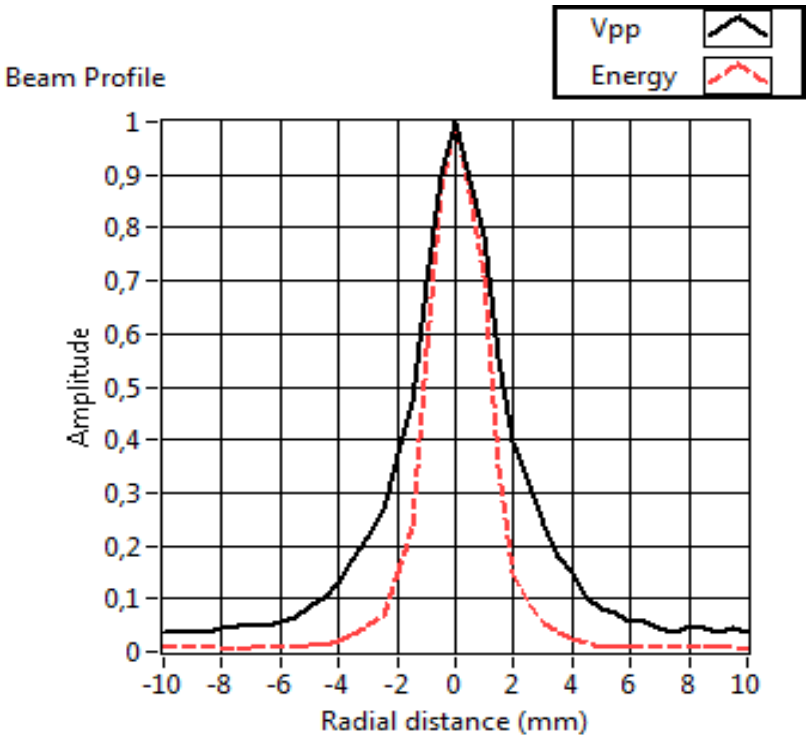

Figure 4.26
Calculated beam profile at z=70mm.

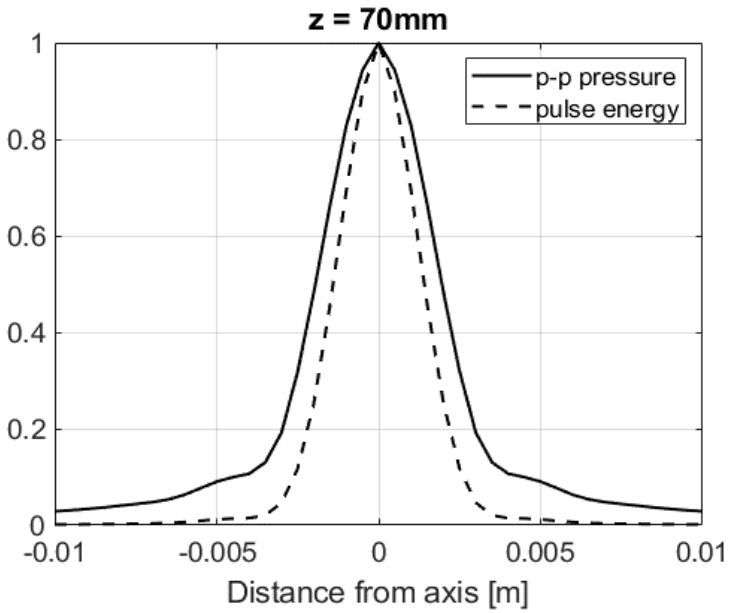

Figure 4.27
Measured beam profile at z=70mm.

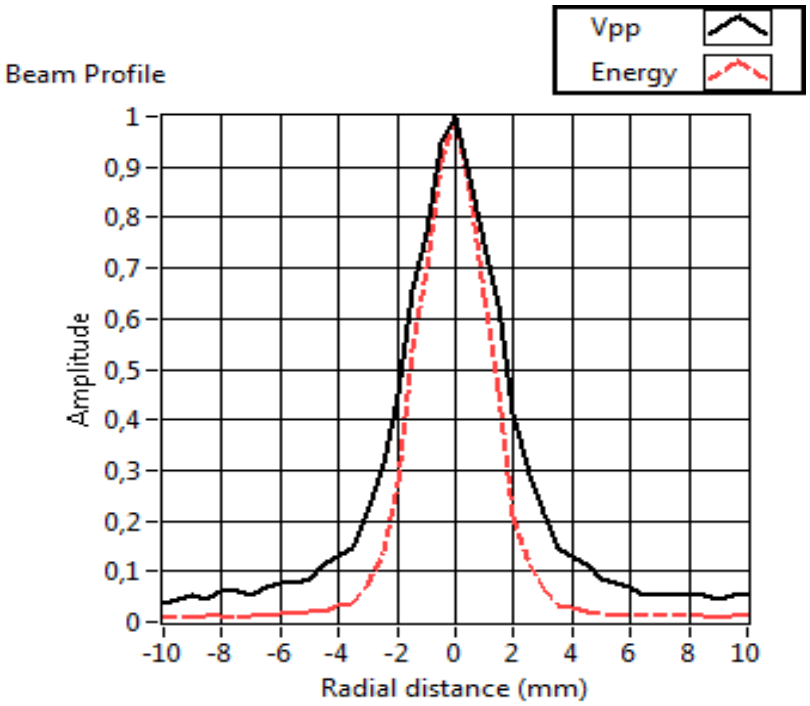

Figure 4.28
Calculated beam profile at z=100mm

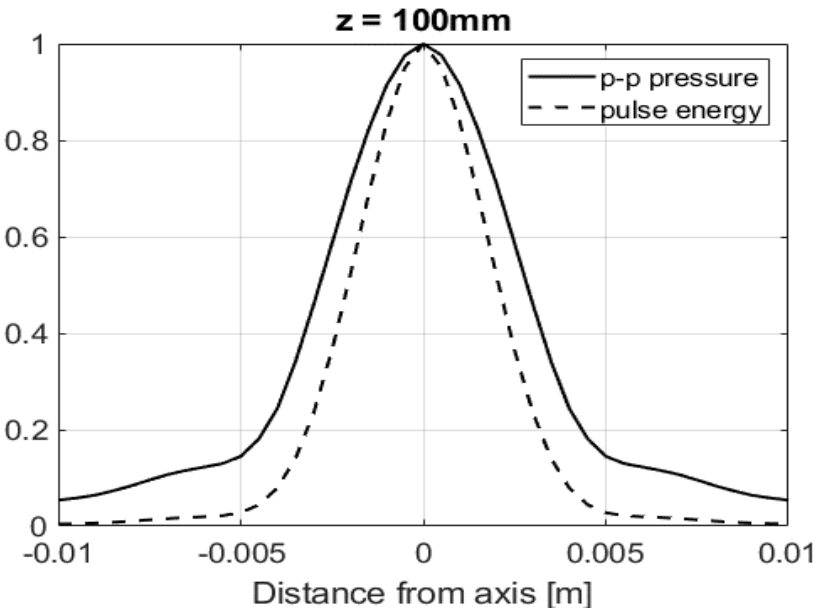

Figure 4.29
Measured beam profile at z=100mm.

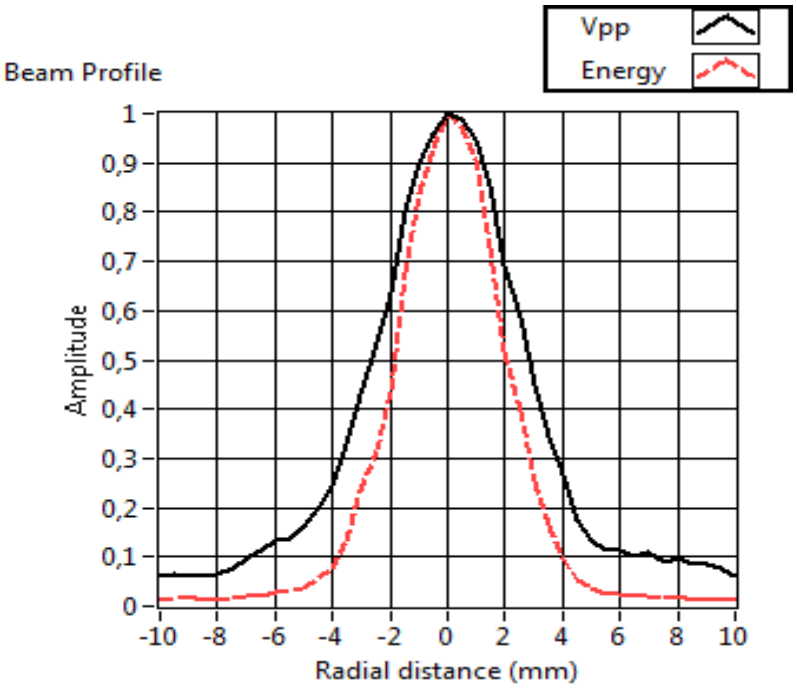

Figure 4.30
Calculated beam profile at z=150mm.

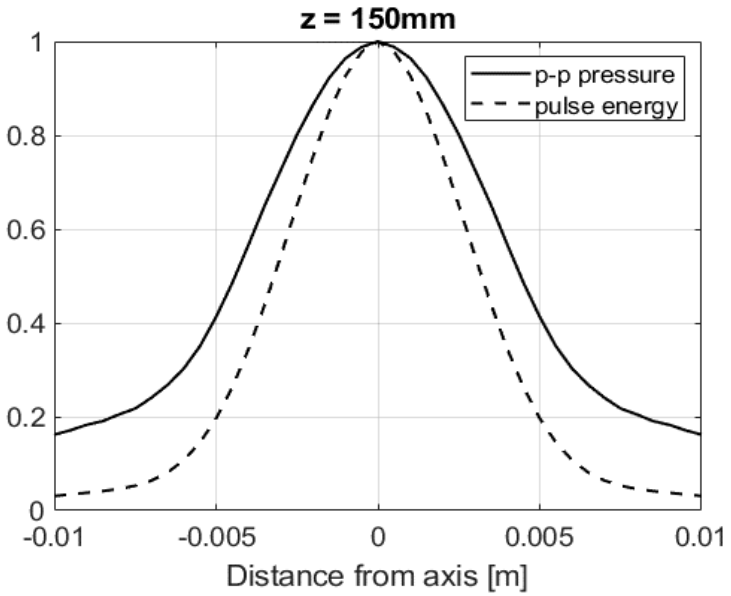

Figure 4.31
Measured beam profile at z=150mm.

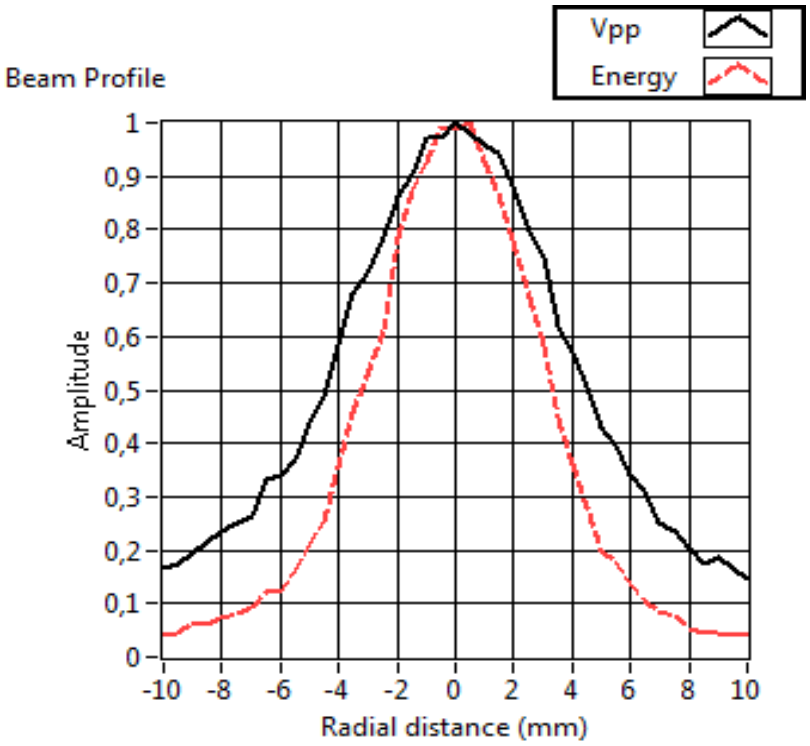

This is a beam with an unacceptable transversal resolution for imaging purposes. To improve the transversal resolution, we will need a lens to focus the transducer. A good lens materiel is silicon rubber because it has a speed of sound less than water and we can design concave/planar lens that is easy to mount on the front of a planar disc transducer. Elastosil 601 (Wacker, USA) was available, and the speed of sound was measured to be about 1000m/s. The refractive index is therefore n = 1.5, and the curvature of the concave face should have a radius of f/2 based on simple geometric optics. For imaging depths up to 150mm a good choice of focal length should be f = 75mm and the curvature radius should be 37mm. A molding form was made, and the produced lens was attached to the transducer without problems.

Figure 4.20 through Figure 4.31 shows calculated and measured beam profiles of the focused transducer at depths z=20, 30, 50, 70,100, and150mm. The calculated first and followed by the measured. The solid curves represent the peak-peak values of the pressure pulses, and the dashed curves shows the pulse energies. The focus is 75mm and the beam waist is at about 40 – 50 mm. The half value beam diameter is 3mm with respect to the peak-peak measure and 2.5mm with respect to the energy measure at depth 50mm. This is an acceptable transversal resolution for

ultrasound imaging. However, the beam is broader in both the near-field and the far-field, and this is why most ultrasound scanners use dynamic focusing.

The measured beam profiles for the focused beam are in better agreement with the calculations for the focused field compared to the unfocused field. The most obvious deviation between the measured and calculated beam profiles for the focused beam is the peak at the center of the beam profile at depth 30mm. The size of the hydrophone and a small displacement can easily explain this deviation.

4.3 Measurements of transducer PA75

Transducer PA75 was manufactured by Precision Acoustics, Dorchester, UK. The transducer has a diameter of 15mm and a focal length of 75mm. It has no matching layer but has a heavy backing about six times the impedance of water. The transducer is also equipped with a proprietary electric matching circuit and the center frequency should be 2MHz.

Figure 4.32 shows the measured pressure pulse of PA75 in the focal point. The pulse has a disappointing long tail. Figure 4.33 shows the frequency response of PA75. In the frequency spectrum we see a third harmonic, due to the 3/2 resonance of disc's thickness mode. The fundamental resonance of the transducer is twin peaked, and this is linked to the long pulse. However, the half value bandwidth of the transducer is about 1.4MHz and it should therefore be possible to design a better image pulse by applying inverse filtering. The center frequency was measured to be 2.3MHz.

Figure 4.32
Measured impulse response of the focused transducer, PA75. The hydrophone was placed in the focal point of the transducer and the excitation pulse is 40ns.

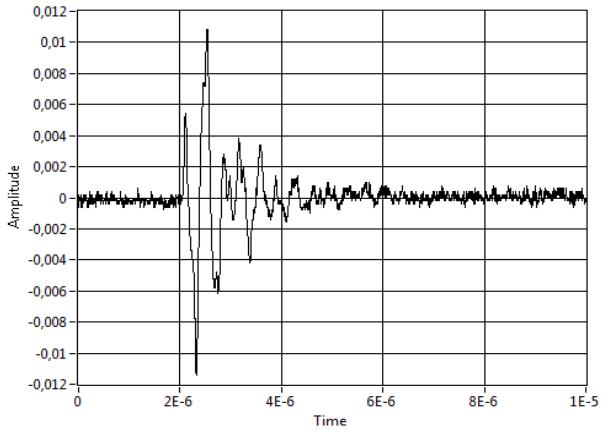

Figure 4.33
Measured frequency response of the focused transducer, PA75. The hydrophone was placed in the focal point of the transducer and the excitation pulse is 40ns.

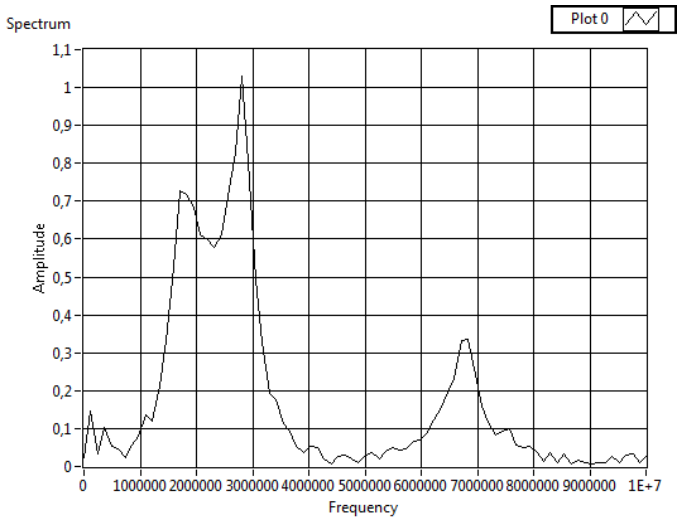

4.3.1 Calculation of the ideal excitation pulse

Figure 4.34 shows the filtered and extrapolated impulse response of transducer PA75 Figure 4.35 shows the amplitude response. To analyze the measured impulse response, the measured data was exported to an Excel file and read into Matlab. The time resolution of the measured data is 4ns and the length of the measured array is 2500 points or 10µs (1µs/div setting on the oscilloscope). Eight and eight

time points were simply added together for the first 128 points in Figure 4.32 and the rest of the time array was filled up with zeros up to 512 points. This gave a time resolution of 32ns and a frequency resolution of 61kHz.

The next step is to select a desired imaging pulse. This is not a given, but a two-period pulse with no tail is often considered to be a good imaging pulse. Inverse filtering will not work if we expect to generate a pulse with much larger bandwidth than the bandwidth of the transducer. The desired imaging pulse of PA75 must therefore be limited to a bandwidth of around 1.4MHz. For this project, a three-period Hanning pulse was chosen, and is given by:

$$u(t)_{H3} = \sin(2\pi f_0 t)\left(1 - \cos\left(2\pi \frac{f_0}{3} t\right)\right) \; \forall \; t \in [0, {}^{3}/_{f_0}]$$

The center frequency for transducer PA75 is f_0 = 2.3MHz. Figure 4.36 and Figure 4.37show the pulse and its frequency spectrum respectively and shows that the half value full bandwidth of this pulse is 1.5MHz or 65% relative bandwidth. This is 5% larger bandwidth than the measured relative bandwidth of the transducer PA75. The frequency spectrum also shows that the third harmonic at 6.8MHz should not be excited.

This imaging pulse require an excitation pulse that can be found as the inverse Fourier transform of the frequency spectrum of the imaging pulse divided by the frequency response of the transducer. Figure 4.38 shows the absolute value of the spectrum after this inverse filtering operation. Only the absolute value is shown, but the calculations also include the phase. The peaks in the spectrum below 1MHz and above 4MHz is a result of division by a small number and should be removed. We can truncate the spectrum at the zeroes in the Hanning pulse spectrum at around 0.8MHz and 3.9MHz. Figure 4.39 also shows the truncated spectrum. Figure 4.40 shows the resulting desired excitation pulse for transducer PA75 and the response pulse of transducer PA75 when this excitation pulse is used. The resulting image pulse is similar to the desired image pulse shown in Figure 4.41, except for some small ripples caused by the truncation.

A standard signal generator cannot generate the calculated excitation pulse in Figure 4.11. The truncated frequency spectrum in Figure 4.8 shows that there are three dominant frequencies in the spectrum, one around 1.2MHz, another around 3.3MHz

and finally the most dominant around the center frequency of 2.3MHz. The excitation pulse also consists of these frequencies. Most of the energy in the time pulse seems to be contained in a one period sinus of frequency 2.3MHZ and a second one period sinus two periods later with an amplitude of 40% of the first. Based on these observations, a simplified excitation pulse was constructed. Figure 4.42 shows the simplified excitation pulse and Figure 4.43 shows the calculated pulse response of transducer PA75. This pulse is close to the desired imaging pulse in Figure 4.36 and must be considered as an acceptable pulse for ultrasonic imaging and measurements.

Figure 4.34
Filtered impulse response and of transducer PA75

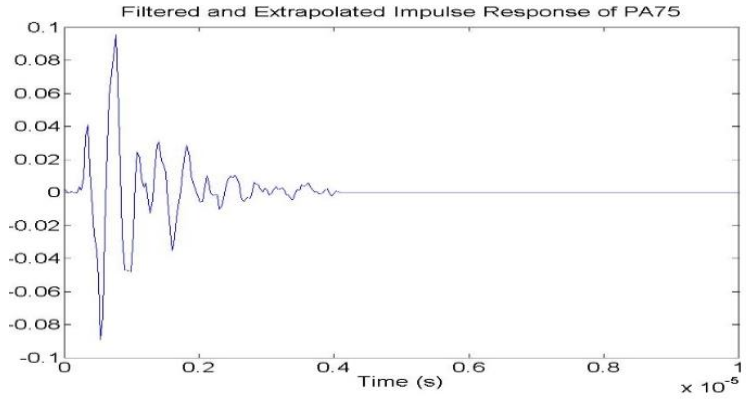

Figure 4.35
Filtered frequency response of transducer PA75

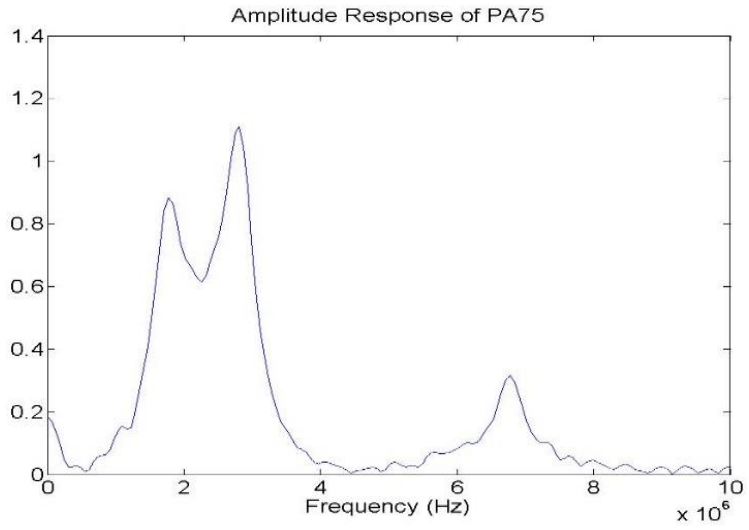

Figure 4.36
A 3-period Hanning pulse at 2.3MHz. This pulse is used as the desired imaging pulse in this project.

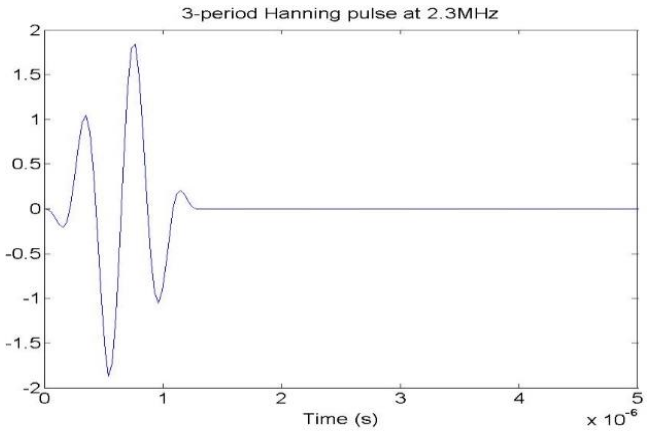

Figure 4.37
The frequency spectrum of the above Hanning-pulse.

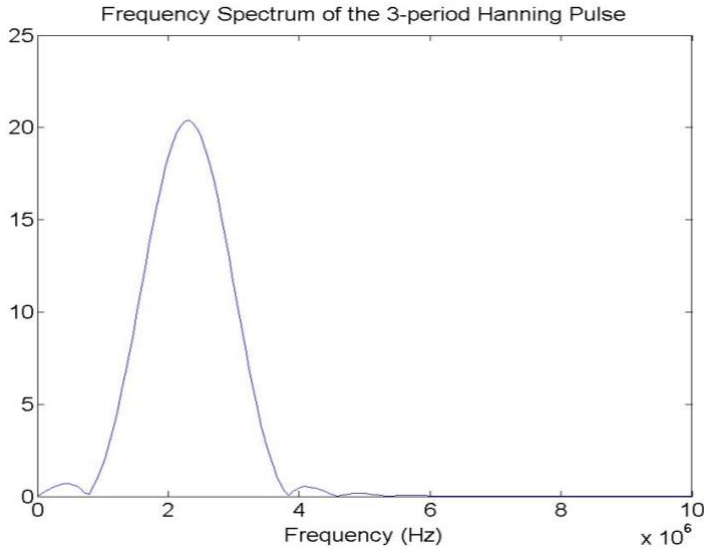

Figure 4.38
The inverse filtered spectrum resulting from transducer PA75 and the 3-period Hanning pulse and the spectrum

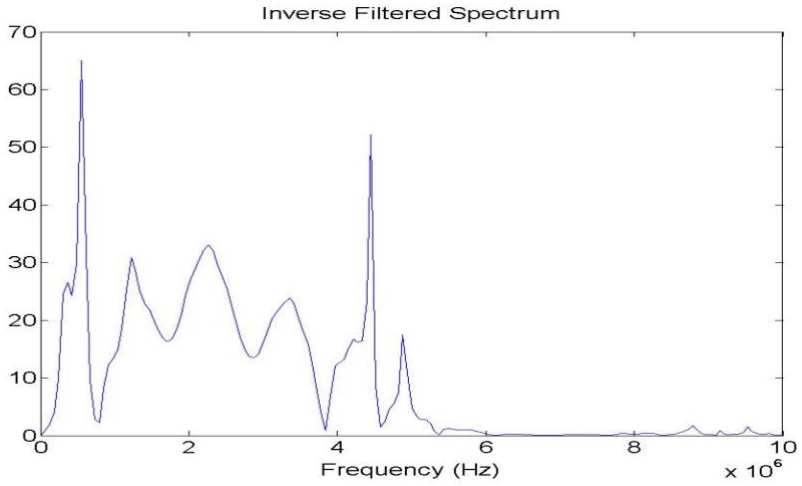

Figure 4.39
The inverse filtered spectrum resulting from transducer PA75 and the 3-period Hanning pulse and the spectrum, truncated at 0.8MHz and at 3.9MHz.

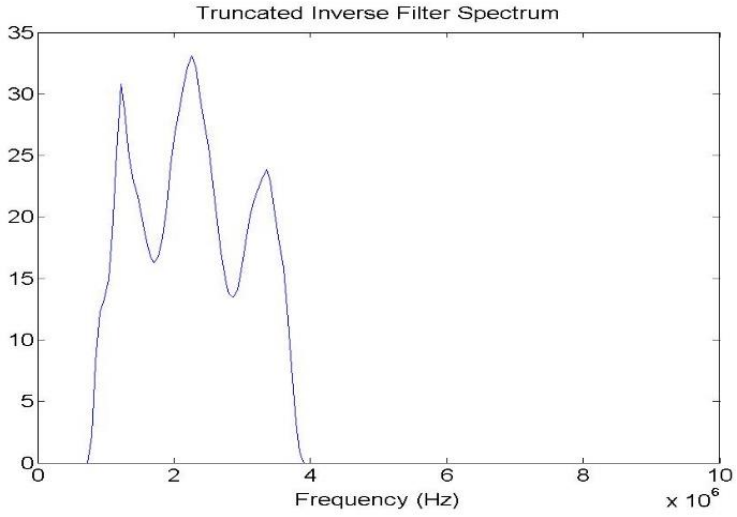

Figure 4.40
The desired excitation pulse for transducer PA75 found as the inverse Fourier transform of the truncated invers filtered spectrum in Figure 4.6. To the right is the resulting response pulse from transducer PA75 when this excitation pulse is applied to the input.

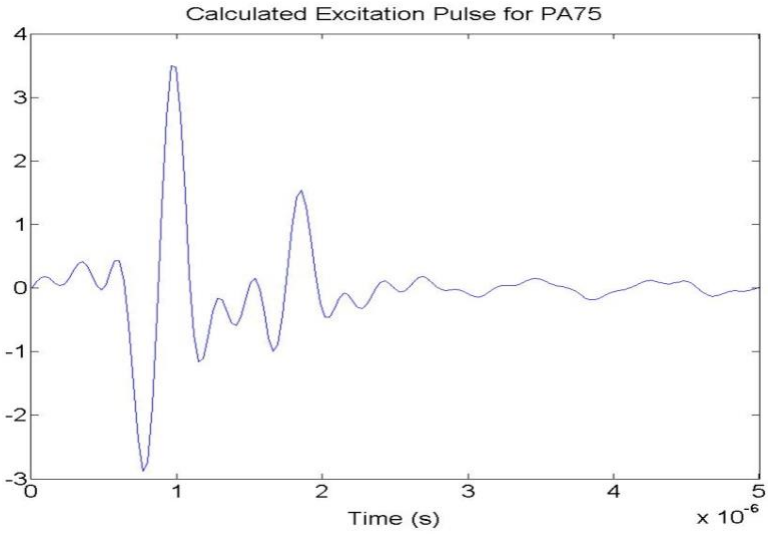

Figure 4.41
The simulated pulse response with the resulting response pulse from transducer PA75 when this excitation pulse is applied to the input.

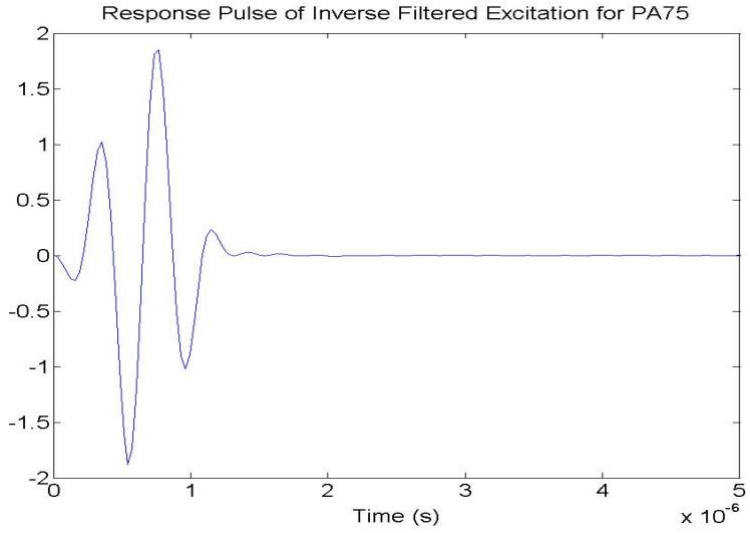

Figure 4.42
The simplified excitation pulse for transducer PA75.

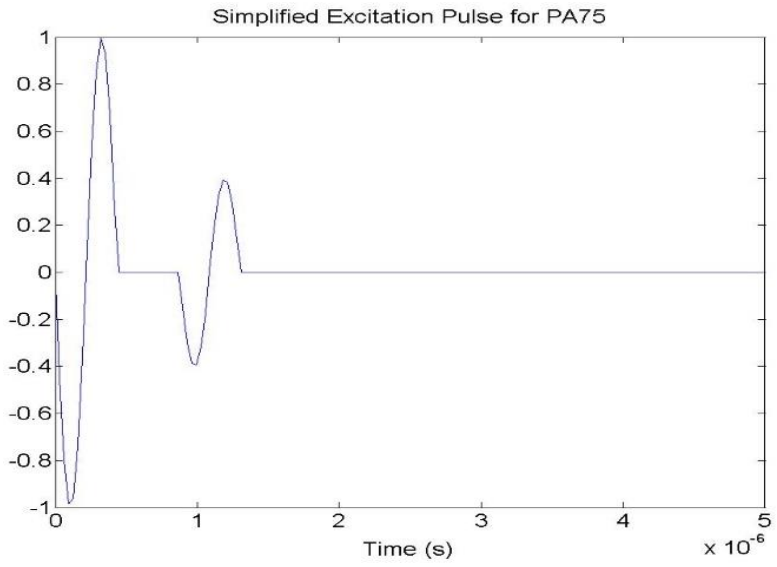

Figure 4.43
The resulting pulse response for transducer PA75 when the simplified excitation pulse is applied.

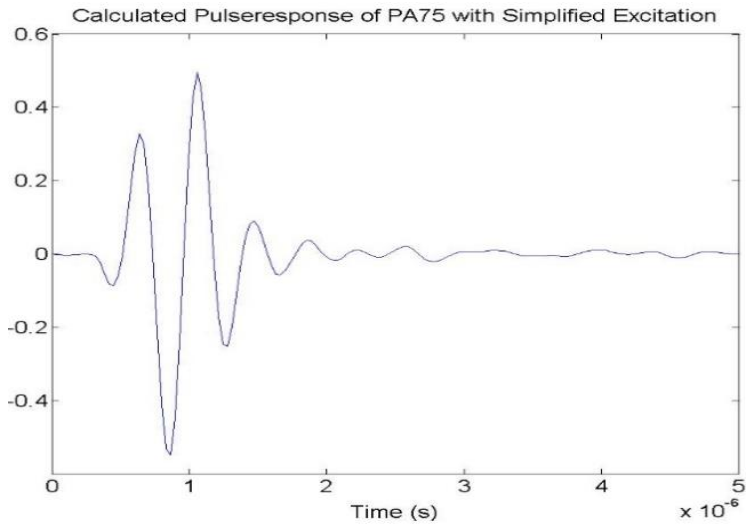

4.3.2 Measurement of simplified excitation pulse for PA75

The simplified excitation pulse for transducer PA75 was constructed and stored in the AFG and measured in the measurement tank. Figure 4.44 shows the measured output from the AFG and Figure 4.45 shows its frequency spectrum. Figure 4.46shows the measured pulse response and Figure 4.47 shows the amplitude response of transducer PA75 when the constructed pulse of Figure 4.46 is used as excitation.

Figure 4.44
The simplified excitation pulse designed for transducer PA75 from the function generator.

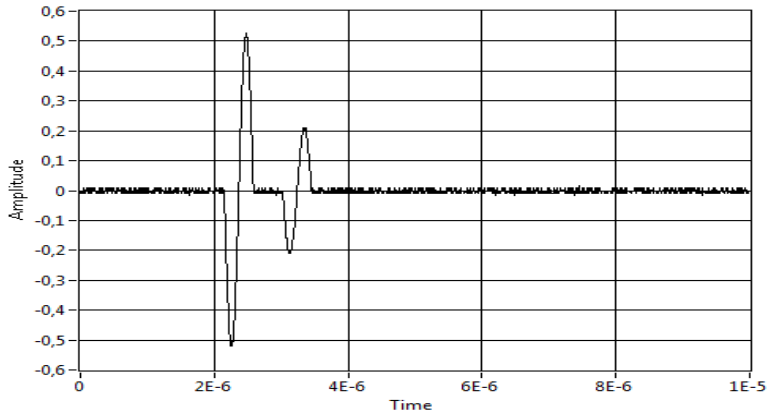

Figure 4.45
The frequency spectrum of simplified excitation pulse designed for transducer PA75.

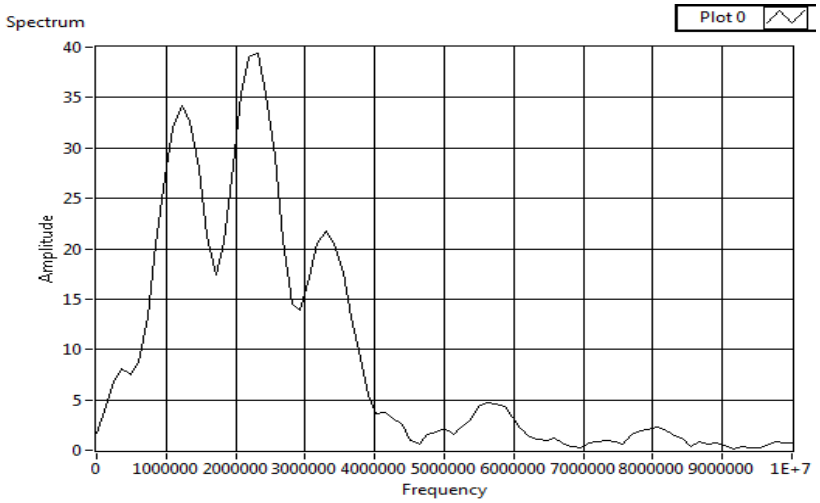

Figure 4.46
The measured pulse response of transducer PA75 when excited with the simplified excitation pulse.

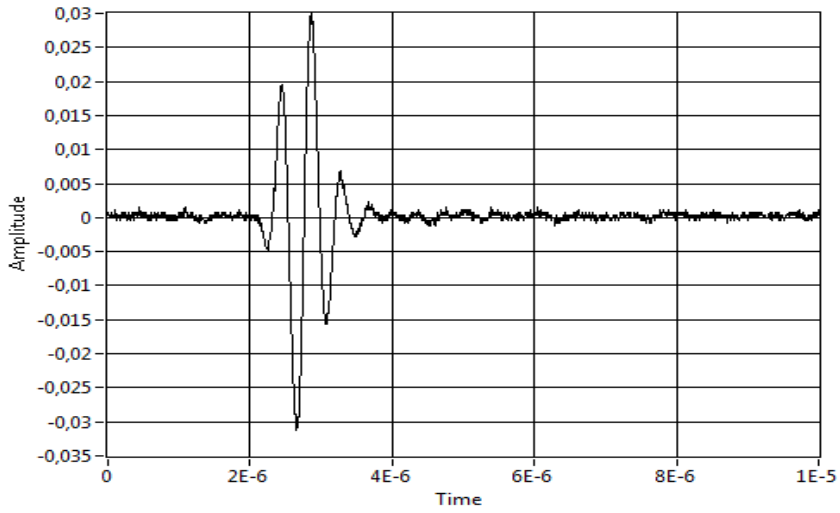

Figure 4.47
The measured frequency response and of transducer PA75 when excited with the simplified excitation pulse.

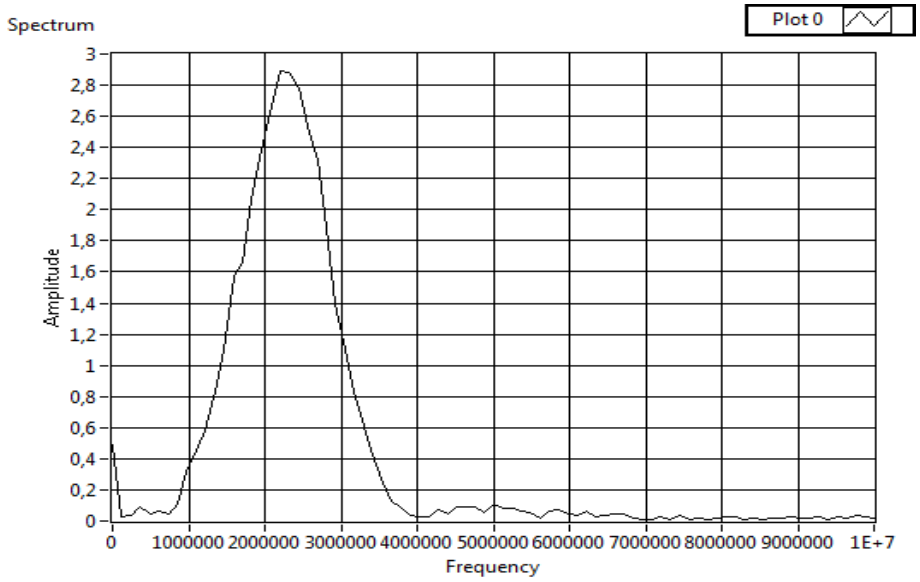

The results in Figure 4.46 show that the pulse has a minimal tail and is well suited for imaging and measurements. The bell shape of the frequency amplitude is linked to the minimal tail of the pulse through the Fourier transform.

4.3.3 Measurements of beam profiles of PA75

Figure 4.48
Calculated beam profiles of PA75 at depths z = 50mm.

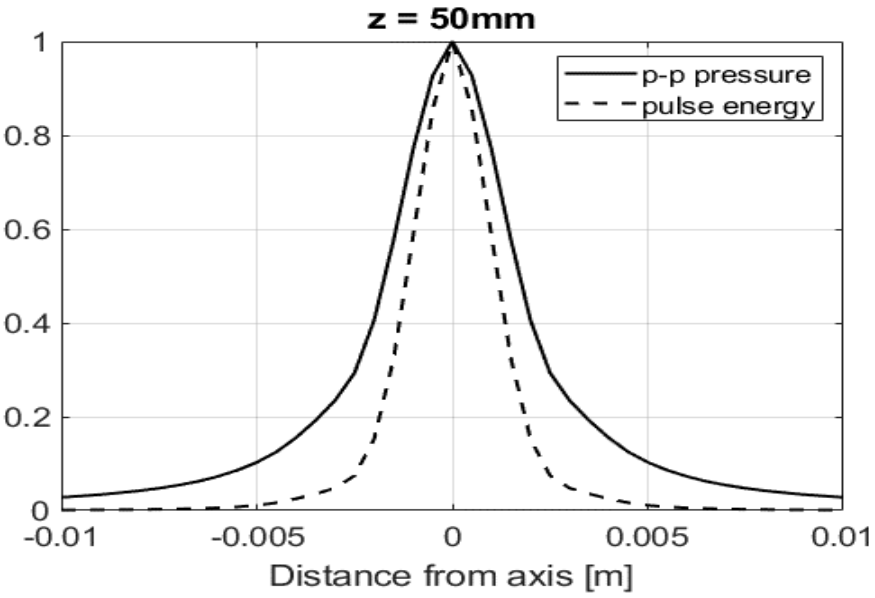

Figure 4.49
Measured beam profiles of PA75 at depths z = 50mm.

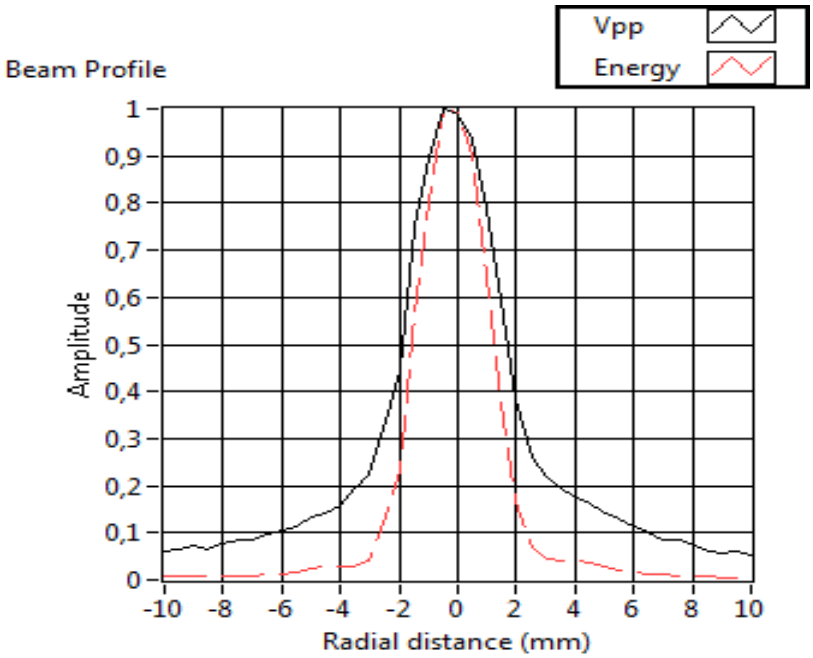

Figure 4.50
Calculated beam profiles of PA75 at depths z = 75mm.

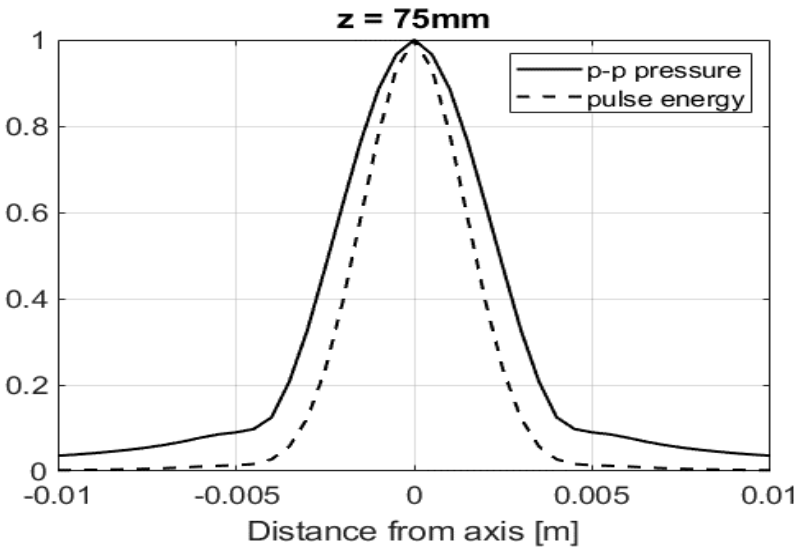

Figure 4.51
Measured beam profiles of PA75 at depths z =75mm.

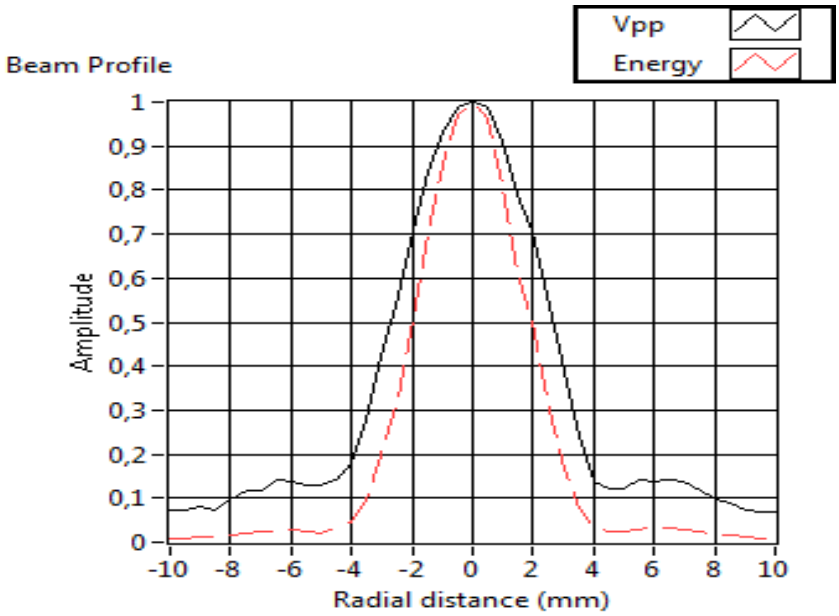

Figure 4.52
Calculated beam profiles of PA75 at depths z = 100mm. The solid curves are peak-peak pressure, and the dashed curves are pulse energy.

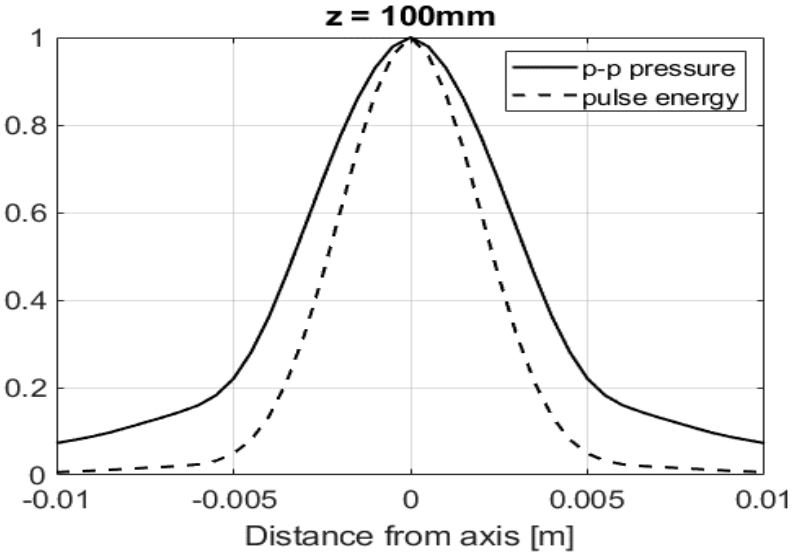

Figure 4.53
Measured beam profiles of PA75 at depths z = 100mm. The solid curves are peak-peak pressure, and the dashed curves are pulse energy.

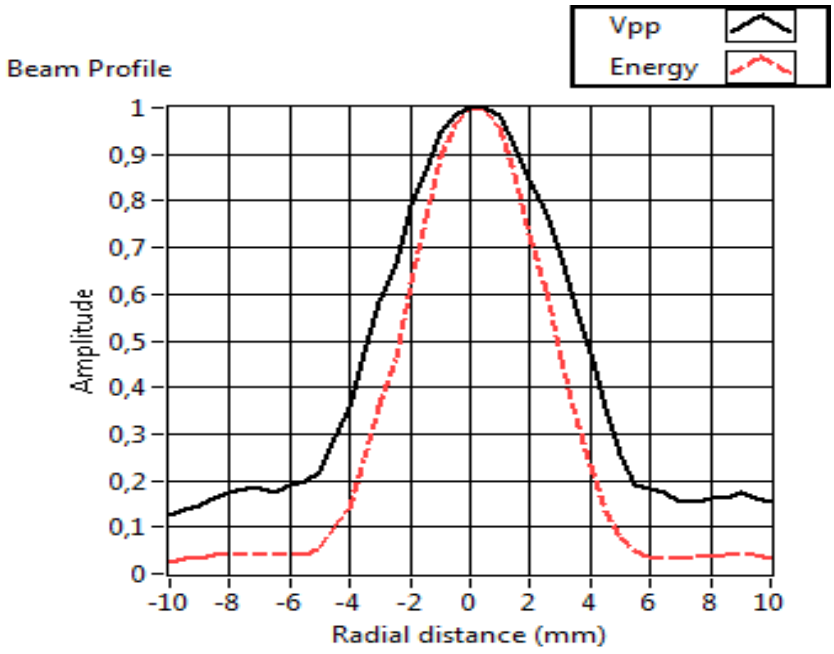

The measured beam profiles in Figure 4.48 through Figure 4.53 are more symmetric than the beam profiles of transducer1. This is probably due to a better support of the PZT-disc for PA75 transducer. The disc is supported by a heavy backing and is

mounted in a metallic cylinder. The agreement with the calculations is also excellent and within the accuracy of 0.5mm set by the size of the hydrophone.

4.3.4 Measurement of non-linear effects

Non-linear effects are well known to be generated in medical ultrasound imaging. No model for non-linear propagation was available, so no calculations were possible. The non-linear effects in water and biological tissue are also known to differ. Only measurements in water will be presented in this report.

To generate significant harmonics in water, a 4-period Hanning pulse with center frequency 2MHz was used. The peak-peak voltage was 400V. Figure Figure 4.54 shows the pressure pulse, andFigure 4.55 its frequency spectrum measured in the focal point. The non-linear effects are obvious. The pressure pulse has sharp positive peaks with almost a shock wave formation in front of the highest peak while the negative peaks have lower amplitude. The frequency spectrum shows the first harmonic centered at 2.1MHz and the second harmonic centered at 4.2MHz and several higher harmonics.

Two Butterworth filters (8^{th} order) were made to separate the 1^{st} harmonic (1-3MHz) and the 2nd harmonic (3-5MHz) pulses. The outputs from the two filters are shown in Figure 4.56 and Figure 4.58. Figure 4.56 shows the pulse of the first harmonic and Figure 4.57its frequency spectrum. Figure 4.58 shows the pulse of the second harmonic and Figure 4.59 its frequency spectrum.

Figure 4.54
The pressure pulse measured at the focal point.

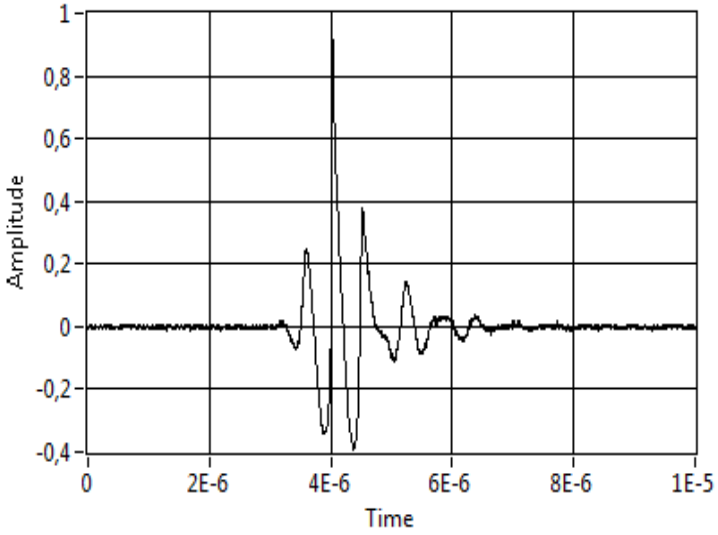

Figure 4.55
The frequency spectrum measured at the focal point.

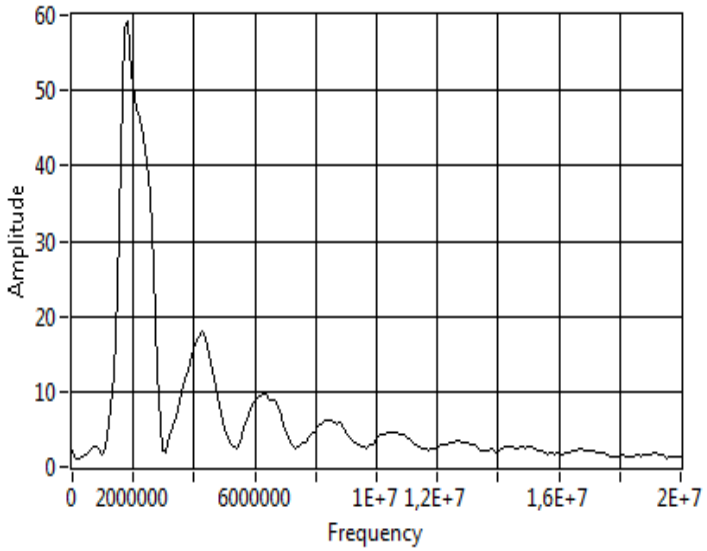

Figure 4.56

The 1st harmonic pulse separated by a 8th- order butterworth filter (1-3MHz)

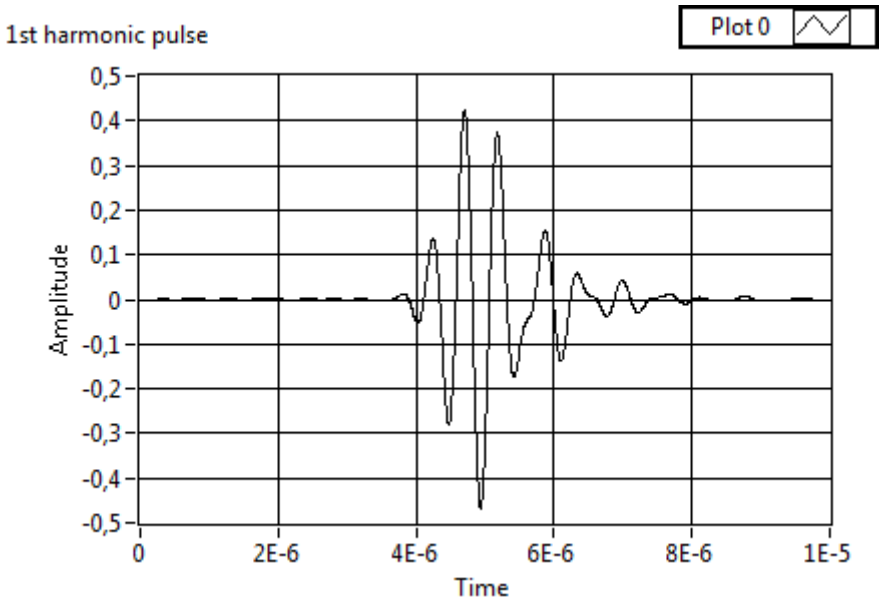

c

Figure 4.57

The frequency spectrum of the 1st-harmonic.

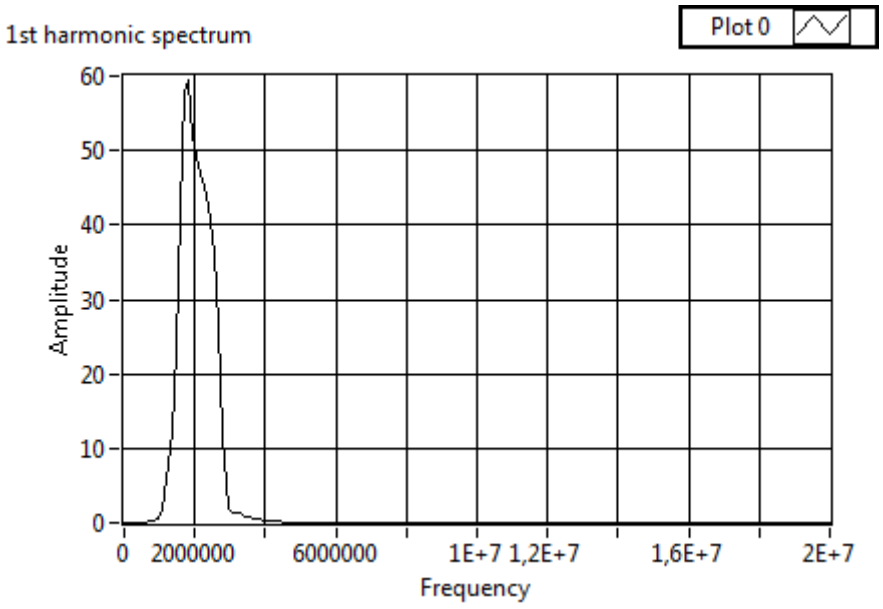

Figure 4.58
The 2nd-harmonic pulse separated from the pulse in Figure 4.16 by an 8-order Butterworth filter (2-5MHz).

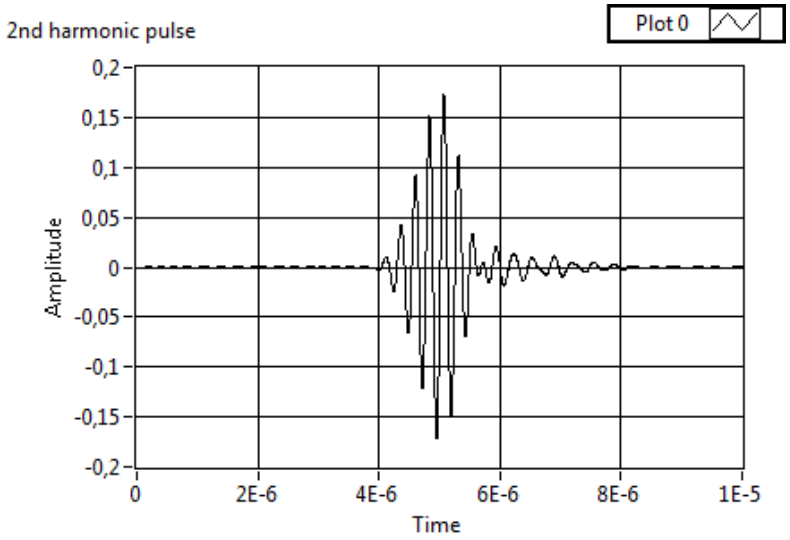

Figure 4.59
The 2nd-harmonic frequency spectrum.

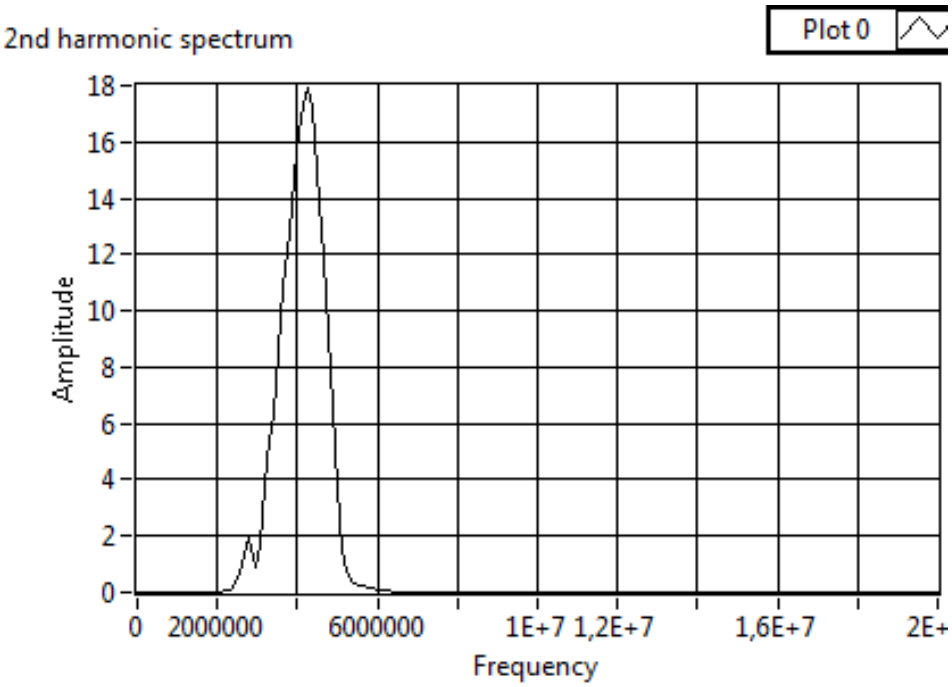

We can see from the frequency spectra that the first and second harmonics are well separated from each other and well separated from the higher harmonics. This separation technique was used to separate the measurements of the first harmonic

beam profile and the second harmonic beam profile. Figure 4.60, Figure 4.61 and Figure 4.624.21 shows the beam profiles measured at depth 50mm. Figure 4.60 include all frequencies of the field, Figure 4.62 include only the first harmonic component of the field, and Figure 4.61 include only the second harmonic component of the field. Figure 4.64 shows the beam profile at depth 75mm for all frequencies. Figure 4.65 shows the beam profile at depth 75mm for the 1st-harmonic and Figure 4.66 the 2nd-harmonic. Figure 4.67, Figure 4.68, and Figure 4.69 show the beam profiles at depth 100mm for all frequencies, the 1st-harmonin and 2nd-harmonic, respectively.

The solid curves in all plots are the peak-peak pressure and the dashed curves are the pulse energy. As expected, the beam profiles of the second harmonic are significantly narrower than the beam profiles of the first harmonic. This is also one of the reasons why second harmonic imaging has become so popular in medical imaging. The higher harmonics are not of the same interest due to the limited bandwidth of the imaging transducers in use.

Figure 4.60
Aii frequency beam profile at depth 50mm

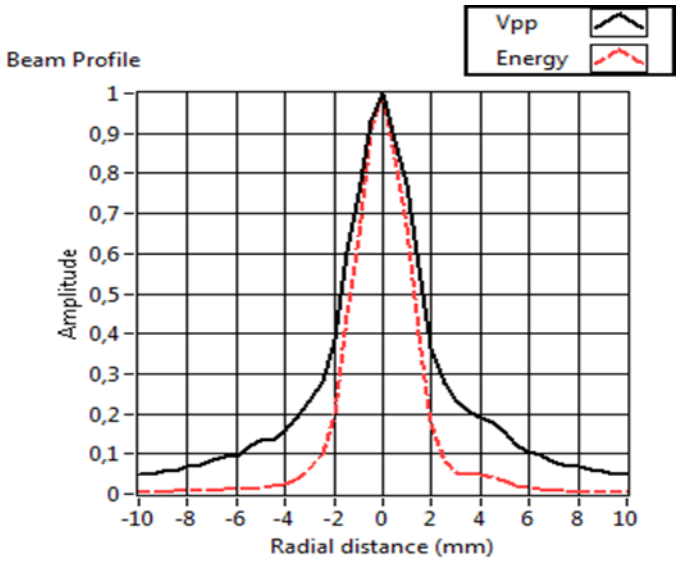

Figure 4.61

1st-harmonic beam profileat 50mm

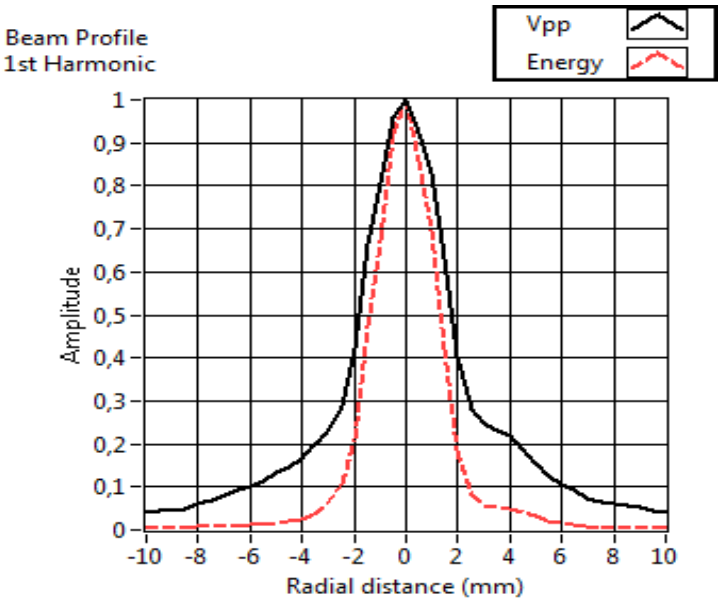

Figure 4.62

1st-harmonic beam profile at depth 50mm

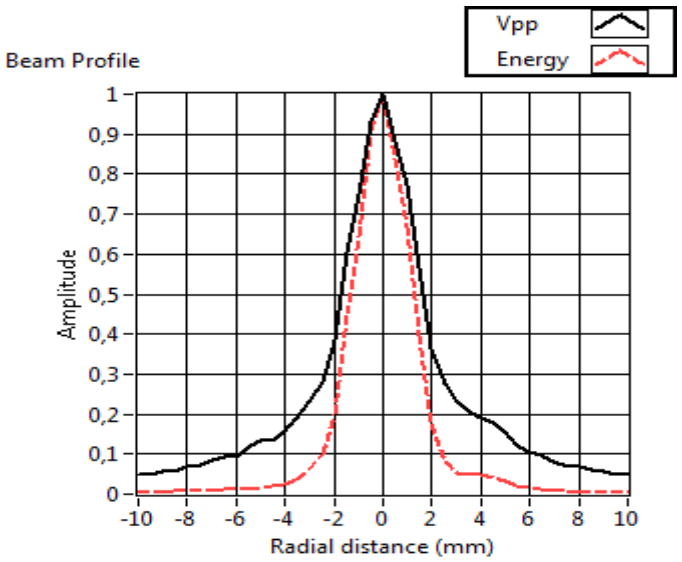

Figure 4.63
The measured 2nd harmonic beam profiles at depth 50mm

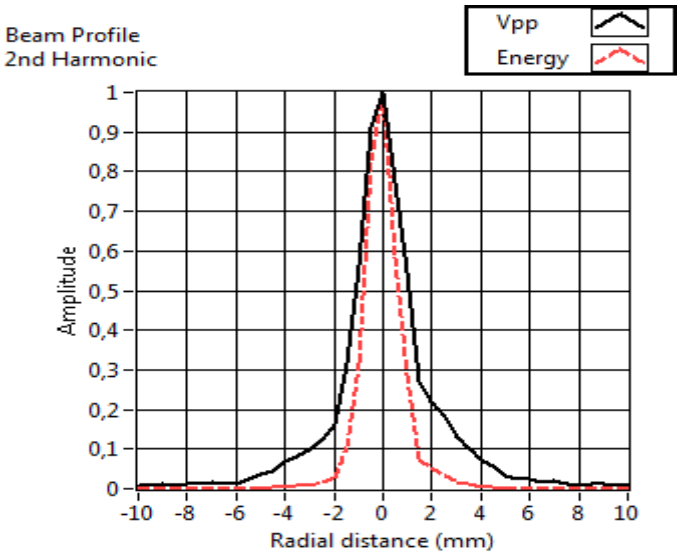

Figure 4.64
All harmonics beam profile at depth 75mm.

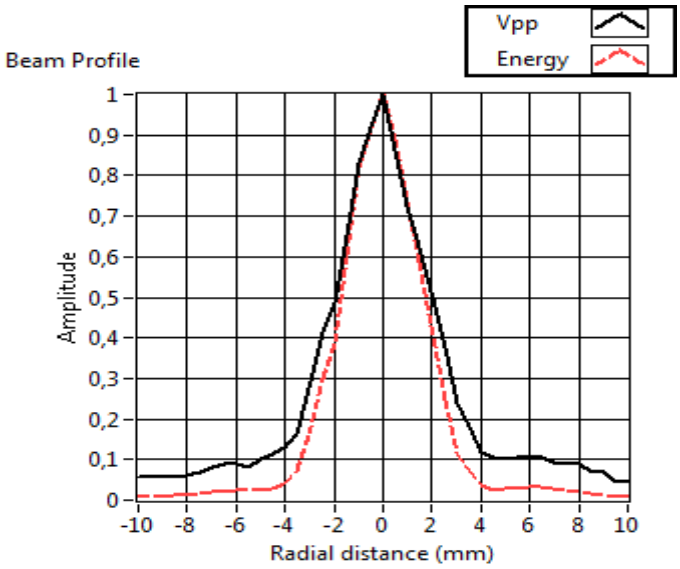

Figure 4.65

The 1st harmonic measured beam profiles at depth 75mm, focal plane..

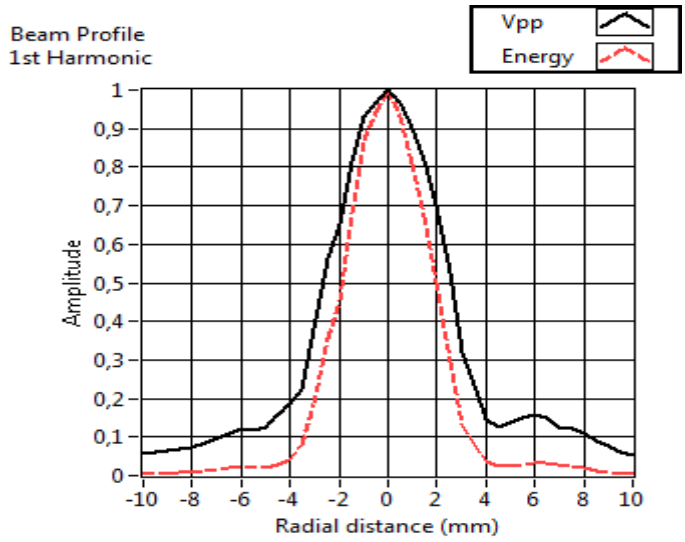

Figure 4.66

The 2nd-harmonic measured beam profiles at depth 75mm, focal plane.

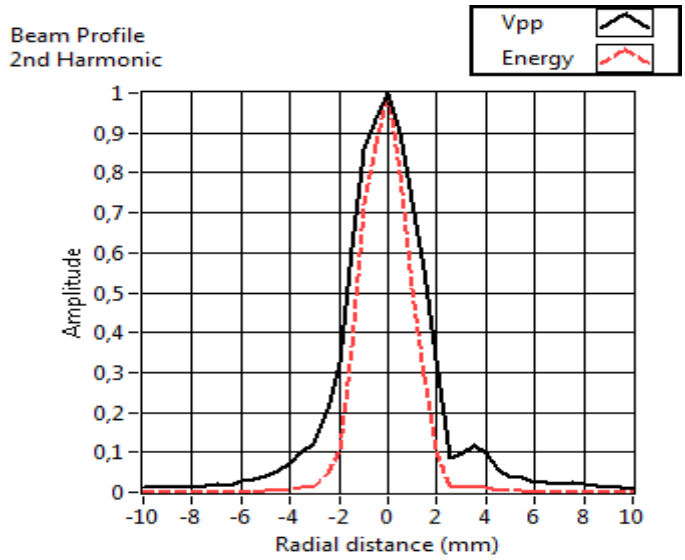

Figure 4.67
All harmonics measured beam profiles at depth 100mm

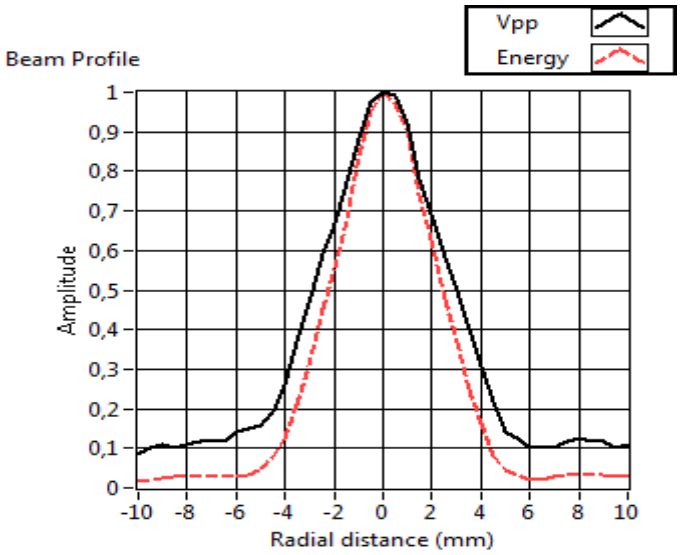

Figure 4.68
The 1st-harmonic measured beam profiles at depth 100mm.

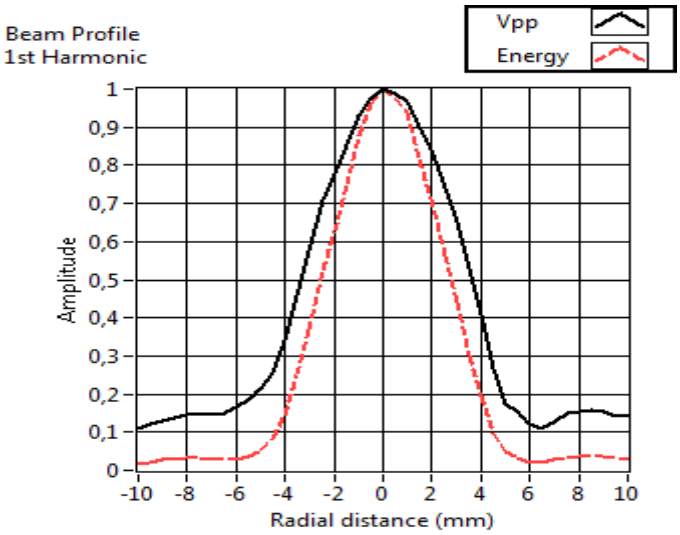

Figure 4.69
The 2nd-harmonic measured beam profiles at depth 100mm.

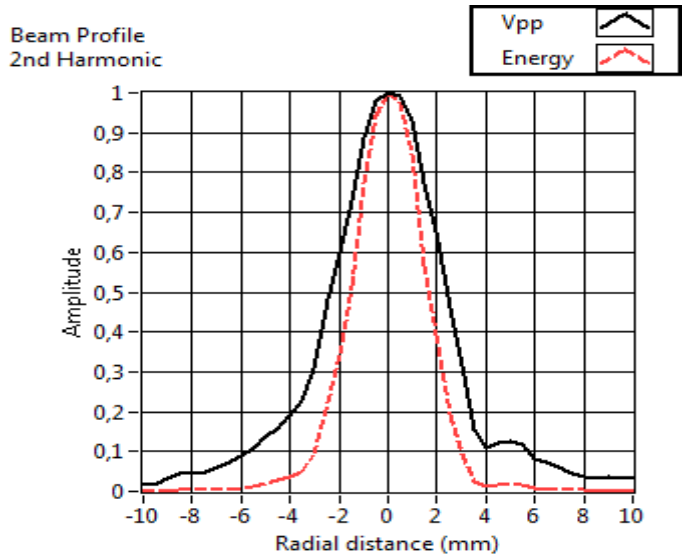

4.3.5 Pulse inversion

An alternative to use filters to separate the harmonics is to apply pulse inversion. Pulse inversion is a method that involves two transmitted pulses where the second pulse is the negative of the first. At receipt the two pulses are added and if the pulse propagation is linear the result will be zero. However, if the pulse propagation is non-linear, we will end up with even harmonic components after adding the two pulses. The two transmitted pulses are related as follows:

$$p_2(t) = -p_1(t)$$

The received pressure field can be written as a Taylor series to account for non-linear effects:

$$\hat{p}(t) = a_1 p(t) + a_2 p^2(t) + a_3 p^3(t) + a_4 p^4(t) + a_5 p^5(t) + \cdots$$

When the two pulses are added, all odd factors will cancel, and the result is a sum of the even factors:

$$\widehat{p_1}(t) + \widehat{p_2}(t) = 2a_2 p^2(t) + 2a_4 p^4(t) + \cdots$$

In terms of frequency, this means that we are left with only the even harmonics. In practice, mainly the second harmonic, due to the limited bandwidth of imaging transducers.

Figure 4.22 shows the measured double pulse with the hydrophone at the focal point of transducer PA75. The second pulse is delayed by 15μs and is the negative of the first.

Figure 4.23 shows the added pulses when the first pulse is delayed by 15μs. The result is non-zero and indicates that there are non-linear effects in the pulse propagation.

Figure 4.24 shows the absolute value of the Fourier transform of the added pulses in in Figure 4.23. The amplitude spectrum shows that most of the power is concentrated around 4MHz, twice the frequency of the transmitted pulses.

Figure 4.70
Measured double pulse where the second pulse is delayed 15μs and is negative of the first pulse.

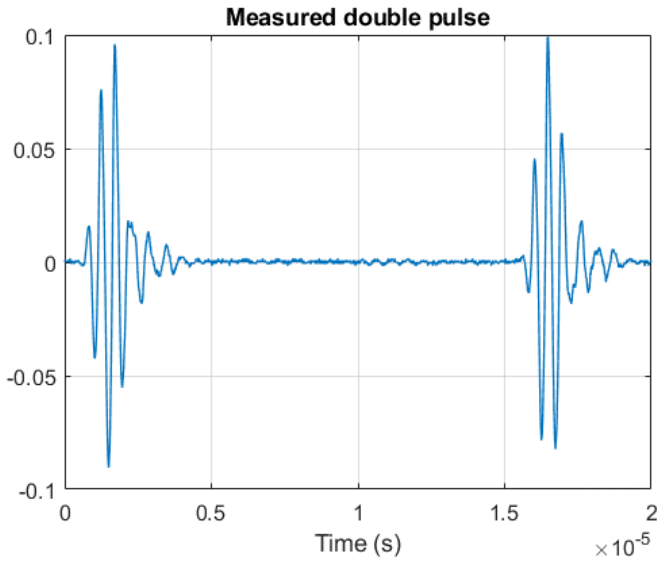

Figure 4.71
The added pulses after delaying the first pulse by 15μs.

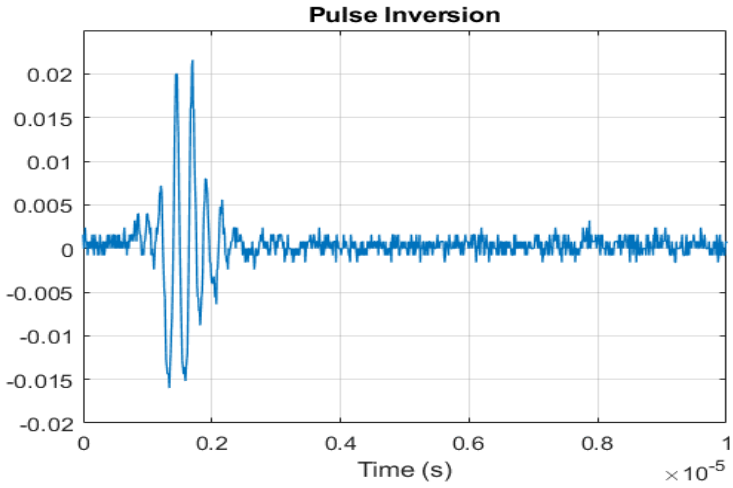

Figure 4.72
Amplitude spectrum of the added pulses in Figure 4.21.

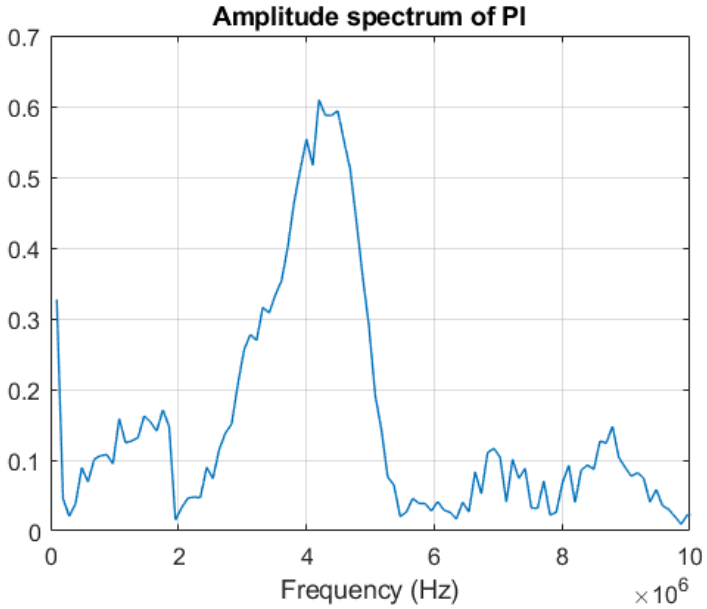

4.4 Measurements of transducer PAplan

Transducer PAplan is also produced by Precision Acoustics, Dorchester, UK. The transducer has a diameter of 15mm and a planar front. It has one quarter-wave matching layer and air backing. The transducer is also equipped with a proprietary electric matching circuit and the center frequency should be 2MHz. For the measurements a lens with focal length of 75mm was attached at the front.

Figure 4.73
Pressure pulse of PAplan measured in the focal point at depth 75mm with a 40ns pulse excitation.

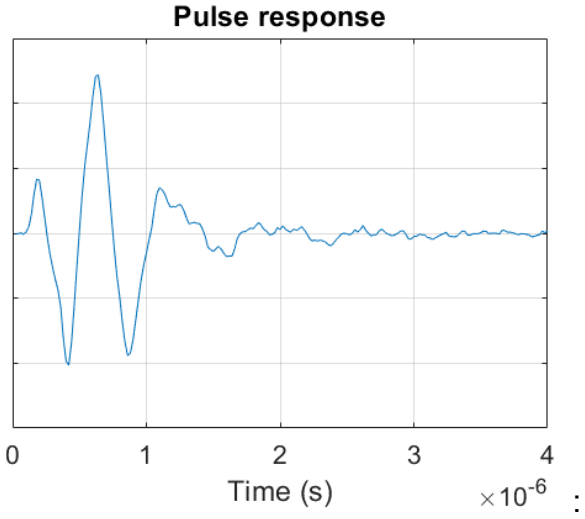

:

Figure 4.74
The amplitude spectrum of PAplan measured in the focal point at depth 75mm with a 40ns pulse excitation.

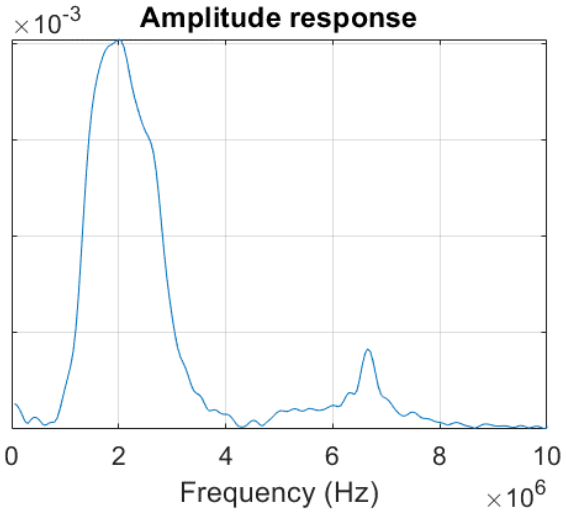

Figure 4.75
Pressure pulse of PAplan measured in the focal point at depth 75mm with a 150ns pulse excitation.

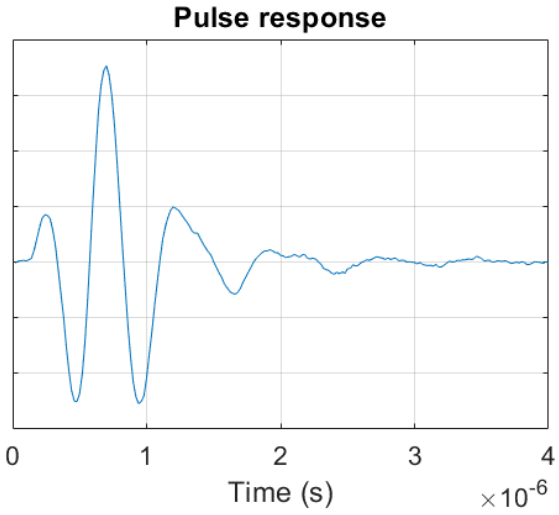

Figure 4.76
The amplitude spectrum of PAplan measured in the focal point at depth 75mm with a 150ns pulse excitation.

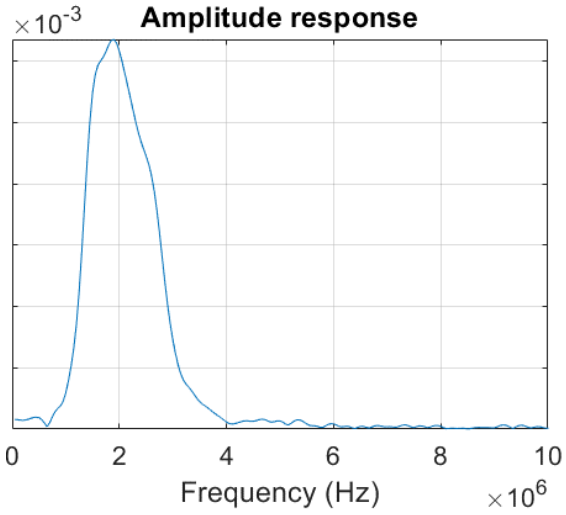

Figure 4.25 shows the measured pressure pulse and the amplitude spectrum in the focal point. The excitation pulse is the short pulse of length 40ns. We see that also for this transducer a third harmonic is excited by the short pulse at frequency 6.6MHz. A rectangular excitation pulse of length 150ns will have a zero in its frequency spectrum at 6.66MHz (= 1/150ns). Figure 4.26 shows the pulse response and the amplitude response when the transducer is excited with the 150ns-pulse. The result is a pulse well suited for imaging and measurements.

Figure 4.27 shows the measured beam profile of the unfocused PAplan at the depth of beam waist ($z = a^2/\lambda = 75$mm). The solid curve shows the measured peak-peak values, and the dashed curve shows measured pulse energy.

Figure 4.28 shows the calculated beam profile under the same conditions as the measured beam profile in Figure 4.27.

Figure 4.77
Measured beam profile of the unfocused PAplan through beam waist (z=75mm)

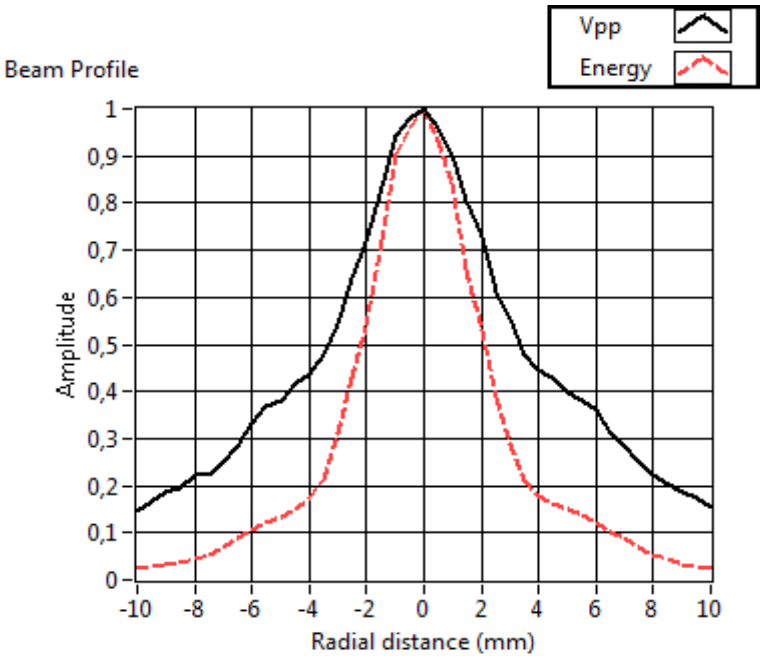

Figure 4.78
Calculated beam profile of the unfocused PAplan through beam waist (z=75mm).

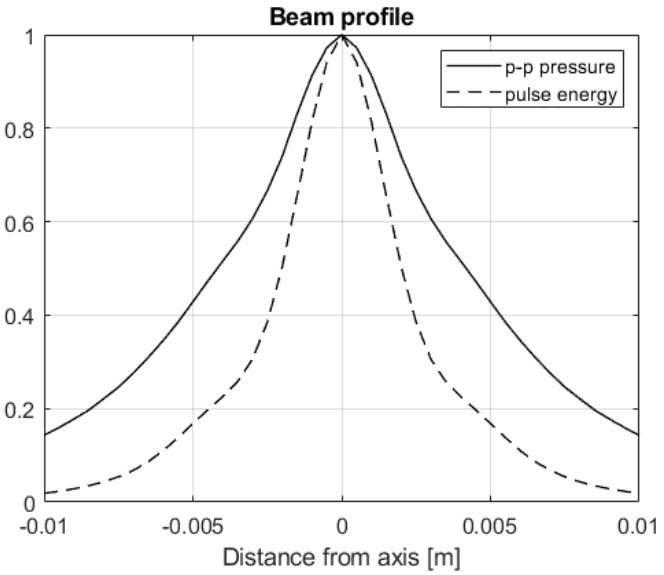

4.4.2 Design and test of lenses for PAplan

Transducer PAplan is unfocused and need an additional lens to work well for measurements and imaging. A lens of silicon rubber was made similar to the description in Chapter 4.2. The focal length was chosen to be 75mm and the curvature radius of the concave side should therefore be 37mm. The diameter of the lens should be 15mm to fit the transducer.

The lens was tested by measuring the acoustic field along the acoustic axis of the transducer PAplan with and without the silicon lens attached. The measurements were compared to calculations with the MATLAB program fieldL.m. For comparison also the PA75 transducer with a fixed focus was measured. The measurements are shown as circles and the calculations as solid lines.

shows the measured and calculated peak pressure field of the unfocused transducer PAplan. The measured and calculated values are normalized in the far field at z = 150mm. For this transducer, the beam waist should be at depth z = 75mm. This is also close to where the pressure is at its maximum. Proximal to the beam waist, the calculated field has huge variations over short distances. The measurements done with a hydrophone with diameter 0.5mm will partially integrate over these spatial variations.

Figure 4.80 shows the measured and calculated pressure along the acoustic axis of transducer PAplan with an attached lens of focal length 75mm. The maximum pressure for both the measurement and the calculation is at depth z= 45mm.

Figure 4.81 shows the measured and calculated pressure along the acoustic axis of transducer PA75 which has a focal length of 75mm. The maximum pressure for both the measurement and the calculation is at depth z= 45mm.

Figure 4.79
Measured and calculated peak pressure along the acoustic axis of unfocused transducer PAplan without any lens.

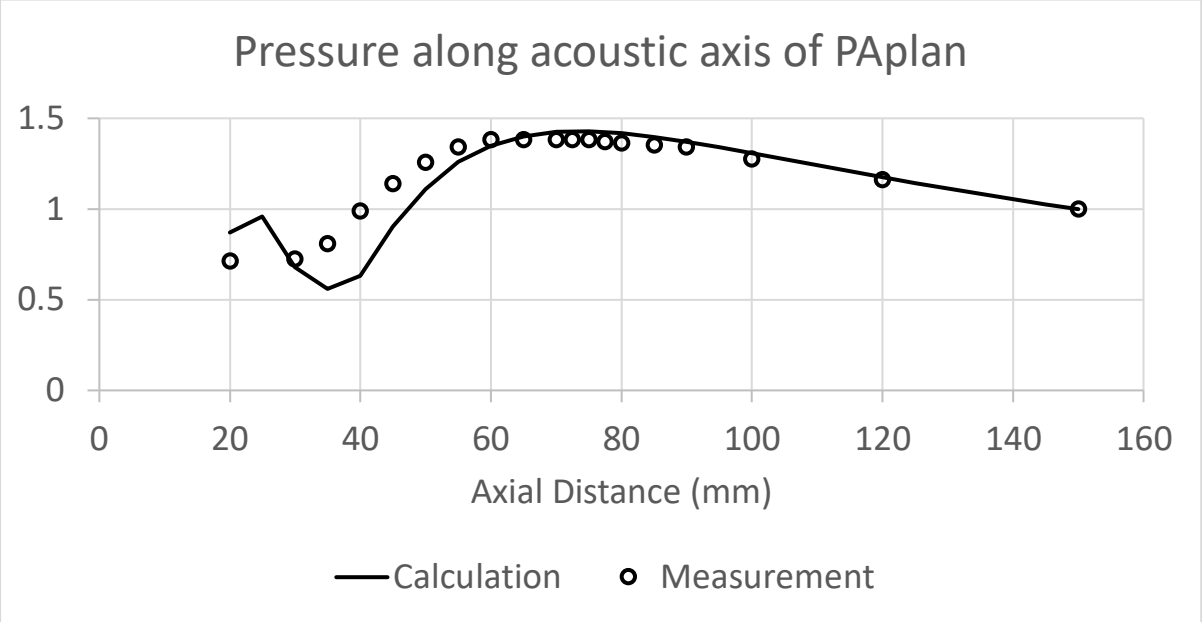

Figure 4.80
Measured and calculated peak pressure along the acoustic axis of transducer PAplan with a lens with a focal length of 75mm.

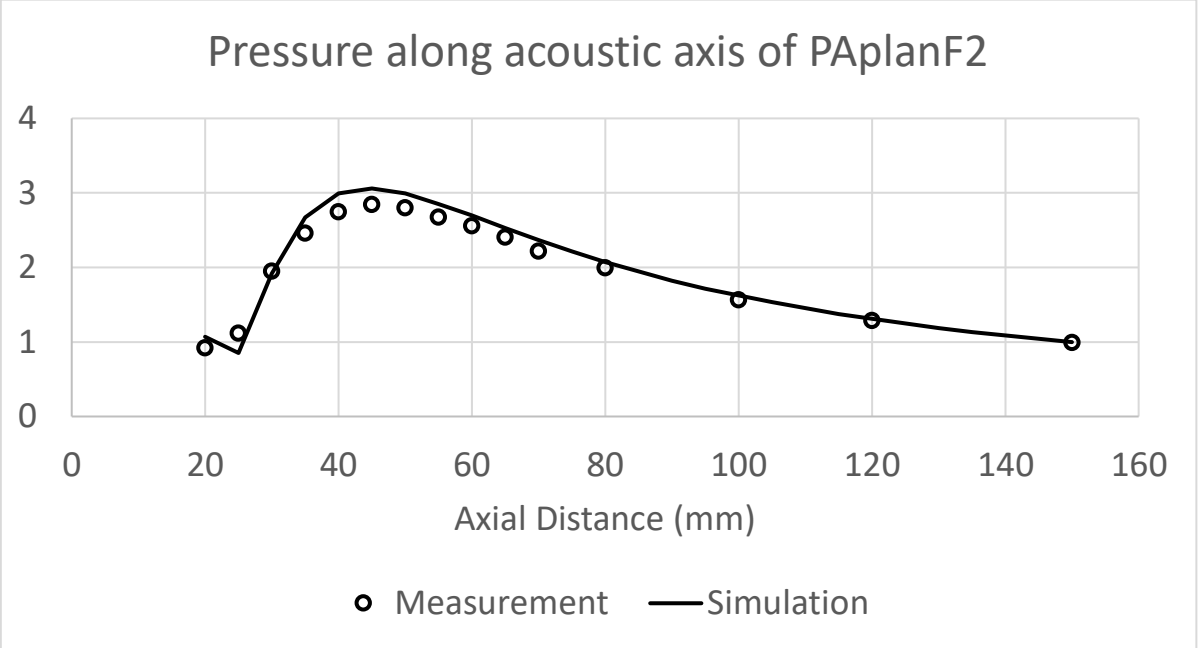

Figure 4.81
Measured and calculated peak pressure along the acoustic axis of the transducer PA75 with a focal length of 75mm.

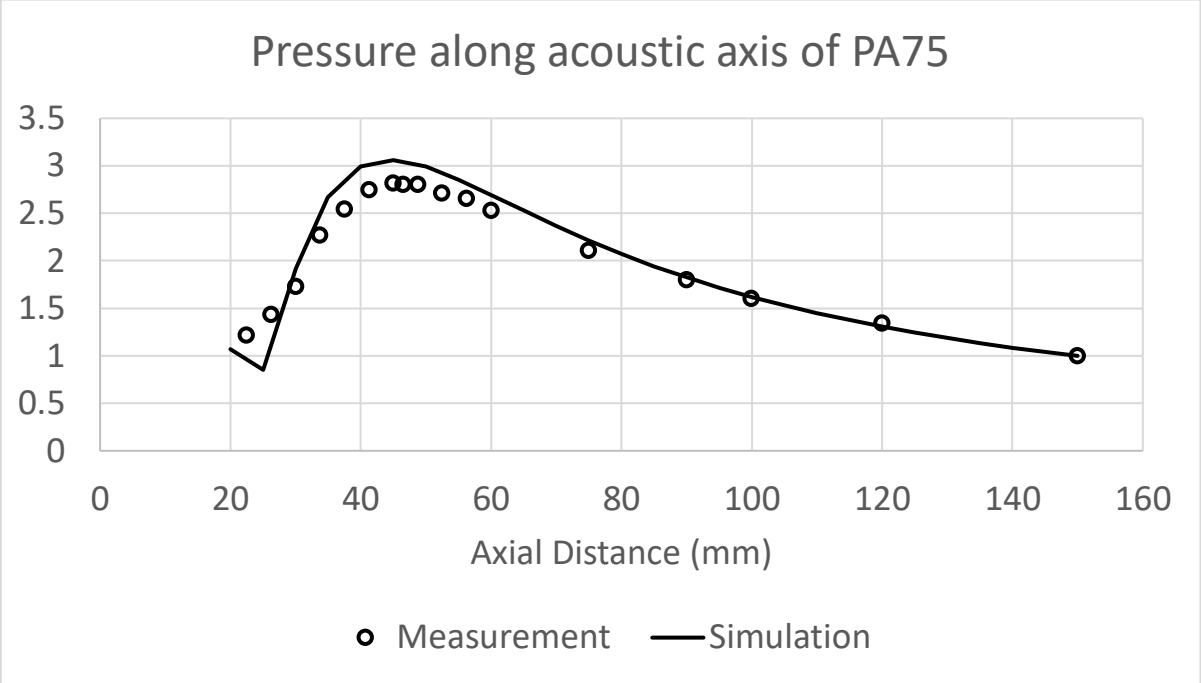

Comparing the two last measurements and calculations in Figures 4.30 and 4.31 indicates that the lens works as it should.

4.5 Measurements of transducer PATR

Transducer PATR was also designed and made by Precision Acoustics Ltd. The transducer was custom designed for both transmit and receipt. It has a PZT ceramic resonant at 2MHz and a quarter wave matching layer at the front made of PVDF that also function as a receiver. The diameter of the transducer is 15mm and it is unfocused. This transducer was built to measure reflections of the transmitted pulse from objects in the water tank.

The lens with focal length 75mm was attached to the front of the transducer. Figure 4.32 shows the measured pressure pulse in the focal point when the transducer is excited with 40ns pulse. Figure 4.33 shows the Fourier transform of the pulse and is the frequency response of transducer PATR.

Figure 4.82
Pressure pulse measured at the focal point of transducer PATR.

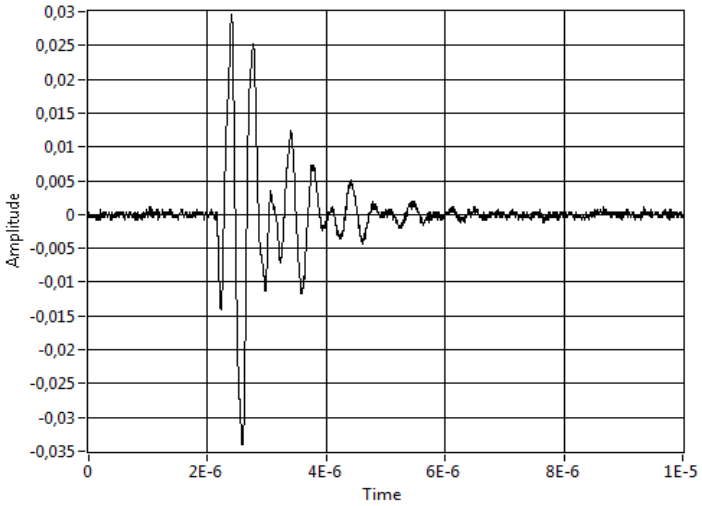

Figure 4.83: Amplitude spectrum measured at the focal point of transducer PATR.

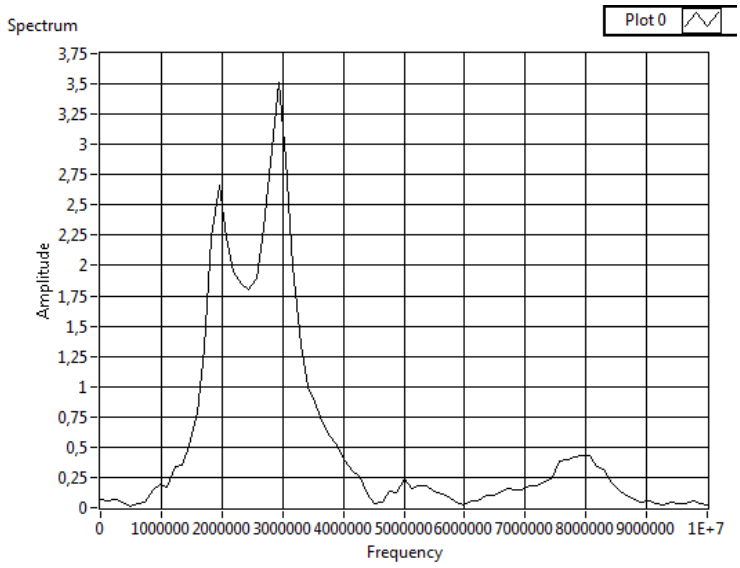

Figure 4.84
Measured beam profile in the focal plane of focused transducer PATR.

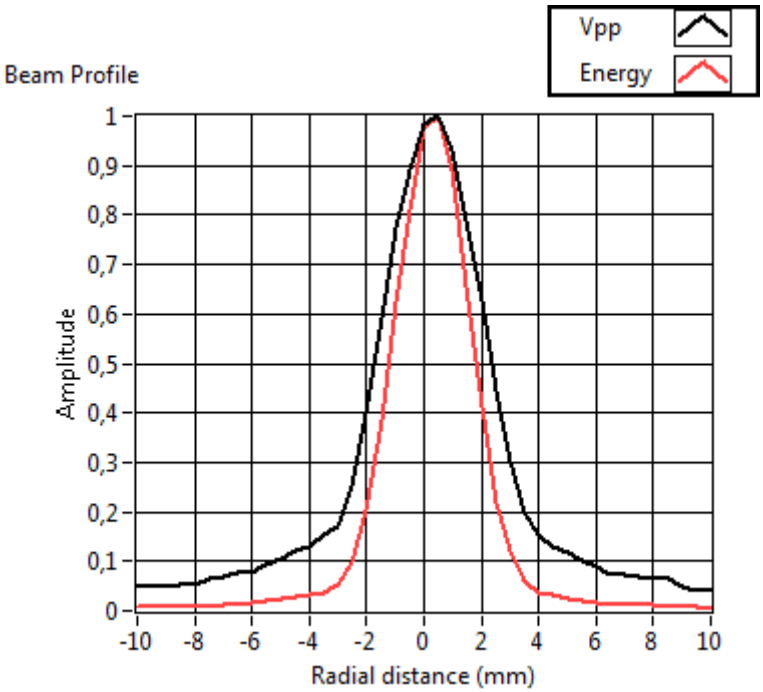

4.5.2 Inverse filtering applied to transducer PATR

The impulse response and the frequency response of transducer PATR as shown in Figures 4.32 and 4.33 were not as expected. The pulse has a big tail, and this is linked to the twin-peaked appearance of the frequency spectrum. To compensate for the twin-peaked spectrum, an inverse filter was computed, and a compensating excitation pulse was found like in Chapter 4.3.1. The calculated excitation pulse was loaded into the AFG and used to excite transducer PATR.

Figure 4.85
Measured excitation pulse for PATR transmitted from the AFG.

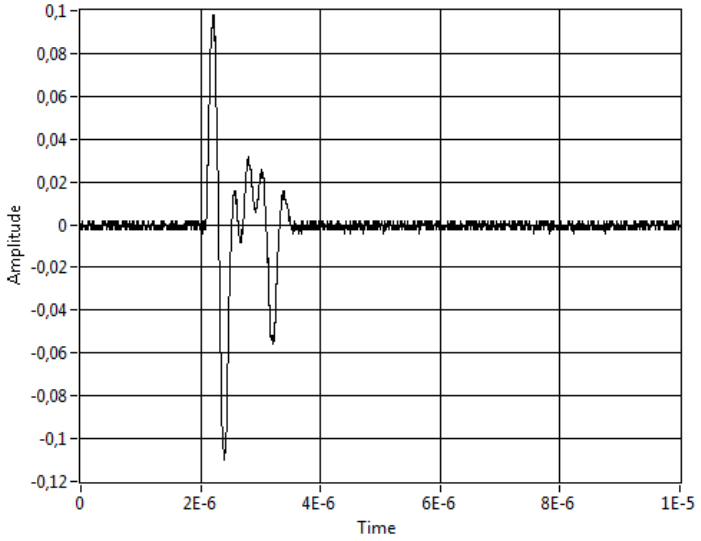

Figure 4.86
The frequency response of the inverse filter for transducer PATR.

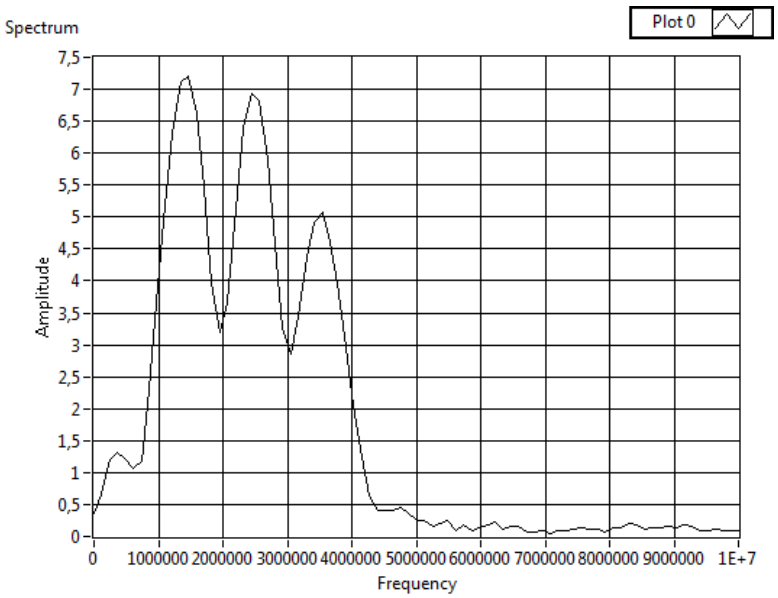

Figure 4.36 shows the frequency response of the inverse filter used to compensate for the twin-peaked frequency response of transducer PATR. The peaks at 2MHz and 3MHz are compensated by the dips at the same frequencies in the frequency response of the inverse filter. Figure 4.35 shows the resulting pressure pulse at focus when the above excitation pulse is used. The tail of the pulse is much smaller

compared to the pulse in Figure 4.32. Figure 4.38 shows the frequency response of the transducer including the inverse filter. The amplitude has a single peak.

Figure 4.87
Measured pressure pulse at focus when the inverse excitation pulse is used.

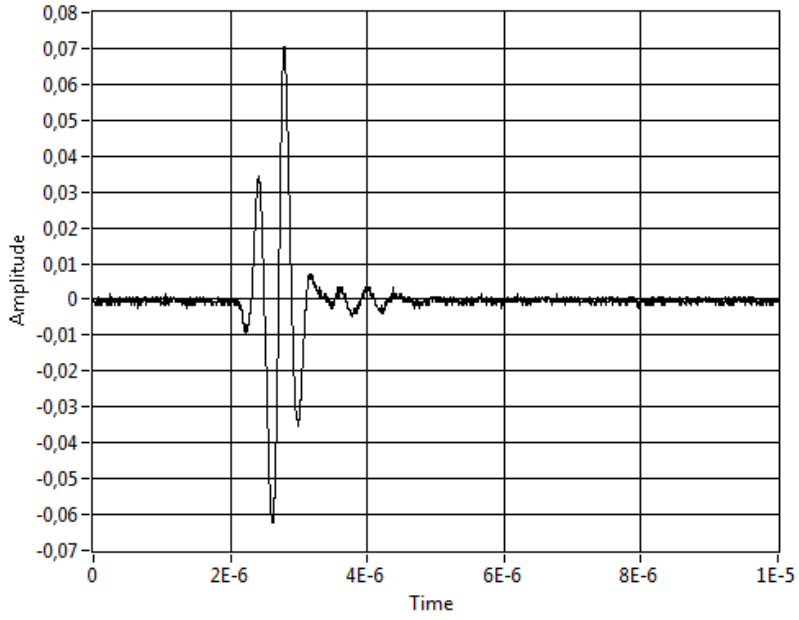

Figure 4.88
Frequency response of transducer PATR including the inverse filter.

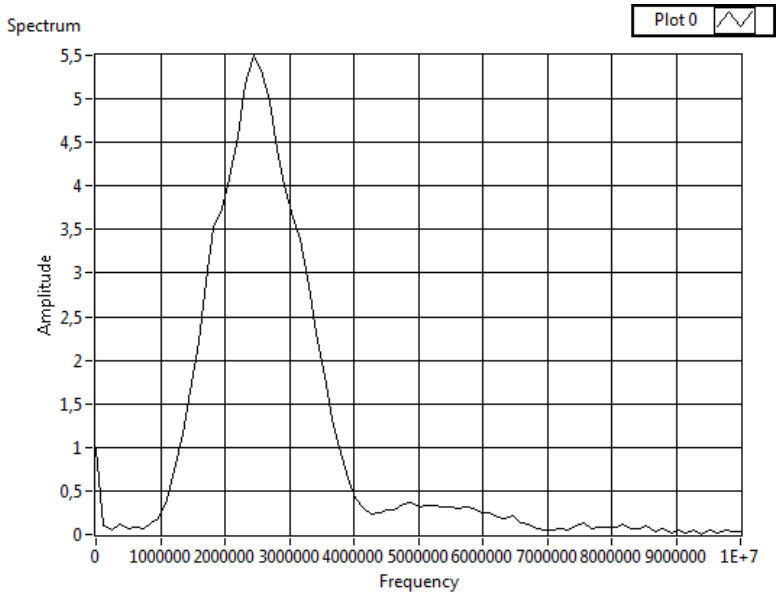

4.5.3 Measurement of reflection

Transducer PATR was designed for measurements of reflections with the PZT layer as transmitter and the PVDF layer as receiver. To test the round-trip performance, a brass object was made. The brass object was made of a cylinder of diameter 8mm and made conical in one end so that the smaller end has a diameter of 1.2mm and therefore an area of 1 square millimeter. The area of the large end is 50 square millimeters. The measurements were done with a lens of focal length 75mm attached to the transducer. Figure 4.39 shows the measured reflex pulse when the small end of the brass object was placed in the focal plane, z = 75mm, and Figure 4.40 shows its frequency spectrum. The signal level in this measurement is relatively low and we see a considerable level of noise in the measured reflex pulse. The pulse has been prolonged with approximately half a period compared to the pulse measured with the hydrophone in Figure 4.37. The center frequency of the reflex pulse is at 3MHz, while the center frequency of the transmitted pulse is at 2.5MHz, see Figure 4.38.

The brass object was also measured with the large end towards the transducer. Figure 4.41 shows the reflex pulse from the large end placed in the focal plane, z = 75mm, and Figure 4.42 shows its frequency spectrum. The signal to noise ratio is considerRably increased in this measurement due to the larger reflector. The reflex pulse in Figure 4.41 has a phase shift of 90 degrees but is not prolonged compared to the transmitted pulse shown in Figure 4.37. The center frequency of the reflex pulse is 2.5MHz as was the case with the transmitted pulse, see Figure 4.42.

The receiver characteristics of the transducer PATR is not known, but it was assumed that the frequency response should be relatively constant over the frequencies between 1 and 3 MHz. A point reflector in the focal point should therefore give a reflex pulse equal to the transmitted pulse in Figure 4.37 and a frequency spectrum equal to the spectrum in Figure 4.38. However, the small end is not a point object, and the reflectors directivity will be a function of the frequency. The transmitted frequency of the transducer is significant between 1.5MHz and 3.5MHz and the directivity will increase with a factor of 5 between 1.5MHz and 3.5MHz. This is why the frequency spectrum in Figure 4.40 has a center frequency around 3MHz.

The larger end of the brass object work as a plane reflector. The diameter of 8mm covers most of the beam as shown in Figure 4.34 where the beam diameter at focus is about 4mm. The directivity of a plane reflector is not frequency dependent. The

frequency spectrum in Figure 4.42 is therefore almost the same as the frequency spectrum of the transmitted pulse in Figure 4.38. The reflected pulse in Figure 4.41 will therefore be used as the reference pulse for the reflection measurements.

Figure 4.89
Reflexpulse from the small end of the brass object

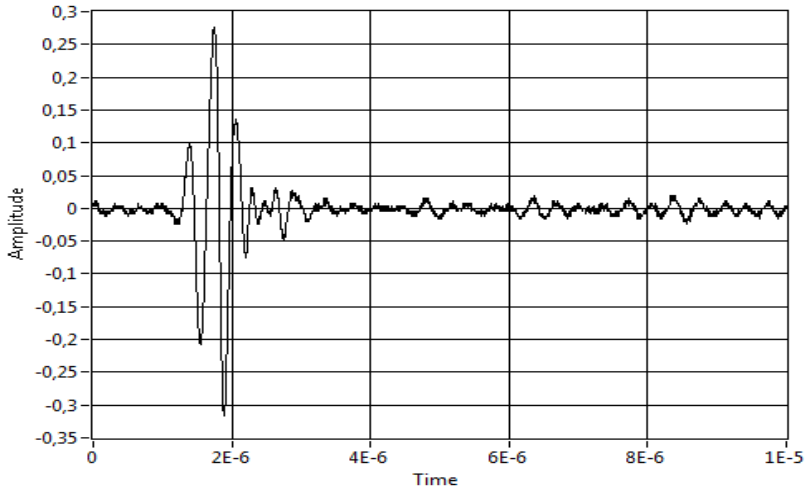

Figure 4.90
Frequency response from the small end of the brass object.

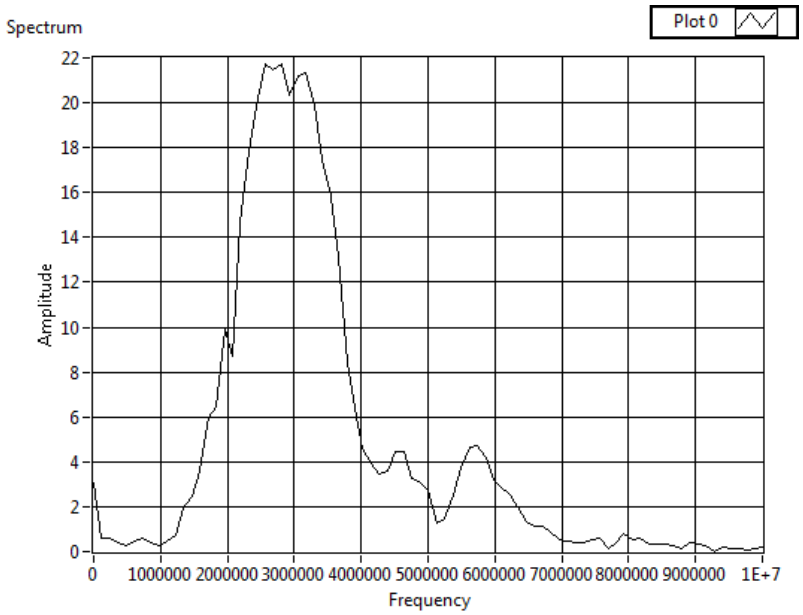

Figure 4.91
Reflex pulse from the large end of the brass object.

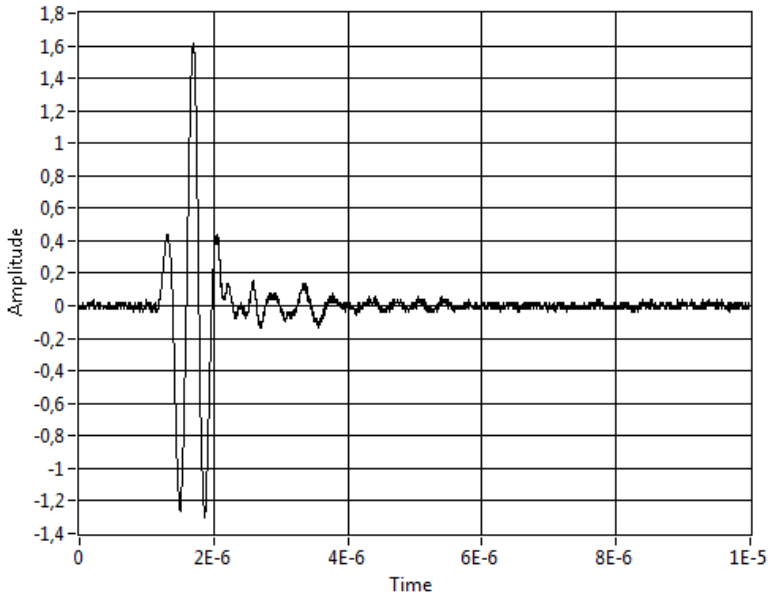

Figure 4.92
Frequency spectrum of reflex pulse from the small end of brass object.

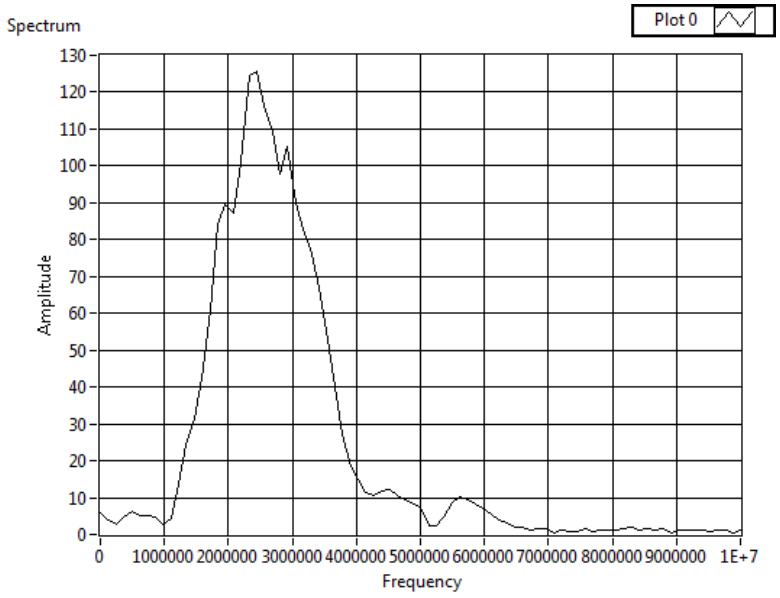

4.5.4 Measurement of thickness

The reflected pulse from the larger brass object is a well-defined short pulse without a disturbing tail. The transducer is therefore well suited for measuring thickness of semi-transparent objects. The thickness of objects that we put in a water tank can be measured up front and rather than measuring the thickness, we can calculate the speed of sound in the material at hand by measuring the time delay between the two reflections. In biological tissue, however, we normally assume a speed of sound and the time delay between reflections can be used to measure thickness. An example is measurement of the intima media thickness (IMT) of the carotid artery for detection of cardiovascular disease.

Four different plastic plates were measured. They were lined up in the water tank, at the focal plane of the transducer, and they were adjusted to give maximum reflection back to the hydrophone. The signal was recorded with the digital storage oscilloscope, and an attempt was made to do amplitude detection of the signal as well as detection by deconvolution of the measured reflections.

The first plastic plate was PMMA (polymethyl methacrylate) with thickness 1.8mm. Figure 4.43 shows the reflection measurement. The recorded signal consists of two pulses. The first pulse is a reflection from the water/plastic interface and the second is from the plastic/water interface. The first pulse is positive, and the second negative as compared to the reflected pulse in Figure 4.41. Thus, we can conclude that the plastic has a higher acoustic impedance than water. Figure 4.44 shows the amplitude detected signal. The signal is multiplied by the center frequency and low pass filtered with the center frequency as cut-off frequency. The time delay between the two reflections is 1.6μs. The thickness of the plate is 1.8mm. The speed of sound in the plastic is therefore (2x1.8mm/1.6μs) = 2250m/s. This is reasonable for a relatively hard plastic as PMMA. The density of PMMA is around 1200kg/m^3 and the acoustic impedance is 2.76Mrayl. The reflection coefficient of the water/PMMA interface becomes (2.76-1.5)/(2.76+1.5) = 0.30 or 30%.

Figure 4.93
Measured reflection from the PMMA of thickness 1.8mm

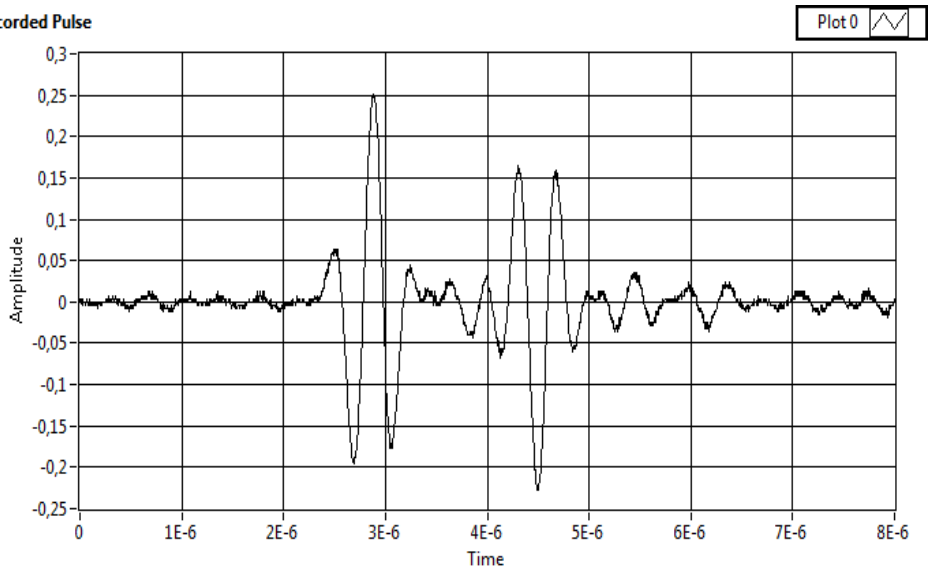

Figure 4.94 Amplitude detected measurement of reflections from a 1.8mm thick plate of PMMA.

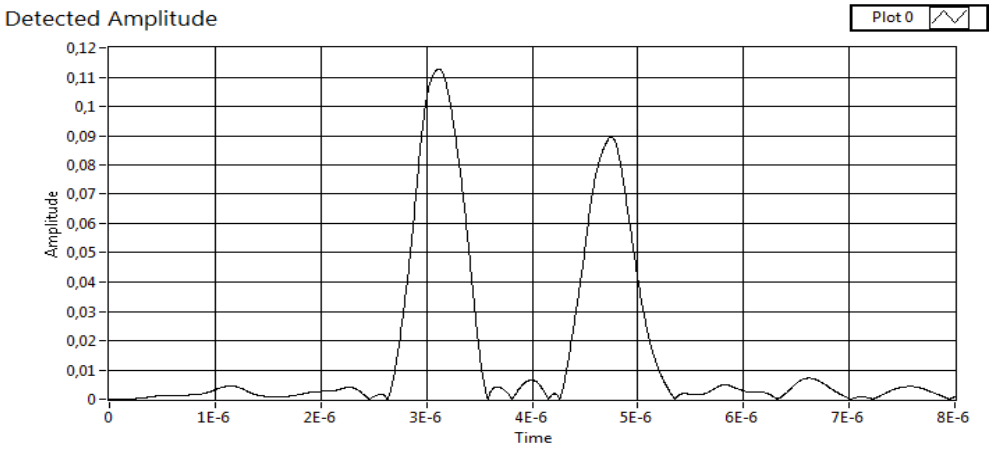

Figure 4.95
Reflection from the 0.75mm PS plate

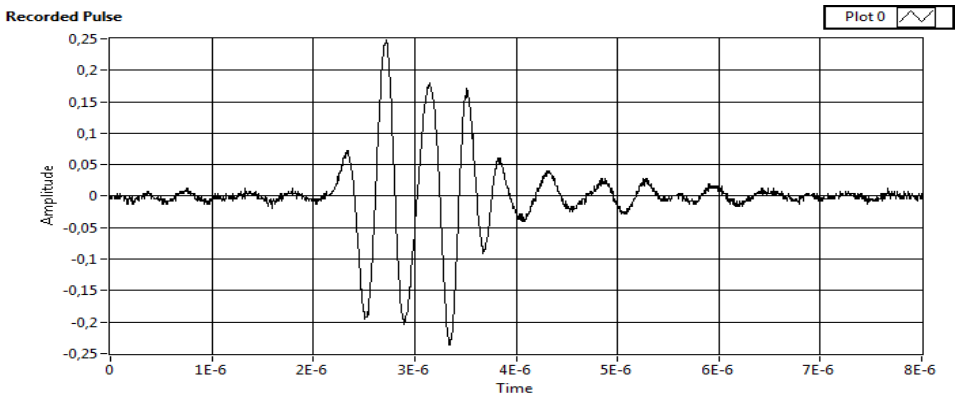

The second plastic plate is of Polystyrene (PS) and is 0.75mm thick. Figure 4.45 shows the measurement. The two pulses are now so close that they interfere with each other, but the peak values can still be identified. The time delay between the two reflections is around 0.65μs and this is also the approximate pulse length of the transducer and therefore at the resolution limit. Using this measurement, we find that the speed of sound in PS is around 2300m/s. Figure 4.46 shows the amplitude detected measurement and the two peaks are barely separable.

Figure 4.96
Amplitude detected measurement of reflections from a 0.75mm thick plate of PS.

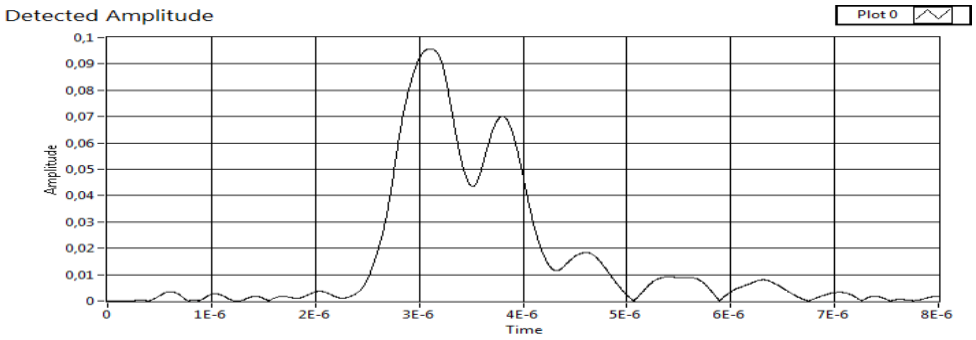

Figure 4.97
Measured reflection from the 0.3mm thick plastic sheet

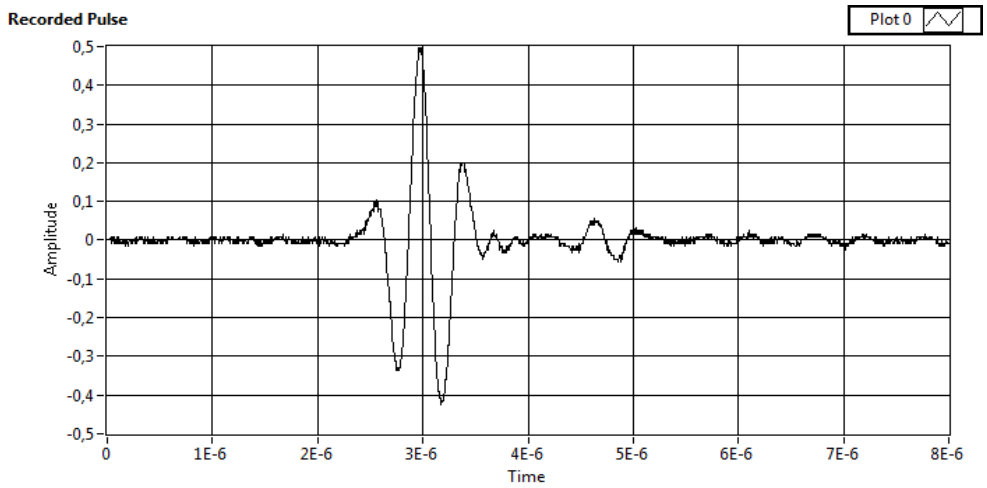

The third plastic came from a plastic packaging of unknown material, but possibly also polystyrene. It was measured to be 0.3mm thick. Figure 4.47 shows the measurements. The two pulses are fully interfered and cannot be separated, but we observe that the amplitude of the pulse in Figure 4.46 is twice that of the pulses in Figure 4.43. This indicates that there is fully constructive interference between the positive and negative pulse. The pulse is only half a period longer than the single reflections and this indicates that the time delay of the second negative pulse is one-half period of the signal. At 2.5MHz, the period is 0.4μs and the time delay between the two pulses is 0.2μs. The amplitude-detected signal in Figure 4.48 is single peaked and the two reflections are not resolved. The width of the signal is however approximately 0.2μs wider than the widths of the peaks in Figure 4.44, also indicating that the pulse is half a period longer. A thickness of 0.3mm and a time delay of 0.2μs gives a speed of sound in this plastic of 3000m/s, but the uncertainty of the measurement is large and the uncertainty of the speed of sound measurement is 3000±1000m/s.

Figure 4.98
Amplitude detection of the measurement of reflections from a 0.3mm thick plastic.

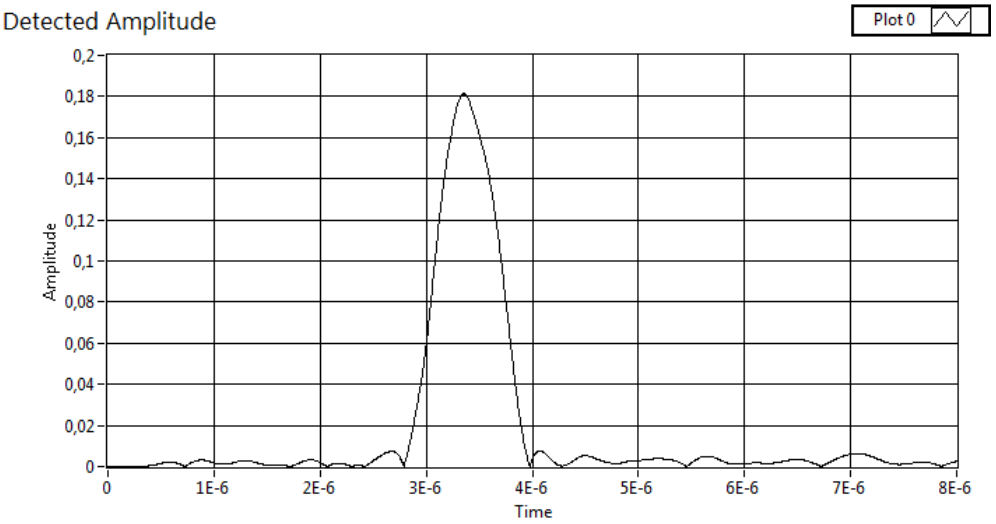

4.5.5 Detection of thickness by deconvolution

The method of deconvolution or inverse filtering has a potential of improving the resolution of the thickness measurement. However, inverse filtering involves the division of a measured frequency response with a reference signal and the frequency response of the reference may be zero within the bandwidth of interest. A bandwidth limitation may therefore be required, and this will in turn compromise the resolution of the method.

As a reference reflex signal, the reflex from the hydrophone holder was used. The hydrophone holder is made of PMMA and should therefore give a reflex that is similar to the chosen objects. The hydrophone holder is an inch thick and the first reflex from the water/plastic interface is easy to separate. The reflex and its frequency spectrum are shown in Figure 4.49.

Figure 4.99
Measured reference pulse used for deconvolution of the measured objects.

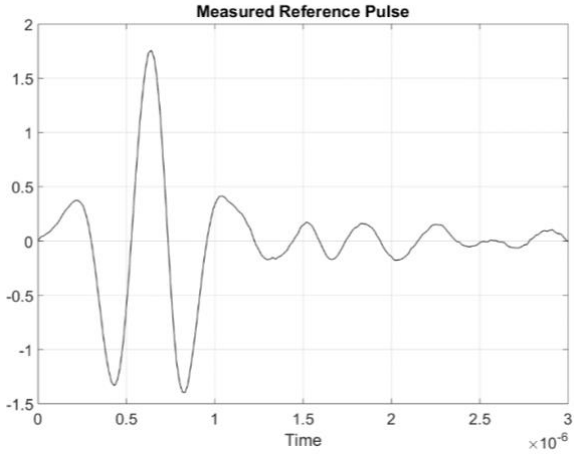

Figure 4.100
Measured reference frequency spectrum used for deconvolution of the measured objects.

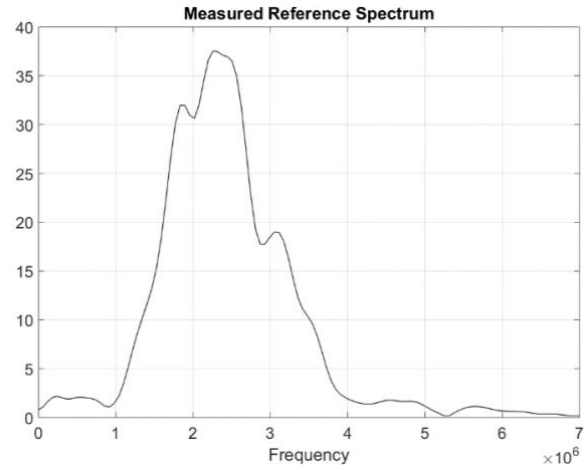

Inverse filtering is a technique that in theory shall expand the bandwidth of the measurement by using the reference as a correcting frequency spectrum. We can compensate for the limited bandwidth by dividing the measured signals frequency spectrum with the reference frequency spectrum. Let us call the measured signal from the object, x(t), and its Fourier transform, X(f). Likewise, we call the reference signal, r(t), and its Fourier transform, R(f). The resulting frequency spectrum after inverse filtering of the measured signal is given by:

$$Y(f) = X(f)/R(f)$$

The resulting time domain signal is:

$$y(t) = \mathcal{F}^{-1}\left\{\frac{X(f)}{R(f)}\right\}$$

the inverse Fourier transform of the ratio between the measured spectrum signal and the reference spectrum. This result, y(t), is also called the deconvolution of x(t) with respect to r(t). In theory, the result should be an impulse function at each reflecting surface of the object. However, the reference signal is bandlimited and the division with R(f) will result in division with zero or values close to zero. The division with the reference must therefore be limited to a bandwidth where R(f) has a significant value. Figure 4.49 shows that R(f) has a significant value only between 1 and 4MHz.

The reflected signal from the 1.8mm thick plate of PMMA was shown in Figure 4.43. The first reflection from the water/plastic-interface and the second reflection from the plastic/water-interface are well separated. As a first test of the method with deconvolution, this object was chosen. Figure 4.50 shows the frequency spectrum of the measured signal from the object as the solid line and the frequency spectrum of the reference signal as the dashed line. The transducer bandwidth is evident in both spectra, between 1 and 4MHz. However, some signal of interest is also apparent over the bandwidth between 0 and 5MHz. The spectrum was therefore rounded off with a half period sine function between 0 and 5 MHz:

$$W(f) = \sin\left(\frac{\pi f}{5MHz}\right)$$

Figure 4.101
The frequency spectrum of the reflected signal from the 1.8mm PMMA object (solid line) and the frequency spectrum of the reference signal from the hydrophone holder (dashed line).

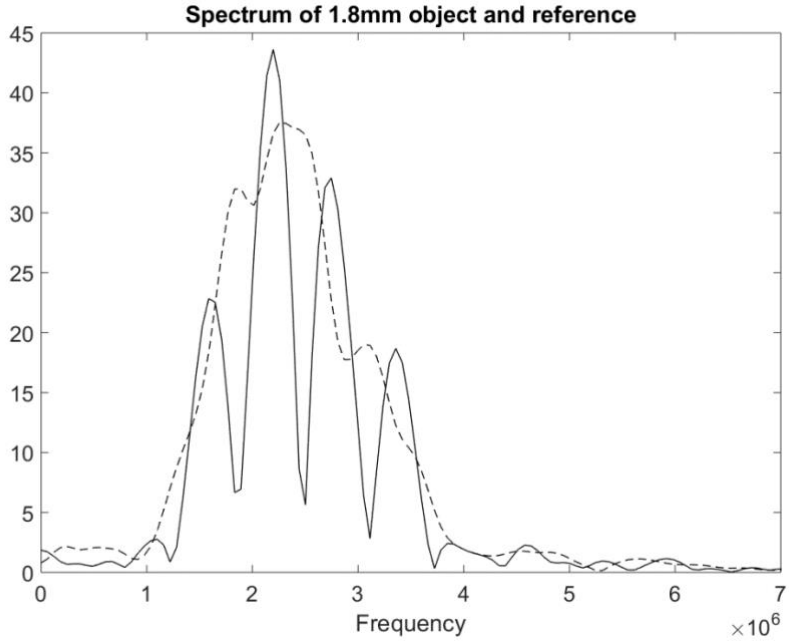

Figure 4.51 shows the frequency spectrum after inverse filtering of the signal from the object. This is the spectrum of the signal, X(f), divided by the spectrum of the reference signal, R(f), and multiplied with the window function, W(f).

$$Y(f) = \frac{X(f)}{R(f)} W(f)$$

Figure 4.102
Spectrum of the inversely filtered reflection from the 1.8mm PMMA object.

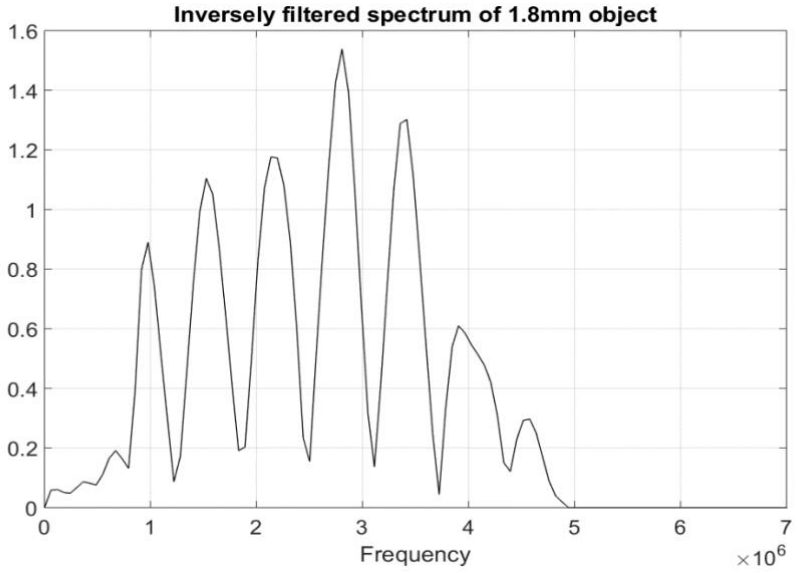

Figure 4.103
The deconvolved reflex from the 1.8mm PMMA object.

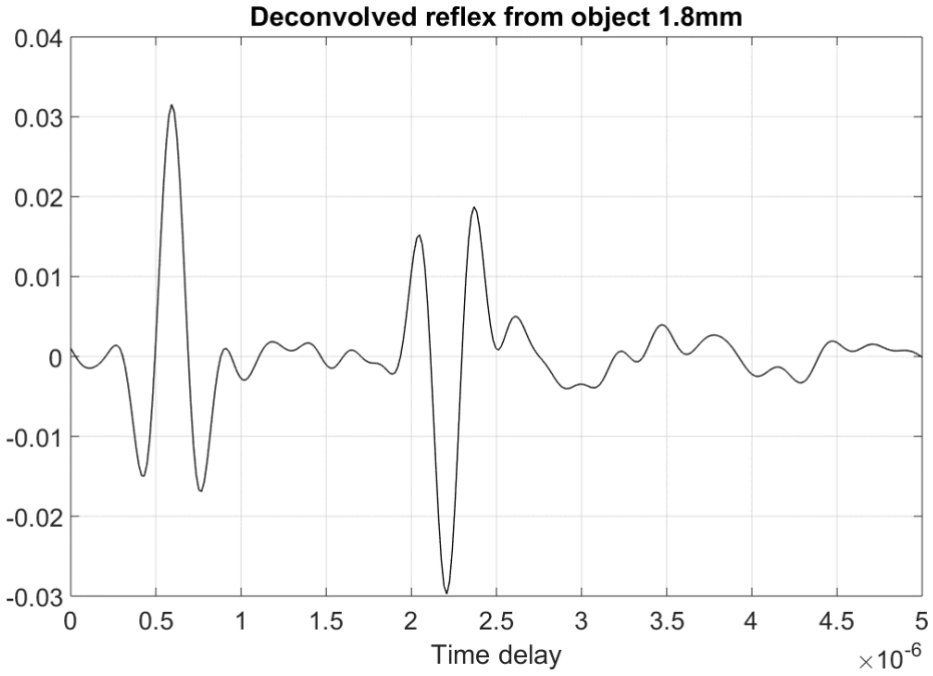

Figur 4.50 shows the deconvolved signal from the 1.8mm PMMA object, which is found by taking the inverse Fourier transform of the spectrum in Figure 4.51. The first positive reflection and the second negative reflection is evident in Figure 4.52.

The time delay between the two reflections is 1.6μs. The speed of sound in this PMMA material is therefore 2250m/s. The same time delay was also measured from the original signal from the 1.8mm PMMA object in Figure 4.53. This was possible due to the good separation of the first and the second reflection.

To test the method further, we look at the reflex from the 0.75mm polystyrene object. The first and the second reflection from this object was hardly resolved in Figure 4.45. Figure 4.53 shows the result of the deconvolution method described above. In this case, it is easy to distinguish the first positive and second negative reflection from the object. The time delay between the two reflections is 0.64μs and the calculated speed of sound in polystyrene is 2340m/s.

To test the resolution of the thickness measurement, the reflections from a packing material of thickness 0.3mm was measured. Figure 4.47 showed the measurement. In this case, the first and second reflection were not separable. Figure 4.54 shows the result after deconvolution, following the same procedure as describe above. The measured time delay between the first and second reflection is 0.24μs. The speed of sound in this material is therefore 2500m/s.

Finally, an even thinner plastic material was measured. A plastic sheet foil used for overhead projectors was measured to a thickness of only 0.13mm. Figure 4.55 shows the measured reflection from the foil and Figure 4.56 shows the measured reflection after deconvolution. The measured time delay between the positive and the negative peak in the signal is 0.155μs. Using this time delay to estimate the speed of sound in this plastic material, give a speed of sound equal to 1680m/s. This estimate is most likely to low, and this is probably due to interference between the two reflections and that the time resolution of the measurement is inadequate for this object.

Figure 4.104
Deconvolved reflex from the 0.75mm polystyrene object. The time delay between first and second reflection is measured to be 0.64μs.

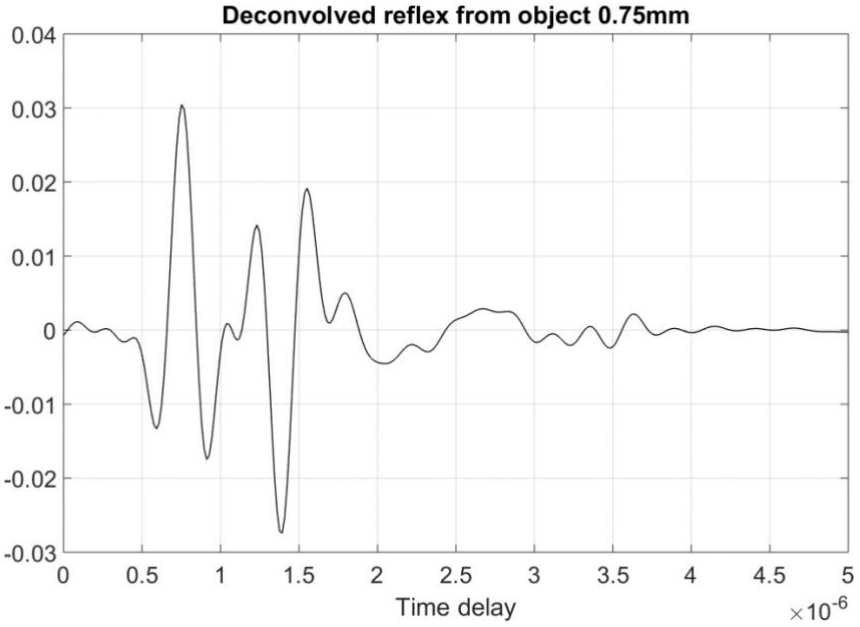

Figure 4.105
Deconvolved reflex from the 0.3mm packing object. The time delay between first and second reflection is measured to be 0.24μs.

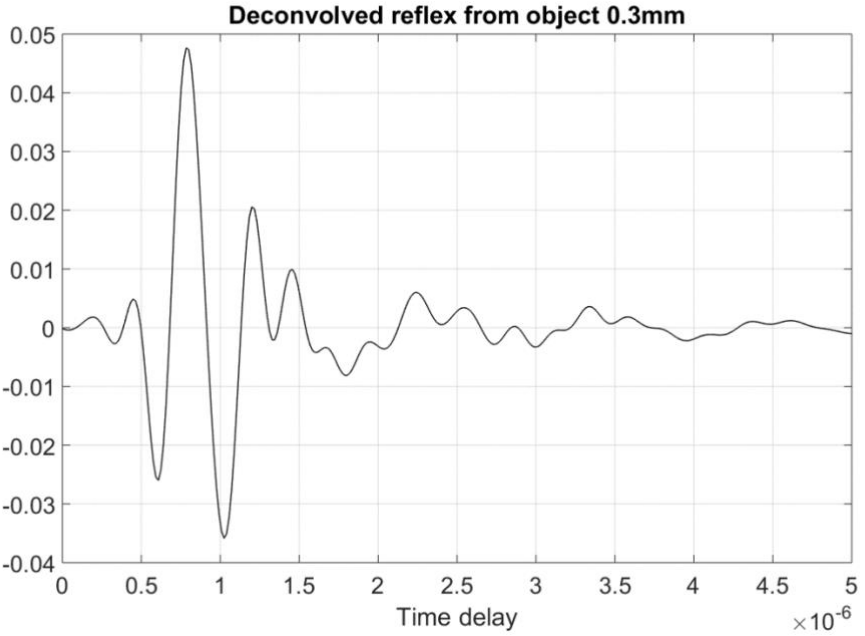

Figure 4.106
Measured reflection from the thin foil of only 0.13mm thickness.

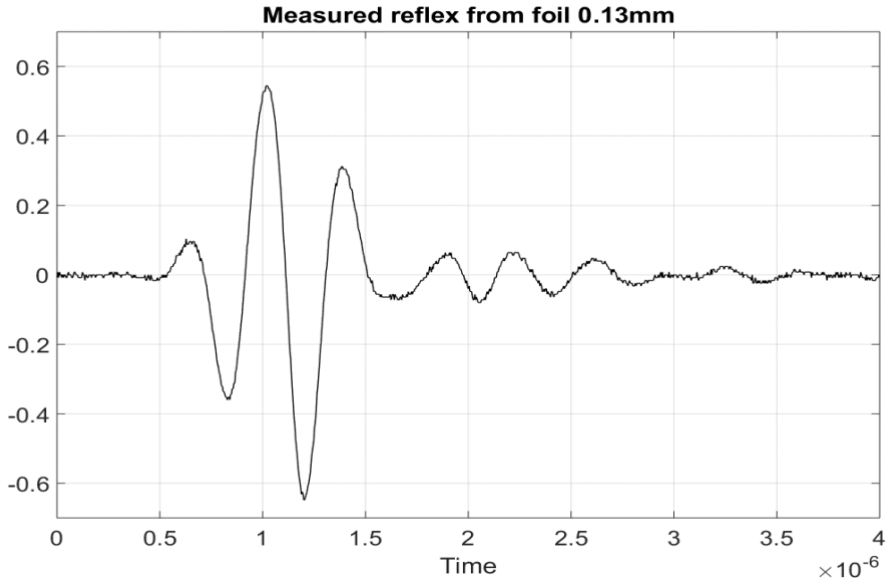

Figure 4.107
Deconvolved reflex from foil 0.13mm thick. The time delay between the positive and the negative peak is 0.155μs.

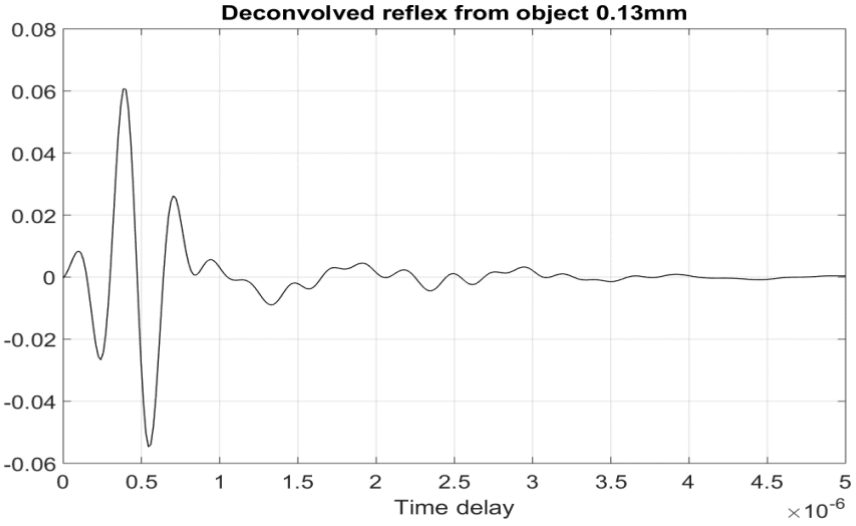

5 Discussion and Conclusions

This report is a summery of my ultrasound activity at Oslomet. The most important result is the development of the novel numeric algorithm for calculating the spatial impulse response of an arbitrary source. There are numerous analytic solutions for calculating the spatial impulse response, but they are only piecewise analytic and special precautions must be taken at the critical timepoints where the analytic functions intercept. A numeric algorithm work for all source functions, but the calculation time will be larger. The bottleneck in the numeric calculation is the calculation of R, the distance from each source element to the observation point. The calculation time is therefore proportional with the number of source elements. The source elements must be smaller than half the wavelength, but to reduce numeric noise the element size is often selected even smaller. The novel numeric method presented in this report reduce the numeric noise with the method of weighted binning and the element size can therefore be set to the limit of half a wavelength of the highest frequency in question. The method of weighted binning can therefore reduce the calculation time with a low noise level. Chapter 3.1 qualify the method and is used in all calculations of pulsed fields in this report.

The measurement tank was built up over time and it is the final version that is described in Chapter 4.1. The measurements were read from Labview in most cases, but the time-pulses could also be read from the oscilloscope and processed in Matlab. Many of the measurement of pulses and beam profiles were done to qualify the calculation. Most of the measurements and calculations were in excellent agreement with a few exceptions linked to the individual transducers.

The first transducer, named transducer 1, was my 40 year old Dr.ing.-transducer. The impulse response and the beam profiles were in good agreement with theory, except in the near field. This was most likely due to asymmetric support of the PZT disc and soldering of the leads.

The hydrophone and the three other transducers were all produced by Precision Acoustics (Durham, UK). The hydrophone including a preamplifier was calibrated for frequencies between 1 and 20MHz and the sensitivity was 200mV/MPa at 2-3MHz. The hydrophone had a diameter of 0.5mm and this is therefore the spatial resolution of the measurements.

The first transducer from PA was the focused transducer with heavy backing and no front matching named PA75. The intension of this transducer was to generate non-linear effects. The first measurement was to find its impulse response and the frequency response. It came out as a surprise that this transducer had a twin-peaked frequency response. A transducer like this should have a maximum response at the center frequency and monotonically fall of towards lower and higher frequencies. The twin peaked frequency response must therefore be caused by the proprietary impedance matching network. Anyway, a twin-peak frequency response results in a pulse response with a significant tail as seen in Figure 4.32. A tailor-made excitation pulse was therefore designed and applied in the measurements. The resulting pulse response in Figure 4.34 shows that this technic of inverse filtering worked well as the pulse response has virtually no tail. The measured and calculated beam profiles in Figure 4.12 through Figure 4.19show excellent agreement for the main lobe, but for the of-axis field there are some disagreements. The measurements are symmetric but at a higher level than the calculations. The transducer seems therefore to vibrate in symmetric modes, but not only as a piston.

Harmonic effects of ultrasound propagation were studied by turning the output voltage of the amplifier up 10-fold to 400Vpp. The non-linear effects are evident in pulse in Figure 4.54 and the frequency spectrum of the pulse shows several harmonics. Ultrasonic transducers for imaging are band limited and only the second harmonic is of practical importance. Two 8^{th}-order Butterworth filters were designed in Labview to separate out the first and second harmonics. The separated pulses and their frequency spectrums are shown in Figure 4.56 through Figure 4.59. These filters were applied when the beam profiles were measured. The first harmonic beam profiles look much like the beam profiles measured under linear condition. The second harmonic beam profiles are narrower also as expected. No software for calculating non-linear propagation was available, so it is difficult to draw any conclusions on the quality of these measurements. The pulse inversion technique is an alternative to using filters.

The second transducer from Precision Acoustics was an unfocused transducer with a quarter wave matching layer in front and air backing, PAplan. This transducers pulse response and frequency response are shown in Figure 4.73 and Figure 4.74. Except for the excitation of a third harmonic, this transducer gives a short pulse well suited for imaging. To eliminate the third harmonic, the transducer was excited with a rectangular pulse of 150ns. The frequency spectrum of a rectangular pulse will have zeros at frequencies f=n/T, where T is the pulse length and n=1, 2, 3… For T=150ns

the first zero is at f=1/150ns=6.7MHz. When this excitation pulse is used, we see in Figure 4.75 and Figure 4.76 that the third harmonic is gone.

Figure 4.77 shows the beam profile through beam waist at z=75mm where the beam is at its narrowest. The beam diameter is more than 6mm and this transducer must be focused with a lens. The lens was made of a silicon rubber and attached to the front of the transducer. The lens was tested by calculating and measuring the on-axis field. The PAplan with the lens performed equal to PA75.

The last transducer from Precision Acoustics was designed to measure reflections from objects in the water tank. The transmitting transducer is a half wavelength PZT element with diameter 15mm. In front the transducer has a PVDF layer designed as a quarter wave matching layer. The PVDF layer also work as the receiver of reflections. The impulse response and the frequency response of this transducer is shown in Figure 4.82 and Figure 4.83. The twin-peaked frequency response and the lager tail of the pulse show that the acoustic matching did not work as expected. An excitation pulse was design with the method of inverse filtering. The outcome was a relatively complex pulse shown in Figure 4.85, but when used as the excitation pulse, the pulse response and frequency response of the transducer were improved as shown in Figure 4.87Figure 4.88 This excitation pulse and a lens with focal length 75mm were used in the following measurements of reflections.

A brass cylinder was used as a test object for the reflection measurements. The cylinder was 8mm in diameter and made conical in one end so that the diameter at the tip was 1.2mm. Thus, we had a plane reflector with a small end that was 1.2mm in diameter and a large end that was 8mm in diameter. The center frequency of this transducer is 2.5MHz and the wavelength is 0.6mm. The small end is 2 wavelengths in diameter and the directivity of the object therefore has a strong frequency dependence and is not suitable as a test object. The large end covers most of the beam in focus, as can be seen from the beam profile in Figure 4.84. This end is therefore suited as a test object. The measured reflection pulse and its frequency spectrum is shown in Figure 4.91 and Figure 4.91.The result is similar to the measured pulse response and frequency response of the transmitting transducer. This implies that the frequency response of the receiver is frequency independent over the frequency band in question.

To test the depth or time resolution of the transducer several planar plastics were measured. The plastics had a measured thickness of 1.8mm, 0.75mm, 0.3mm and

0.13mm. Two detection methods were used to detect the time difference between the two reflected pulses, amplitude detection and deconvolution. Deconvolution turned out to give the best resolution. The plastic of thickness 0.3mm gave a time delay between the two pulses of 0.24μs and the plastic of thickness 0.13mm gave a time delay of 0.16μs. The last one with a degree of uncertainty. The time resolution was therefore estimated to be 0.2μs. At frequency 2.5MHz the period is 0.4μs, implying that the time resolution is one half period when using deconvolution to detect the reflected pulses.

References

[1] G. E. Tupholme, ‘Generation of acoustic pulses by baffled plane pistons’, Mathematika 16, 209-224 (1969).

[2] P.R. Stepanishen, ‘The time-dependent force and radiation impedance on a piston in a rigid infinite planar baffle’, J. Acoust. Soc. Am. 49, 841-849 (1971).

[3] P.R. Stepanishen, ‘Transient radiation from pistons in an infinite planar baffle’, J. Acoust. Soc. Am. 49, 1629-1638 (1971).

[4] G. R. Harris, ‘Review of transient field theory for a baffled planar piston’, J. Acoust. Soc. Am. 70, 10-20 (1981).

[5] M. Arditi, F. S. Foster, and J. W. Hunt, ‘Transient fields of concave annular arrays’, Ultrason. Imaging 3, 37-61 (1981).

[6] D. R. Dietz, S. J. Norton and M. Linzer, ‘Wideband annular array response’, 1978 IEEE Ultrasonic Symp., 206-211, (1978).

[7] A. Penttinen and M. Luukkala, ‘The impulse response and pressure nearfield of a curved ultrasonic radiator’, J. Phys. D 9, 1547-1557 (1976).

[8] G. R. Harris, ‘Transient field of a baffled planar piston having an arbitrary vibration amplitude distribution’, J. Acoust. Soc. Am. 70, 186-204 (1981).

[9] J. N. Tjotta and S. Tjotta, ‘Nearfield and farfield of pulsed acoustic radiators’, J. Acoust. Soc. Am. 71, 824-834 (1982).

[10] J. D’hooge, J. Nuyts, B. Bijnens et al, ‘The calculation of the transient near and far field of a baffled piston using low sampling frequency’, J. Acoust. Soc. Am. 102, 78-86 (1997).

[11] A. Ortega, L. Tong and J. D’hooge, A new analytic expression for a fast calculation of the transient near and far field of a rectangular baffled piston’, Ultrasonics 54, 1071-1077, (2014).

[12] J. Cheng, J. Lu, W. Lin and Y.-X. Qin, ‘A new algorithm for a spatial impulse response of rectangular planar transducers’, Ultrasonics 51, 229-237, (2011).

[13] J. A. Jensen and N. B. Svendsen, ‘Calculation of pressure fields from arbitrary shaped, apodized and excited ultrasound transducers’, IEEE trans. UFFC, Vol. 39, No. 2, 262-267 (1992).

[14] N. Sponheim, ‘An error reduction algorithm for numeric calculation of the spatial impulse response’, POMA 22, 020003 (2014). [DOI: 10.1121/2.0000008]

[15] N. Sponheim, ‘Simulation of pulsed ultrasonic fields of rectangular sources’, Report Oslo Met, 2015.

[16] R. Krimholtz, D. Leedom and G. Matthaei,’New Equivalent Circuit for Elementary Piezoelectric Transducers’, Electronics Letters 6, 398-399, 1970.

[17] N. Sponheim, ‘Transient ultrasonic fields of efficient broadband piezoelectric transducers’, Dr.ing.-thesis submitted to The Norwegian Institute of Technology in August 1985.

Appendix: Program code

Figure A.1
Overview of programs for calculation of pulsed ultrasonic fields.

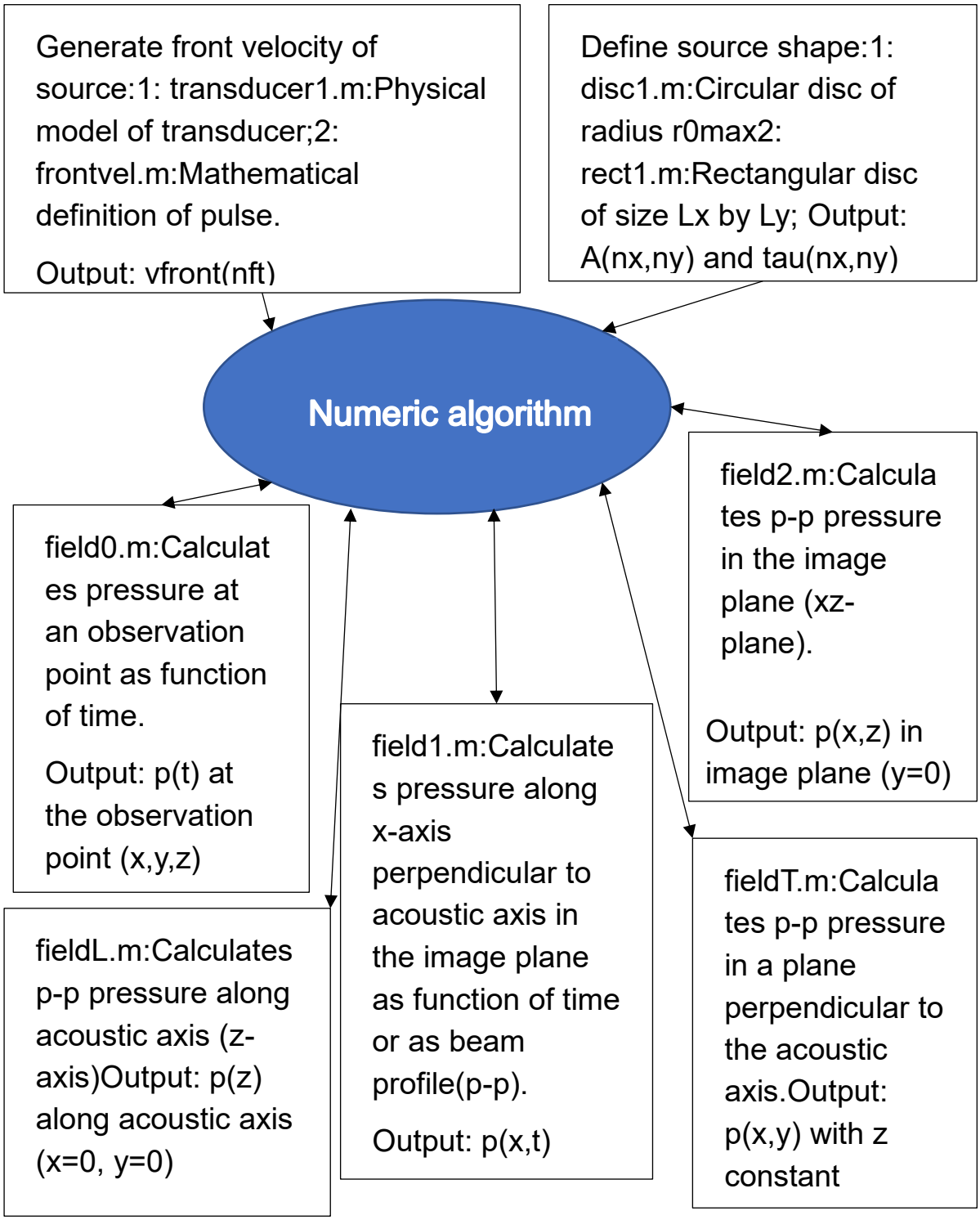

Figure A.1 shows an overview of the programs used to calculate the pulsed ultrasonic fields. The pulsed fields are calculated for different observation geometries with the different field programs. They all use the same numeric algorithm that is based on weighted binning. But prior to embarking on the field calculation, the source must be defined. The source is defined by the normal velocity on the front of the source and by the shape of the source surface. The normal velocity of the source can be generated by two different programs. The simplest program is frontvel.m. This program is just a mathematical description of a pulse that is used in the following calculations. A more complex program is transducer1.m. This program is a mathematical model of a thin disc piezo-electric disc. The program calculates the electric input impedance of the transducer, the frequency response from the electric port to the front velocity of the transducer and the corresponding impulse response of the transducer. This impulse response is used as the front velocity in the following calculations. This require that the transducer is excited with an impulse at the electric port.

The shape of the source front must also be defined before calculating the field. In medical ultrasound, two different shapes are in regular use. These are circular disc transducers and rectangular transducers as phased arrays or linear arrays. A circular disc transducer can be defined with the program disc1.m. The inputs to this program are the diameter of the disc and the focal length of the disc. A rectangular transducer can be defined with the program rect1.m. The inputs to this program are the length and the width of the transducer front as well as the focal length in azimuth and elevation.

When the source is properly defined, the field calculations can start. The parameters and the results from the source definition programs must be stored in the working space of MATLAB. The pressure field is a function of the observation coordinates, (x,y,z), as well as time, p(x,y,z,t). In order to present the calculations, the 4-dimensional function is simplified by calculating the field along characteristic axis and planes. The time dimension is in most calculations reduced to a peak-peak value of the pressure. The spatial axes are standardized, so that the z-axis is the acoustic axis starting at the center of the source and the x-axis is defining the image plane, so that the xz-plane is the assumed image plane of a 2D-ultrasound scanner. The program field0.m calculates the pressure field in a single observation point as function of time, p(t). The program field1.m calculates the pressure field along the x-axis at a given z-position. The field is presented as a pulse in space as a function of time or as a beam profile as peak-peak pressure. The program field2.m calculates the peak-peak pressure in the image plane, p(x,z). The field is presented as a contour plot or a beam in space. The program fieldL.m calculates the pressure field along the acoustic axis, p(z), and presents the peak-peak value. Finally, the program fieldT.m calculates the pressure field transversal to the acoustic axis at a given

depth, p(x,y). The field is presented as a contour plot of the peak-peak pressure. This is to accommodate the rectangular shaped sources, for circular sources the transversal field will be circular symmetric.

A.1 Transducer1.m

This program utilizes a simple one-dimensional model of a thin disc piezo-electric transducer. The model is referred to as the KLM-transmission line model after Krimholtz, Leedom and Matthaei [16]. The transducer is modelled as a transmission line with a half period length at the design frequency. The electro-acoustic coupling is modelled at the center of the disc, see Figure A.2.

Figure A.2
The KLM-transmission line model of a thin disc piezoelectric transducer

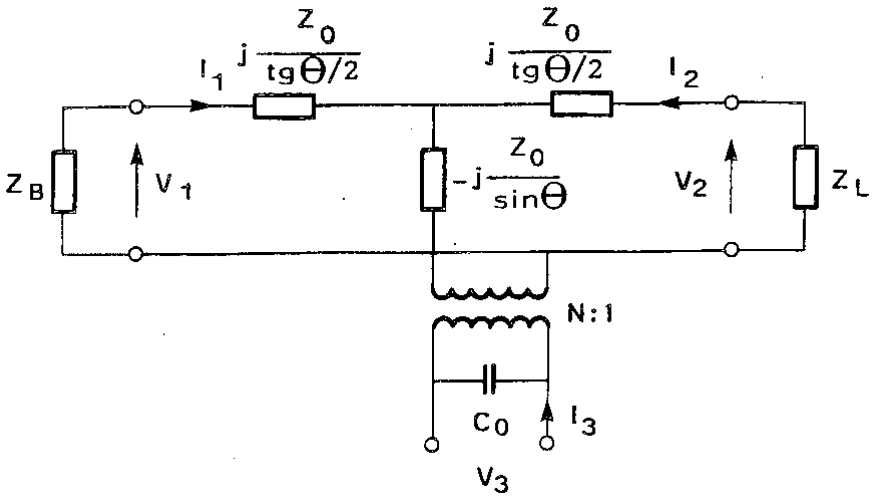

Here the following definitions and notations are used:

Wavenumber: $k_0 = \omega\sqrt{\rho/\kappa}$

Angular frequency: ω

Mass density: ρ

Compressibility: κ

Angular thicknesfs: $\theta = k_0 th$

Thickness of disc: th

Acoustic Impedance: $Z_0 = k_0 \kappa A/\omega$

Area of disc: A

Capacitance: $C_0 = \varepsilon_0 \varepsilon A/t$

Dielectric constant: $\varepsilon_0 \varepsilon^S$ (constant strain)

Coupling factor: $N = hC_0 = C_0/d_{33}$

Piezoelectric constant: $h = 1/d_{33}$

Backing impedance: Z_B

Load impedance: Z_L

Front port force: V_1

Velocity into front port: I_1

Back port force: V_2

Velocity into back port: I_2

Voltage at electric port: V_3

Current into electric port: I_3

The equivalent circuit in Figure A.2 can be used to calculate the electric input impedance of the transducer as: $Z_{in}(\omega) = V_3(\omega)/I_3(\omega)$.

The frequency response from voltage at the electric port to the acoustic velocity at the front port can be found as: $H(\omega) = I_2(\omega)/V_3(\omega)$.

Finally, the impulse response of the transducer can be found as the inverse Fourier transform of H(ω): $h(t) = \mathcal{F}^{-1}\{H(\omega)\}$.

To increase the bandwidth of the transducer, we can add a quarter wave matching layer on the front. The matching layer can be modelled as its cascade matrix:

$$\begin{pmatrix} V_2 \\ I_2 \end{pmatrix} = \begin{pmatrix} cos\theta & -jZ_0 sin\theta \\ j\dfrac{sin\theta}{Z_0} & -cos\theta \end{pmatrix} \begin{pmatrix} V_1 \\ I_1 \end{pmatrix}$$

Here θ is the angular thickness of the matching layer and Z_0 is its acoustic impedance. Index 1 is towards the active element and index 2 is towards the

acoustic front. This model can be used for several matching layers in cascade if required. We can also increase the bandwidth by using a heavy backing.

The program transducer1.m use the above model and is listed below. First, the physical parameters of the active element must be entered including the size and material constants. Secondly, the parameters of the backing and load as well as the quarter wave matching layer, must be entered. The frequency variable is defined as a vector, f, and the input impedance and the frequency response of the transducer can be calculated. The time variable is also defined as a vector, t, and the impulse response of the transducer can be calculated

```
%---------------------------------------------------------------
%   transducer
%---------------------------------------------------------------
% This progam simulates a thin disc ultrasound transducer using the KLM
% transmissionline model.
%
% The outputs from the program are:
% 1.The electroacoustic transferfunction, Helac=I2/Vg, from generator
% voltage, Vg, to acoustic front velocity, I2.
% 2.The electric input impedance, Z3=V3/I3, at the electric port.
% 3.The impulse response as acoustic front velocity, vfront, with a
% Diracs-delta from voltage generator.
%
% The inputs are:
%
% Transducer disc dimensions: thickness, th, and diameter, diam.
diam=12.7*10^-3;
th=0.69*10^-3;
ta=pi*(diam/2)^2;   % transducer area
%
% Transducer disc electro-acoustic parameters (PZ27)
epsstrain=830;      % relative dielectric constant under constant strain
eps0=8.85*10^-12;   % dielectric constant in vacuum
eps=epsstrain*eps0; % dielectric constant in disc
hdisc=22*10^8;      % piezoelectric coefficient
cdisc=4350;         % wave velocity in disc
Z0=34*10^6;         % characteristic impedance in disc
Zdisc=Z0*ta;        % acoustic impedance in disc
Rm=0.33*10^6*ta;    % mechanical loss equivalent in disc
%
% Calculate KLM model constants
Cdisc=eps*ta/th;    % capacitance of disc
Ndisc=hdisc*Cdisc;  % disc coupling factor
%
```

```
% Load and backing impedances
Zwater=1.5*10^6;
Zfront=ta*Zwater+Rm;   %load impedance including loss
Zair=0.4*10^6;         %divinycell
Zback=ta*Zair+Rm;      %backing impedance including loss
%
% Front matching layer
Zmatch=4.25*10^6*ta;%acoustic impedance of matching layer
cmatch=2800;        %velocity in matching layer
tmatch=0.23*10^-3;  %thichness of matching layer
%
% Calculate electric input impedance, Zin=ZA+ZB(ZC+ZD)/(ZE+ZF)
%
j=complex(0,1);     % imaginary unit
fdel=50000;        % frequency resolution
fmin=300000;        % minimum frequency
fmax=6000000;       % maximum frequency
f=(fmin:fdel:fmax); % frequency vector from fmin to fmax in steps of fdel
w=(2*pi)*f;         % angular frequency
theta=(th/cdisc)*w; % angular thickness of disc
thetamatch=(tmatch/cmatch)*w;   % angular thichness of matching layer
Zfront=Zmatch*(Zfront+j*Zmatch*tan(thetamatch))./(Zmatch+j*Zfront*tan(thet
amatch));
ZA=(-j/Cdisc)./w;
ZB=(hdisc^2/Zdisc)./w.^2;
ZC=2*Zdisc.*(cos(theta)-1);
ZD=j*(Zfront+Zback).*sin(theta);
ZE=(Zfront+Zback).*cos(theta);
ZF=j*(Zdisc-Zfront.*Zback/Zdisc).*sin(theta);
Zin=ZA+ZB.*(ZC+ZD)./(ZE+ZF);
Zphase=(180/pi).*angle(Zin);
%
% Plot input impedance
figure;
plot(f,abs(Zin),'k',f,Zphase,'k--','linewidth',2)
%plot(f,real(Zin),f,imag(Zin))
hold on
plot([1.e6 5.e6],[0 0],'k') % zero line
set(gca,'fontsize',15)
xlabel('Frequency [Hz]')
title('Transducer Input Impedance')
legend('module','phase')
axis([1000000 5000000 -100 100])
%
% Calculate transfer function Helac=I2/Vg from generator impedance to
```

```
% front velocity, I2.
%
HA=-j*Zdisc./tan(theta);
HB=-j*Zdisc./sin(theta);
HC=-j*hdisc./w;
HD=Zback-j*Zdisc./tan(theta);
Htrans=(HB-HD)./(Zfront.*HD./Ndisc-HC.*Zfront+HA.*HD/Ndisc-HA.*HC-
HB.^2/Ndisc-HC.*HD+2.*HB.*HC);
%
% Transfer through front matching layer
Hmatch=cos(thetamatch)-j*(Zfront/Zmatch).*sin(thetamatch);
Htrans=Hmatch.*Htrans;
%
% Include generator impedans
Zg=50;
Helac=Htrans.*Zin./(Zg+Zin);
Hphase=(180/pi).*angle(Helac);
%
% Plot amplitude response
figure;
plot(f,abs(Helac),'k','linewidth',2)
set(gca,'fontsize',15)
xlabel('Frequency [Hz]')
title('Transducer Amplitude Response')
%plot(f,Hphase)
%
% Find the impulse response of the transducer, vfront.
%
nft=1000;
tdel=1/(fdel*nft);
t=(0:tdel:tdel*(nft-1));
vfront=ifft(Helac,nft);
Helacint=fft(vfront,nft); % prolongation of Helac to nft points
%
% Plot front velocity
figure;
plot(t,real(vfront),'k','linewidth',1.5)
set(gca,'fontsize',15)
axis([0.0 5*10^-6 -inf inf])
xlabel('Time [s]')
title('Transducer Front Velocity')
```

The impulse response of the transducer can be used as the front velocity of the transducer, provided that, the electric excitation at the electric port is an impulse function.

A.2 Frontvel.m

The pulse shown in Figure 3.6 is a realistic imaging pulse and well suited for an imaging system. An easier way of generating a front velocity pulse is to use the program frontvel.m. This program generates a pulse as a mathematical function of time. Any pulse may be defined, from very short pulses to semi continuous pulses. In the MATLAB code below, a Hanning weighted four period pulse with center frequency of 3MHz is generated. Also, in this case a time vector and a frequency vector must be defined. A center frequency must be chosen, and the function must be defined and calculated.

```
%
%--------------------------------------------------------------------------
% FRONTVEL
%--------------------------------------------------------------------------
% Defines a front velocity vfront
%--------------------------------------------------------------------------
%
tdel=20.0*10^-9;    % time resolution
f0=3.0*10^6;         % center frequency
T0=1/f0;             % center period
iT0=round(T0/tdel); % integer of period
%
nft=1000;           % time array length
fdel=1/(tdel*nft);  % frequency resolution
t=(0:tdel:tdel*(nft-1));    % time axis
f=(0:fdel:fdel*(nft-1));    % frequency axis

% A three period Hanning pulse
%
vfront=zeros(1,nft);    % array for front velocity
for i=0:3*iT0
    vfront(i+1)=sin(2*pi*f0*tdel*i)*(1-cos(2./3.*pi*f0*tdel*i))/2;
end

% Plot front velocity
figure;
plot(t,vfront,'k','linewidth',1.5)
set(gca,'fontsize',15)
axis([0.0 5*10^-6 -inf inf])
xlabel('Time [s]')
title('Source Front Velocity')
%
% Find frequency spectrum
```

```
%
Vfront=fft(vfront,nft);
%
% Plot amplitude spectrum
figure;
plot(f,abs(Vfront),'k','linewidth',2)
set(gca,'fontsize',15)
axis([0.0 10e6 -inf inf])
xlabel('Frequency [Hz]')
title('Front Velocity Spectrum')
```

A.3 Circular disc; disc1.m

The program disc1.m defines the shape of a circular disc transducer, by defining the size of the elements and the number of elements depending on the radius of the disc. Each element is given an amplitude A, and a time delay tau. Both A and tau are two-dimensional arrays. The matrix, A, accounts for the shape as well as possible apodization of the source. The matrix, tau, accounts for the focusing of the source. The input to the program is simply the focal length and the program calculates the required time delay. The matrices A and tau are stored in the workspace.

```
%
%-------------------------------------------------------------------------
% SOURCE circular single element disc
%-------------------------------------------------------------------------
% This program calculates the source amplitude function A(x0,y0) and
% the source time delay tau(x0,y0) for a single element circular disc
% transducer with focal length F and radius r0max.
%
%-------------------------------------------------------------------------
%
% Define a uniform circular disc with unit amplitude A of radius, r0max
% and a timedelay giving a focus at F.
%
c=1500;     %speed in water
F=0.075;     % Focal length of source, if F>0.9 then infinite focus
diam=15*10^-3;   % diameter of source disc
r0max=diam/2;   % radius of source disc
%
% Define source numerical grid
delx0=0.1*10^-3; % element size of source in x-direction
dely0=delx0; % element size of source in y-direction
nr0=round(r0max/delx0); % number of radial source elements
```

```
nx0=2*nr0; % number of source elements in x-direction
ny0=2*nr0; % number of source elements in y-direction

x0=(-delx0*(nx0-1)/2:delx0:delx0*(nx0-1)/2); % x0-vector at source
y0=(-dely0*(ny0-1)/2:dely0:dely0*(ny0-1)/2); % y0-vector at source
%
% Calculate A(nx0,ny0) and tau(nx0,ny0)
taumax=(sqrt(r0max^2+F^2)-F)/c; % maximum timedelay at center of disc
A=zeros(nx0,ny0);   % Matrix for amplitude
tau=zeros(nx0,ny0); % Matrix for time delay
for i=1:nx0
    for j=1:ny0 % element position, r0
        r0=sqrt((delx0*(i-(nx0-1)/2))^2+(dely0*(j-(ny0-1)/2))^2);
        if r0<r0max
            A(i,j)=1;   % Uniform source amplitude
            if F<0.9
                tau(i,j)=taumax-(sqrt(r0^2+F^2)-F)/c;
            else
                tau(i,j)=0; % Infinite focus
            end
        else
            A(i,j)=0;   % Outside disc
            tau(i,j)=0;
        end
    end
end
figure; % Plot of source amplitude
mesh(x0,y0,A)
set(gca,'fontsize',15)
title('Source Amplitude')
xlabel('Size (m)')
figure; %Plot of source time delay
mesh(x0,y0,tau)
set(gca,'fontsize',15)
title('Source Time delay')
xlabel('Size (m)')
```

A.4 Rectangular disc rect1.m

The program rect1.m defines the shape of a rectangular disc transducer, by defining the size of the elements and the number of elements depending on the length, Lx, and width, Ly, of the disc. Each element is given an amplitude A, and a time delay tau. Both A and tau are two-dimensional arrays. The matrix, A, accounts for the

shape as well as possible apodization of the source. The matrix, tau, accounts for the focusing of the source. The inputs to the program are the focal length in azimuth, Fx, and elevation, Fy. The program calculates the required time delay. The matrices A and tau are stored in the workspace.

```
%
%------------------------------------------------------------------------
% RECT1 rectangular source function
%------------------------------------------------------------------------
% This program calculates the source amplitude function A(x0,y0) and
% the source time delay tau(x0,y0) for a rectangular Lx by Ly
% transducer with focal length Fx in azimuth or x-direction and Fy in
% elevation or y-direction. Apodization is given by Ax in the x-direction
% and by Ay in the y-direction.
%
%------------------------------------------------------------------------
%
% Define source numerical grid
%
delx0=0.1*10^-3; % element size of source in x-direction
dely0=0.1*10^-3; % element size of source in y-direction
Lx=0.02;   % Transducer length in x-direction (azimuth)
Ly=0.012;   % Transducer width in y-dimension (elevation)
nx0=round(Lx/delx0);   % Number of elements in x-direction
ny0=round(Ly/dely0);   % Number of elements in y-dimension
x0=(-delx0*(nx0-1)/2:delx0:delx0*(nx0-1)/2); % x0-vector at source
y0=(-dely0*(ny0-1)/2:dely0:dely0*(ny0-1)/2); % y0-vector at source
%
% Define a uniform source function A(x0,y0) with unit amplitude
% Define the time delay tau(x0,y0) Fx and Fy focal lengths.
%
c=1500;     % velocity in water
Fx=0.075;     % Focal length of source in x-direction
Fy=0.075;   % Focal length of source in y-direction

A=zeros(nx0,ny0);   % array for amplitude
Ax=zeros(nx0,1);    % array for apodization in x-direction
Ay=zeros(ny0,1);    % array for apodization in y-direction
tau=zeros(nx0,ny0); % array for total time delay
taux=zeros(nx0,1);    % array for time delay in x-direction
tauy=zeros(ny0,1);    % array for time delay in y-direction
tauxmax=sqrt(Fx^2-(Lx/2)^2)/c;  % maximum time delay due to Fx
for i=1:nx0  % loop for x-direction
    taux(i)=sqrt(Fx^2-x0(i)^2)/c-tauxmax; % time delay in x-direction
    %Ax(i)=sin(pi*(i-0.5)/nx0);  % Apodization in x-direction
```

```
    Ax(i)=1.;                   % No apodization
end

tauymax=sqrt(Fy^2-(Ly/2)^2)/c;  % maximum time delay due to Fy
for j=1:ny0  % loop for time delay in y-direction
    tauy(j)=sqrt(Fy^2-y0(j)^2)/c-tauymax;   % time delay in y-direction
    Ay(j)=1.;   % No apodization in y-direction
end
for i=1:nx0     % Setting time delay and apodization for all elements
    for j=1:ny0
        A(i,j)=Ax(i)*Ay(j);
        tau(i,j)=taux(i)+tauy(j);
    end
end
%
figure; %Plot of source amplitude
mesh(x0,y0,A.')
set(gca,'fontsize',15)
title('Source Amplitude')
xlabel('x0 (m)')
ylabel('y0 (m)')
figure; %Plot of sorce timedelay
mesh(x0,y0,tau.')
set(gca,'fontsize',15)
title('Source Time Delay')
xlabel('x0 (m)')
ylabel('y0 (m)')
%
```

A.5 Subroutine numwbin.m

The subroutine numwbin.m is the central numeric algorithm. The routine is called from all the field calculation programs. The input to the routine comes from the MATLAB workspace. For the routine to work, the source must be defined and stored in workspace. The source shape is defined by running disc1.m for a circular disc or rect1.m for a rectangular transducer. The normal velocity of the source is defined by running transducer1.m or frontvel.m. The field programs define the observation points and call numwbin. for each observation point with spatial coordinates (x,y,z) and numwbin.m returns the pressure as function of time.

```
%-----------------------------------------------------------------------
% NUMNEW Numerical integration using weighted binning to find the SIR
%-----------------------------------------------------------------------
```

```
% This program calculates the spatial impulse response, velocity
% potential
% and pressure pulse of a piston disc transducer into infinite half-
% space.
% The source function, S(x0,y0,t), is defined by the source amplitude
% function A(x0,y0), the source time delay,tau(x0,y0), and the normal
% velocity of the source surface, v(t):
%
% S(x0,y0,t)=A(x0,y0)*v(t-tau(x0,y0))
%
% where x0 and y0 are the coordinates of the source and t is time.
% A(x0,y0), tau(x0,y0) and v(t) must be precalculated and stored in
% workspace!
%
% The velocity potential, fi(x,y,z,t), where x, y, and z are the
% coordinates of a predefined observation point in the infinite half-
% space (z>0).
%
% fi(x,y,z,t)=sir(x,y,z,t)*v(t)
%
% The pressure field is calculated from the velocity potential as:
%
% p(x,y,z,t)=ro*d/dt[fi(x,y,z,t)]
%------------------------------------------------------------------------
%
% Define time resolution and time vector in order to calculate the spatial
% impulse response, sir(t):
%
delt=0.02*10^-6;    % time resolution: 0.02 microseconds
itmax=500;          % length of time array for calculation
itmaxplot=250;      % length of time array for plotting
tmin=-0.98*10^-6;   % minimum time for calculations
tmax=9*10^-6;       % maximum time for calculations
tmaxplot=4*10^-6;   % maximum time for plotting
t=(tmin:delt:tmax); % timevector span from -1 to 9 microseconds, 1001
% elements for calculations
tfi=(tmin:delt:tmaxplot); % timevector span from -1 to 4 microseconds, 501
% elements for plotting
%
%
% Calculate sir by integrating over source coordinates
%
sir=zeros(1,itmax);
delA=delx0*dely0/delt;  % Source element strength
zz=z^2;
```

```
for i=1:nx0
    xx=(x-delx0*(i-(nx0+1)/2))^2;
   for j=1:ny0
       yy=(y-dely0*(j-(ny0+1)/2))^2;
      R=sqrt(xx+yy+zz); % distance from source element to observation
      % point
      T=(R-z)/c+tau(i,j);         % retarded time delay
      tind=floor(T/delt)+50;      % time index, element 50 at T=0
      Terr=T/delt-double(tind-50); % error in time due to integer index
      % the i,j'th elements weighted contribution to SIR:
      sir(tind)=sir(tind)+(1.-Terr)*delA*A(i,j)/(2*pi*R);
      sir(tind+1)=sir(tind+1)+Terr*delA*A(i,j)/(2*pi*R);
   end
end
%
% Calculate velocity potential from sir and vfront
%
fi=ifft(fft(sir).*fft(vfront,500));
%
% Calulate pressure from velocity potential, p(t)=ro*d/dt[fi(t)]
ro=1000;
pres=zeros(itmaxplot,1);
for it=1:itmaxplot
   pres(it)=ro*(fi(it+1)-fi(it))/delt; % derivation to find pressure
   %pres(it)=sir(it); % returning sir to field
end
%
% Return to field calculations with pressure pulse p(x,y,z,t)
% for the given observation point (x,y,z).
%
% END
```

A.6 Field0.m

The program field0.m calculates the pressure field at a single observation point in space. The input to the program is the coordinates of the observation point in space, x, y, and z. The resulting pressure is plotted as a function of retarded time. Retarded time is defined as the time measured from T=z/c, where z is the depth of the observation point and c is the speed of sound.

```
%
%--------------------------------------------------------------------
```

```
% FIELD0 single point of observation
%-----------------------------------------------------------------------
% This program calculates the pressure field from a piston disc
% transducer into infinite half-space for a single point of observation.
% The subroutine disc1.m or rect1.m must on beforehand generate the
% source amplitude function A(x0,y0) and the time delay tau(x0,y0).
% The subroutine transducer1 or frontvel.m must have calculated the normal
% velocity of the source surface v(t).
% The subroutine numwbin.m is used to calculate the pressure pulse,
% p(x,y,z,t)
%-----------------------------------------------------------------------
%
% Define observation point (x,y,z)
%
x=0*10^-3;
y=0*10^-3;
z=75*10^-3;
%
% Call routine numint.m for calculating pressure pulse, p(x,y,z,t).
%
numwbin
%
% Plot pressure pulse
%
figure;
plot(tfi,real(pres),'k','linewidth',1.5)
set(gca,'fontsize',15)
title('Pressure pulse')
xlabel('Time (s)')
legend('(x,y,z)=(0,0,75)mm')
%
% END
```

A.7 Field1.m

The program field1.m calculates the pressure field along the x-axis. The x-axis is perpendicular to the acoustic axis in the image plane. For a circular source, we have circular symmetry so that the x-axis and y-axis are interchangeable. For a rectangular source, however, the difference is important.

The inputs to the program are the distance between the observation point and the number of observation points. The subroutine numwbin.m calculates the pressure

field at each observation point. The pressure field is presented in two different plots. The first is a plot of the pressure field as function of time and distance from the acoustic axis. The second plot is referred to as the beam profile. From the calculated pressure pulse, we find the peak-peak pressure and pulse energy at each observation point and plot it as a function of the distance from the acoustic axis. The pressure field is symmetric around x=0 and the plot is therefore symmetric. For a circular source, the beam profile will in addition be circular symmetric. The width of the beam profile determines the resolution in an imaging system.

```
%-------------------------------------------------------------------------
% FIELD1
%-------------------------------------------------------------------------
% This program calculates the pressure field from a piston disc
% transducer along a line perpendicular to the acoustic axis, beam
% profile. The subroutine disc1.m must on beforehand generate the source
% amplitude function A(x0,y0) and the source time delay tau(x0,y0).
% The subroutine transducer1 must have calculated the normal velocity of
% the source surface v(t).The subroutine numint is used to calculate the
% pressure pulse, p(x,y,z,t) at each point along the axial distance in the
% x-dimension.
%-------------------------------------------------------------------------
%
% Define observation point (x,y,z)
x=0*10^-3;
y=0*10^-3;
z=100*10^-3;
%
% Loop over the distances from the acoustic axis in the x-dimension.
%
nx=21;       % number of observation points along the x-dimension
delx=0.5*10^-3;  % distance between observation points along x-axis.
xvector=(0:delx:(nx-1)*delx); % position vector in x-dimension
%
itmaxplot=250;
%
% Initiate array for beam profile calculations
%
pres2D=zeros(nx,itmaxplot); % array for pressure pulse in 2 dimensions
peakbeam=zeros(1,2*nx-1);  % array for peak pressure beam profile
energybeam=zeros(1,2*nx-1);  % array for pulse energy beam profile
%
% Loop over the observation points in the x-direction
%
for n=1:nx
```

```
        x=(n-1)*delx;
        %
        % Call numwbin.m to calculate pres(t) at observation point
        % (x,y,z)
        %
        numwbin
        %
        % Store 2D pressure pulse for plotting
        pres=real(pres);
        pres2D(n,:)=pres;
        %
        % Sum up the energy of the pressure pulse
        energy=0;
        for it=1:itmaxplot
            energy=energy+pres(it)^2*delt; % Summing up the energy of
            % pulse
        end
        energybeam(nx+n-1)=energy;
        energybeam(nx-n+1)=energy;
        %
        % Find peak-to-peak pressure
        presmin=min(pres);
        presmax=max(pres);
        peakbeam(nx+n-1)=presmax-presmin;
        peakbeam(nx-n+1)=presmax-presmin;
end
%
% Plot the beam profiles
xbeam=(-delx*(nx-1):delx:delx*(nx-1));  % x-vector for beam profile
peakbeam=peakbeam/max(peakbeam);        % normalizing peakbeam
energybeam=energybeam/max(energybeam);  % normalizing energybeam
figure;
plot(xbeam,peakbeam,'k-',xbeam,energybeam,'k--','linewidth',1.5)
set(gca,'fontsize',15)
xlabel('Distance from axis [m]')
title('Beam profile')
legend('p-p pressure','pulse energy')
%
% Alternatively plot 2D pressure pulse
figure;
surfl(tfi,xvector,pres2D)
set(gca,'fontsize',12)
xlabel('Time [s]')
ylabel('Distance to axis [m]')
title('Pressure pulse')
```

```
%
% END
```

A.8 Field2.m

The program field2.m calculates the pressure field in two spatial dimensions, in the xz-plane. This is the image plane for an imaging system. For a circular source, the pressure field will have circular symmetry around the acoustic axis, the z-axis. The inputs to the program are the distances between the observation points in the two dimensions and the number of points in the two dimensions. The results are plotted in perspective as a beam in space or as a contour plot. The peak-peak pressure is normalized for depth in the contour plot.

```
%---------------------------------------------------------------------
% FIELD2 Two dimensional field calculation
%---------------------------------------------------------------------
% This program calculates the pressure field from a piston disc transducer
% in a rectangular grid in image plane (x,z) where z is the acoustic axis.
% The subroutine disc1.m or rect1.m must on beforehand generate the
% source amplitude function A(x0,y0) and the source time delay
% tau(x0,y0). The subroutine transducer1 or frontvel must have calulated
% the normal velocity of the source surface vfront(t). The subroutine
% numwbin is used to calculate the pressure pulse, p(x,y,z,t) at each
% point in the xz-grid.
%---------------------------------------------------------------------
%
% Calculate Beam profile at different depths (z-dimension)
%
mz=15;      % number of depths (z-values)
delz=10*10^-3;      % distance between the calulation depths
zvector=(2*delz:delz:(mz+1)*delz); %position vector in z-dimension
%
% Calculate Spatial impulse response as function of time and distance
% from axis in the x-dimension.
%
nx=21;              % number of observation points along the x-dimension
delx=0.5*10^-3;     % distance between observation points in the x-dim.
xvector=(0:delx:(nx-1)*delx); % position vector in x-dimension
%
y=0.; % Beamprofile in horisontal plane (image plane)
%
% Initiate array for 2D-beam calculations
```

```
%
peakbeam=zeros(mz,2*nx-1); %array for peak pressure beam profile
%
% Lopp over the different depths in the z-direction
for m=1:mz
    z=(m+1)*delz;
    %
    % Loop over the observation points in the x-direction
    for n=1:nx
        x=(n-1)*delx;
        %
        % Call numwbin.m to calculate p(t) at observation point (x,y,z)
        %
        numwbin
        % pressure is a real entity
        pres=real(pres);
        %
        % Find peak-to-peak pressure
        %
        presmin=min(pres);
        presmax=max(pres);
        peakpres=presmax-presmin;
        %
        % Contruct beam profiles of p-p pressure and pulse energy
        %
        peakbeam(m,nx+n-1)=peakpres;
        peakbeam(m,nx-n+1)=peakpres;
    end
end
%
% Plot 2D-beam
%
xbeam=(-delx*(nx-1):delx:delx*(nx-1)); % x-vector for beam profile
%
% Value of contour lines
vplot=[1.0,0.708,0.501,0.355,0.251];
% contours at 0dB, -3dB, -6dB, -9 and -12dB

figure; % Contour plot
contour(xbeam,zvector,peakbeam,10,'k-')
set(gca,'fontsize',15)
xlabel('Distance to axis [m]')
ylabel('Distance to source [m]')
title('Peak pressure beam')
```

```
figure; % 3D-plot
surfl(xbeam,zvector,peakbeam)
set(gca,'fontsize',12)
xlabel('Distance to axis [m]')
ylabel('Dist. to source [m]')
title('Peak pressure beam in space')
%
% Normalize beam profiles at each depth, z (m):
%
for m=1:mz
peakbeam(m,:)=peakbeam(m,:)/max(peakbeam(m,:));
end
%
% Plot normalized beam
%
figure;
contour(xbeam,zvector,peakbeam,vplot,'k-')
set(gca,'fontsize',15)
xlabel('Distance to axis [m]')
ylabel('Distance to source [m]')
title('Normalized pressure beam')
legend('-3dB')
%
%END
```

A.9 FieldL.m

The program fieldL.m calculates the pressure field along the acoustic axis (z-axis) with the x- and y-coordinates set to zero. The inputs to the program are the number of observation points along the acoustic axis and the distance between them. The outcome of the program is a plot of the peak-peak pressure as function of the depth, z.

```
%-----------------------------------------------------------------
% FIELDL
%-----------------------------------------------------------------
% This program calculates the pressure field from a piston disc transducer
% along the acoustic axis. The subroutine disc1.m or rect1.m must on
% beforehand generate the source amplitude function A(x0,y0) and the
% source time delay tau(x0,y0). The subroutine frontvel.m or transducer1.m
% must have calulated the normal velocity of the source surface v(t). The
% subroutine numwbin is used to calculate the pressure pulse, p(x,y,z,t)
% at each point.
%-----------------------------------------------------------------
```

```
%
% Define calculation grid along acoustic axis(z-dimension)
%
x=0.0;              % acoustic axis
y=0.0;
delz=2*10^-3;       % distance between the calculation depths
znear=0.01;         % start depth
mnear=uint16(znear/delz);
zfar=0.15;          % stopp depth
mfar=uint16(zfar/delz);
mz=mfar-mnear+1;     % number of depths (z-values)

zvector=(znear:delz:zfar); % position vector in z-dimension (depth)
%
% Initiate array
%
longplot=zeros(mz,1); % array for peak pressure along acoustic axis
%
% Lopp over the different depths in the z-direction
for m=1:mz
    z=double(m-1+mnear)*delz;
    %
    % Call numwbin.m to calculate pres(it) at observation point (x,y,z)
    %
    numwbin
    pres=real(pres); % pressure is a real quantity
    %
    % Find peak-to-peak pressure
    %
    longplot(m)=max(pres)-min(pres);
end
%
% Noralize longplot
longplot=longplot/max(longplot);
%
% Plot peak pressure field along acoustic axis
%
figure;
plot(zvector,longplot,'k','linewidth',2)
set(gca,'fontsize',15)
axis([0 0.15 0 1.2])
xlabel('Distance to source [m]')
title('Peak pressure along acoustic axis')
%
%END
```

A.10 FieldT.m

The program fieldT.m calculates the peak-peak pressure field in a transversal plane normal to the acoustic axis. This calculation is intended for rectangular sources because circular sources are circular symmetric and a beam profile, as the one in Figure 3.13 will give sufficient information. The inputs to the program are the depth (z) of the transversal plane, the number of points in the x- and y-dimension and the distance between them.

```
%---------------------------------------------------------------------
% FIELDT Two dimensional field calculation transverse acoustic axis
%---------------------------------------------------------------------
% This program calculates the pressure field from a piston disc transducer
% in a rectangular grid x-y transvers the acoustic axis. The subroutine
% rect1 must on beforehand generate the source amplitude function A(x0,y0)
% and the source time delay tau(x0,y0). The subroutine frontvel.m must
% have calculated the normal surface velocity, v(t) of the source.
% The subroutine numnew.m is used to calculate the pressure pulse,
% p(x,y,z,t) at each point in the xy-grid.
%---------------------------------------------------------------------
%
% Define distance from source, set z value
z=100e-3;
%
% Define xy-grid.
%
nx=21;              % number of observation points along the x-dimension
delx=0.5*10^-3;     % distance between observation points in the x-
dimension
xvector=(0:delx:(nx-1)*delx); %position vector in x-dimension
%
ny=21;              % number of observation points along the y-dimension
dely=0.5*10^-3;     % distance between observation points in the y-
dimension
yvector=(0:dely:(ny-1)*dely); % position vector in y-dimension
%
% Initiate array for 2D-pressure calculations
%
peakbeam=zeros(2*ny-1,2*nx-1);  %array for peak pressure beam profile
%
% Lopp over the obsevation points in the y-direction
for m=1:ny
    y=(m-1)*dely;
    %
```

```
    % Loop over the observation points in the x-direction
    for n=1:nx
        x=(n-1)*delx;
        %
        % Call numwbin.m to calculate pres(it) at point (x,y,z)
        %
        numwbin
        pres=real(pres);
        %
        % Find peak-to-peak pressure
        %
        presmin=min(pres);
        presmax=max(pres);
        peakpres=presmax-presmin;
        %
        % Contruct matrix of p-p pressure
        %
        peakbeam(ny+m-1,nx+n-1)=peakpres;
        peakbeam(ny+m-1,nx-n+1)=peakpres;
        peakbeam(ny-m+1,nx+n-1)=peakpres;
        peakbeam(ny-m+1,nx-n+1)=peakpres;
    end
end
%
% Plot 2D-beam
%
xbeam=(-delx*(nx-1):delx:delx*(nx-1));  % x-vector for grid
ybeam=(-dely*(ny-1):dely:dely*(ny-1));  % y-vector for grid
%
% Normalize peakbeam
peakbeam=peakbeam./max(max(peakbeam));
vlog= 0:-3:-30;     % contours in dB
vplot=10.^(vlog/20); % contours in linear scale
figure;
mesh(xbeam,ybeam,peakbeam)
set(gca,'fontsize',15)
title('Transvers beam profile')
xlabel('Image plane [m]')
%
% Contour plot
figure;
contour(xbeam,ybeam,peakbeam,vplot,'k','linewidth',1.5)
set(gca,'fontsize',15)
title('Transvers beam profile')
xlabel('Image plane [m]')
```

```
legend('-3dB')
%
%END
```